İSTANBUL TECHNICAL UNIVERSITY ★ INSTITUTE OF SCIENCE AND TECHNOLOGY

MULTIDIMENSIONAL MODELING OF COMBUSTION AND POLLUTANT EMISSIONS IN DIESEL ENGINES

M.Sc. Thesis by

Abdurrahman İMREN

(503021019)

Date of submission : 27 December 2004
Date of defence examination : 27 January 2005

Supervisor (Chairman): Prof. Dr. Cem SORUŞBAY

Members of the Examining Committee Prof.Dr. Metin ERGENEMAN (İTÜ.)

Assoc. Prof.Dr. Osman Azmi ÖZSOYSAL (İTÜ.)

JANUARY 2005

İSTANBUL TEKNİK ÜNİVERSİTESİ ★ FEN BİLİMLERİ ENSTİTÜSÜ

DİZEL MOTORLARINDA YANMA VE KİRLETİCİ EMİSYONLARIN ÇOK BOYUTLU MODELLENMESİ

YÜKSEK LİSANS TEZİ

Abdurrahman İMREN

(503021019)

Tezin Enstitüye Verildiği Tarih : 27 Aralık 2004
Tezin Savunulduğu Tarih : 27 Ocak 2005

Tez Danışmanı : Prof.Dr. Cem SORUŞBAY

Diğer Jüri Üyeleri Prof.Dr. Metin ERGENEMAN (İ.T.Ü.)

Doç.Dr. Osman Azmi ÖZSOYSAL (İ.T.Ü.)

OCAK 2005

ACKNOWLEDGMENTS

First of all, I would like to thank Prof. Cem Soruşbay and Prof. Metin Ergeneman for their constant support and valuable instructions. Without their help, this work would not have been possible. Appreciation also goes to many other people in the Automotive Engineering Division for their help and suggestions.

Ford Otosan is acknowledged for its funding and supplying experimental part of this project.

Last but not least, I wish to thank my family for their continuous support, encouragement and understanding.

December, 2004 Abdurrahman İMREN

TABLE OF CONTENTS

ABBREVIATIONS

3D : Three Dimension
ALE : Arbitrary Lagrangian Eulerian
ATDC : After Top Dead Center
BDC : Bottom Dead Center
BTDC : Before Top Dead Center
CAD : Crank Angle Degree
CDM : Continuum Droplet Model
CFD : Computational Fluid Dynamics
CGS : Cray Graphics System
CPU : Central Processing Unit
DDM : Discrete Droplet Model
DI : Direct Injection
DNS : Direct Numerical Simulation
DOI : Duration of Injection
DPF : Diesel Particle Filter
EBU : Eddy BreakUp Model
EGR : Exhaust Gas Recirculation
EOI : End of Injection
HACA : H Abstraction C_2H_2 Addition
ICE : Internal Combustion Engine
IFP : Institut Français du Pétrole
KH : Kelvin Helmhotz
MH : Magnussen-Hijertager
ODE : Ordinary Differential Equation
PAH : Polycyclic Aromatic Hydrocarbon
PaSR : Partially Stirred Reactor
PDC : Partial Donor Cell
PDF : Probability Distribution Function
RNG : Renormalization Group
QSOU : Quasi Second Order Upwind
RNG : ReNormalization Group
RPM : Revolution per Minute
RT : Rayleigh-Taylor
SCR : Selective Cataytic Reduction
SGS : Sub Grid Scale
SI : Spark Ignition
SIMPLE : Semi Implicit Method for Pressure Linked Equations
SOI : Start of Injection
TAB : Taylor Analogy Breakup model
TDC : Top Dead Center

LIST OF TABLES **Page No**

LIST OF FIGURES **Page No**

LIST OF SYMBOLS

c_0 : Initial average concentration in PaSR model
c : Unknown concentration in the reactive zone
c_1 : Time average value of reactor exit concentration
c_p : Constant pressure specific heat
C_D : Drag coefficient
C_f : Collision frequency of reactant atoms
C_{mix} : Constant for micro mixng time
C_ε : Coefficients for the turbulence model
D : Diffusion coefficient
D : Droplet diameter
e : Specific internal energy
E_a : Activation energy
F : Acting force on the droplet
$\vec{F}^s$: (rate of momentum gain)/(volume) due to spray
$f_m(c)$: Chemical source term
$f(r)$: Probability distribution function
$\dot{f}_{bu}$: Source due to droplet break-up
$\dot{f}_{coll}$: Source due to droplet collision
$\vec{g}$: Specific body force
h_m : Specific enthalpy
I : Specific internal energy
J : Heat flux vector
k : Global reaction rate coefficient
k : Turbulent kinetic energy
k_b : Backward reaction rate coefficient
k_f : Forward reaction rate coefficient
K : Thermal conductivity
$L(T_d)$: Fuel latent heat of vaporization
Nu : Nusselt number
Oh : Ohnesorge number
p : Pressure
Pr : Prandtl number
Q_d : The rate of heat conduction
$\dot{Q}^c$: Source term due to chemical heat release
$\dot{Q}^s$: Source term due to spray interactions
R_0 : Universal gas constant

Re	: Reynolds number
r	: Droplet radius (equilibrium)
r_c	: Diameter of child droplets
$\mathbf{S}$	: Rate of strain tensor
Sc	: Schmidt number
Sh	: Sherwood number
T	: Taylor number
T	: Temperature
T_d	: Temperature of droplet
t	: Time
$\mathbf{u}$	: Velocity vector
$\mathbf{u_d}$	: Droplet velocity
$\mathbf{u_{rel}}$	: Relative velocity
We	: Weber number
W_m	: Molecular weight of species m
Y_m	: Mass fraction of species m
y	: Distortion from sphericity
α	: Dimensionless swirl constant
Δt	: Integration step
$\left(\Delta h_f^0\right)_m$	: Heat of formation of species m at absolute zero
∇	: Vector operator
δ_{m1}	: Dirac delta function
ε	: Dissipation rate of turbulent kinetic energy
ϕ	: Equivalence ratio
ρ	: Total gas mass density
ρ_m	: Mass density of species m
ρ_l	:Droplet/liquid density
$\dot{\rho}_s$	:Total liquid evaporation rate per unit volume
κ^*	: Volume fraction of the reacting mixture
κ	: Reaction rate multiplier
Λ	: Wavelength of maximum growth rate of KHwaves
Λ_t	: RT wavelength
μ	: Gaseous dynamicviscosity
σ	: Viscous stress tensor
σ	: Collision transition probability function
σ	: Surface tension
Ω	: Maximum growth rate of KH waves
Ω_t	: Fastest growing rate of RT waves
τ_c	: Chemical time scale
τ_k	: Kolmogorov time scale

τ_{mix} : Micro mixing time scale

τ_t : Taylor time scale

τ_{kt} : Geometric mean of Kolmogorov and Taylor time scales

τ_u : Momentum relaxation time

τ_e : Evaporation relaxation time

τ_h : Heat transfer relaxation time

ν : Gaseous kinematic viscosity

ν_i : Stoichiometric coefficients

$\dot{\omega}_r$: Chemical reaction rate

DİZEL MOTORLARINDA YANMA VE KİRLETİCİ EMİSYONLARIN ÇOK BOYUTLU MODELLENMESİ

ÖZET

Egzoz gazı emisyonlarının çevre ve insan sağlığı açısından yönetmeliklerle sınırlandırılması ve emisyon sınır değerlerinin gün geçtikçe daha düşük değerlere çekilmesi, kirletici emisyon değerleri daha da düşük motorların üretimini zorunlu kılmaktadır. Standardlarla tanımlanan bu hedeflere ulaşabilmek için alternatif çözüm yolları bulunmaktadır. Ancak öncelikli hedef yanma performansının yüksek tutulması ve egzoz gazı emisyonlarının kaynağında kontrol edilmesidir. Bu amaçla karışım oluşumu ve yanma olaylarının karmaşık yapısının tanımlanması, olaya etki eden parametrelerin belirlenmesi ve genelde bu parametrelerin optimize edilmesi gerekmektedir.

Böylesine karmaşık fiziksel olaylar hakkında detaylı bilgi edinmek ve bu olaylara etkiyen parametrelerin kontrolünü deneylerle yapmak oldukça zor ve pahalıdır. Bu yüzden motor tasarımında matematiksel modelleme önemli bir yere sahiptir. Matematiksel modeller ise genelde termodinamik ve çok-boyutlu modeller olmak üzere iki gruba ayrılır.

Bu çalışmada Diesel motorlarında karışım oluşumu ve yanmanın modellendiği çok-boyutlu bir model kullanılmıştır. Ford-Otosan Ecotorq 7.3 litre NHDD motoru söz konusu model yardımı ile KIVA kodu kullanılarak motor performansı ve egzoz gazları emisyonu bakımından incelenmiştir. Oluşturulan model motorun mevcut deney sonuçları ile doğrulandıktan sonra, performansı iyileştirici ve kirletici emisyonları azaltıcı etkilerin belirlenmesi amacıyla püskürtme zamanlaması üzerine parametrik inceleme yapılmıştır.

Kullanılan KIVA kodunda zamana bağlı, sıkıştırılabilir,üç boyutlu, iki fazlı, türbülanslı, çok bileşenli reaktif gazların ve çeşitli motor geometrilerinin de düşünüldüğü akış alanı korunum denklemleri çözülür. KIVA'nın açık bir kod olması alternatif modellerin koda aktarılması avantajını getirmektedir.

Bu çalışmada KHRT yakıt demeti parçalanma modeli KIVA kodunda standart olan TAB modeli ile değiştirildi. Türbülansın ortalama reaksiyon hızına olan etkisini hesaba katmak için standart M-H modeli yerine Chalmers Üniversite'sinin PaSR modeli kullanıldı. Global tek adımlı reaksiyon seti yerine detaylı mekanizma yaklaşımı kullanıldı. Kullanılan indirgenmiş mekanizma 68 bileşen ve 279 reaksiyondan oluşmaktadır.

Model katsayılarının ayarlanması ile deney ve hesaplama sonuçları karşılaştırıldığında motor performansını belirleyen basınç eğrileri için çeşitli devir ve yüklerde uyumlu sonuçlar alındı. %45 yükte ise deney ve hesaplanan basınç eğrilerinde tutuşma gecikmesinden kaynaklanan ayrılıklar gözlemlendi. Ayrıca, püskürtme debisinin motorun emisyon ve basınç eğrileri üzerinde etkin bir parametre olduğu belirlendi. Hesaplanan emisyonlar incelendiğinde NOx emisyon düzeyinin

egzoz ölçümleri ile uyum içerisinde olduğu is emisyonlarının ise ölçülen değerlere göre çok düşük olduğu görüldü. Fakat, püskürtmenin geciktirilmesiyle yapılan parametrik analizde is emisyonlarının deney sonuçlarıyla beklenen trendi takip ettiği gözlemlendi. Çeşitli ayrık zamanlamalı püskürtme stratejileri uygulanarak hem NOx ve is emisyonlarını birlikte azaltacak hem de motor performansı ve yakıt tüketimini çok etkilemeyecek en uygun zamanlama arandı.

KIVA kodu Intel Fortran Compiler 8.0 ile derlenerek Linux SUSE 9.0 işletim sistemi üzerinde koşuldu. Ağ yapısı k3prep ile hazırlandı ve sonuçlar GMV, Tecplot ve MS Excel paket programları ile görselleştirildi. Ayrıca eğitim amaçlı olarak ICEM CFD ile çeşitli ağ sistemleri ve CEI Ensight programı kullanılarak sonuçların görselleştirilmesi denendi.

MULTIDIMENSIONAL MODELING OF COMBUSTION AND POLLUTANT EMISSIONS IN DIESEL ENGINES

SUMMARY

Due to stringent and continuously tightened emission standards with respect to environmental concerns and human health, improvement in Diesel engine technology is required. Although there exist several alternative exhaust aftertreatment systems in order to meet these future emission norms, first aim is to attain a better combustion performance and to control pollutant emisssions in the source where combustion takes place. In this case, it is essential that mixture formation and intricate structure of combustion process be defined and influencing parameters be optimised.

Furthermore, it is quite expensive and may extremely be difficult to do sophisticated experiments so as to obtain detailed information of such complex processes and to control affecting parameters. This is because, mathematical modeling is of great importance in engine research and development. Generally speaking, mathematical models can be categorized into two main groups, so called thermodynamic and multidimensional models.

In this study, multidimensional modeling approach has been utilized as a predictive tool to investigate mixture formation and combustion process in Diesel engines. This approach has been carried out by using KIVA-3V code in order to understand the effects of certain parameters on NOx and soot emissions of a new heavy duty engine of Ford, so called Ecotorq NHDD. Having compared the computed results with the experimentally obtained data from Ford Otosan, several parametric analyses on injection scheme have been investigated to obtain better engine performance and to reduce both NOx and soot emissions.

For diesel engine applications, KIVA code, which solves the conservation equations for evaporating fuel sprays coupled with the three-dimensional turbulent fluid dynamics of compressible, multi-component, reactive gases in cylinder with arbitrary shaped piston geometries, has been selected due to being an open source code. In the code, some modifications have been done in order to increase its modeling capability.

The KHRT spray model has been used to replace the TAB model, which is standard in KIVA for diesel spray modeling. Detailed chemistry approach, accounting tri-molecular reactions and third body influence, has been used both ignition modeling and combustion process. PaSR model of the Chalmers University of Technology, applicable to the whole reaction set, have been implemented. The diesel fuel surrogate model comprises 70/30% mixture of n-heptane, C_7H_{15}, and toluene, C_7H_8. The mechanism consists of 68 species and 279 reactions. In the simulation, the physical properties like vapor pressure, critical temperature, latent heat of vaporization of the model fuel have been considered as the same as those of the real diesel oil#2.

Having calibrated the code by means of cycle modeling on a specific rpm and load, computational and experimental pressure histories were compared for different load and rpms. Quite satisfactory results were obtained except low load cases, e.g. lower than 45% load, where discrepancy between the computed and measured pressure traces was considered because of not predicting the ignition delay well enough. From the point of view of computed emissions, it was seen that NOx emission level was in agreement with that of the measurements, whereas soot was predicted extremely small. Moreover, it was shown that injection rate parameters, such as its shape and timing, played important role on both pressure histories and emissions. In the case of retarded injection, the fact that both NOx and soot emissions followed the expected emission trend was dealt. Several split injection strategies were tested to come up with the best scheme resulting in both reducing NOx and soot emissions simultaneously without a penalty of fuel consumption and engine performance.

KIVA code was compiled with Intel Fortran 8.0 program and run on Linux SUSE 9.0 platform. Model grid was built with k3prep and results were visualized by GMV, Amtec Tecplot and MS Excel softwares. For educational purposes, ICEM CFD and CEI Ensight were tested to generate several grids and to visualize the computed results respectively.

CHAPTER 1

INTRODUCTION

Internal combustion engines, utilized to propel the vehicles on roads, have more than a 100 year long history. During this period, there always have been such researches to alleviate fuel consumption and to get more efficient combustion in order to control its products causing pollution of environment. For last decade, continuously tightened emission legislations have accelerated these researches of engine technology.

Diesel engine applications are getting increase in automotive industry due to the advantages of especially having high thermal efficiency in part loads, subsequently, resulting low specific fuel consumption. Recently, in European countries, Diesel engine applications, which are widespread in conventional heavy duty vehicles, are of great amount of increase in automobiles as well **(Dohle et al, 2004).** Also, some innovations in injection systems like electronic controlled, high pressure, multiple injection are able to yield lower pollutant emissions and noise in regard to the past.

Since exhaust gas emissions with respect to environment and human health are continuously regulated by legislations, it is unavoidable for the engine manufacturers to produce less pollutant emission-out-engine. Therefore, alternative solution procedures that will satisfy the norms of these legal requirements are being developed extensively by both the industry and academicians. In this regard, the first aim is to have higher combustion performance and to control emissions in the source where combustion takes place. Thus, it is essential that mixture formation and complex phenomena of combustion be defined and affecting parameters be optimized.

To challenge with future emission limits, controlling in-cylinder combustion is not adequate, and it requires some additional precautions or aftertreatment systems such as application of EGR (exhaust gas recirculation) and SCR (selective catalytic reduction) for lower NOx; oxidation catalyst and DPF (Diesel particle filter) for soot **(Penny et al, 2004).** In Diesel engines, one of the effective method to have better performance and low engine-out emissions is turbocharging that supply more power and less specific emission concentrations.

As noted above, it is plausible to give priority to control of combustion phenomena in order to get higher engine performance and lower engine-out emissions. However, improvement of combustion performance can be achieved by examining the parameters relying on combustion, for instance, resolving local conditions can yield substantial information especially for Diesel engines in which mixing has quite significance. Furthermore, heat and mass transfer, air movements (swirl, squish) in the combustion chamber are some of the important parameters influencing combustion as much as local conditions. In internal combustion engines sprays are utilized in order to mix the liquid fuel with air and increase its surface area for rapid evaporation and combustion. Since fuel is injected directly into the combustion chamber so as to form an ignitable mixture with air, the spray is one of the most effective measures to control the combustion process. Moreover, spray represents the main source for turbulence that governs the micro-scale air fuel mixing.

Experiments of such complex physical processes or parameters governing the mixture formation and combustion are too expensive and difficult to obtain local information. Therefore, mathematical modeling can be an invaluable tool to get three dimensional resolved information, that experiments can hardly yield. Despite their advantages, mathematical models have shortcomings either because of oversimplifying assumptions or because of insufficient knowledge of the real processes.

Mathematical models utilized in internal combustion engines are divided into two groups: thermodynamic and multi dimensional models. First law of the thermodynamics is applied to combustion chamber represented as single or multi zones in a cycle, that's why, it is called as thermodynamic model. It is also helpful to provide the heat release rate according to a given pressure history. On the other hand, multidimensional models take into account many details as turbulent flow, spray,

combustion and their interactions with arbitrary shaped combustion chamber. Since they provide all the variables at every geometrical point, they are more predictive and can better supply fundamental information on combustion phenomena.

In this study, multidimensional modeling approach has been considered to investigate mixture formation and combustion process in Diesel engines. This modeling approach has been carried out by means of a modified KIVA-3V code in order to get better performance and less pollutant emissions. At first stage, numerical simulation results were compared with those of experimentally obtained from Ford-Otosan Ecotorq engine. The latter is to carry out parametric analysis to have lower pollutant emissions.

CHAPTER 2

MODELING OF COMBUSTION PROCESS

In direct injection Diesel engines, evolution of combustion process and spray undergoes in a logical sequence as atomization, breakup, collision, evaporation, mixing with surrounding air, combustion and heat release, finally emission formation. **(Dec, 1997)**. This logical sequence gives an opportunity to consider these physical processes as sub-models in numerical modeling.

There are several kinds of modeling approaches considering the physical processes above. In this chapter, comparisons of modeling approaches and, of those, CFD multidimensional approach will be dealt, as well as spray formation, breakup and combustion processes.

Additionally, mixing-controlled combustion is of great significance. In this kind of combustion, mixing time scales are dominant for the overall combustion process, and both molecular and turbulent diffusion play important roles on mixing rate. Therefore, in engine modeling approach, it is essential that combustion process be modeled as accurate as possible. Hence, in the next sections, combustion process and its chemistry/turbulence interaction and implementation into KIVA code, was described in detail.

In diesel engines, pollutant engine-out emissions are carbon monoxide (CO), unburned hydrocarbons (HC), nitrogen oxides (NOx) and particulate matter which is often approximated as soot. Depending on the quality of the fuel there may also exist sulphur oxides (SOx). With respect to legislations, there is typically a focus on the NOx and soot standards. In addition, reducing both soot and NOx is a challenging task, known as ‘The Diesel dilemma’. Therefore, in the latter section, parametric analysis has been realized to investigate pollutant emissions and how to reduce their amounts regarding computational approach.

2.1. The Classification of Models

Engine modeling approaches are usually divided into two categories as: thermodynamic and multidimensional models (CFD). In addition to these approaches, phenomenological models are sometimes considered as a separate group. (see Figure 2.1).

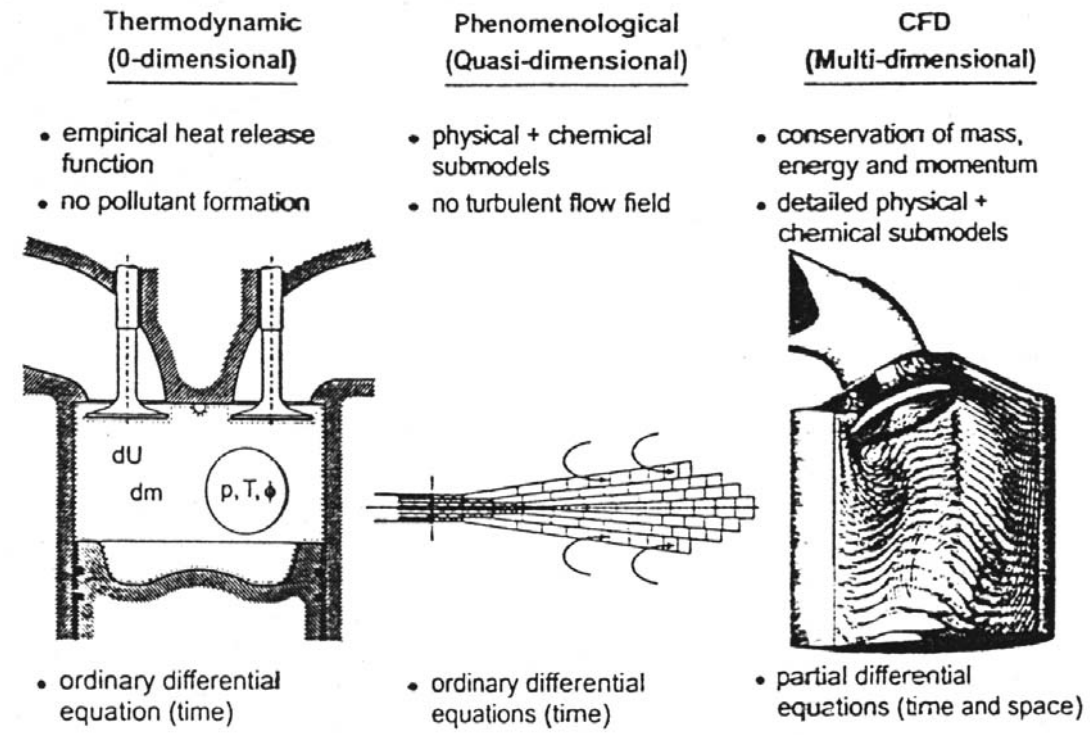

Figure 2.1. Classification of the models **(Stiesch, 2003)**

2.1.1. Thermodynamic Models

Thermodynamic models are based on the first law of thermodynamics and mass balances (conservation of mass and energy). The principles of momentum conservation are not considered in this category. Since spatial variations of composition and thermodynamic properties are ignored, combustion chamber is treated as a single, homogeneously mixed zone.

Governing equations of the thermodynamic models are those of the conservation of mass and energy.

$$\frac{dm_{cv}}{dt} = \sum_i \dot{m}_i - \sum_e \dot{m}_e \qquad (2.1.1)$$

$$\frac{dU_{cv}}{dt} = \dot{Q} + \dot{W}_t + \sum_i \dot{m}_i h_i - \sum_e \dot{m}_e h_e \qquad (2.1.2)$$

These assumptions profoundly simplify the problem and prohibit the usage of thermodynamic models in order to obtain locally resolved information. However, in some applications such as heat release analysis, the great advantage of these models is the fact that they are both easy to handle and computationally very efficient. Moreover, it is possible to use numerous zones that have different thermodynamic properties and compositions. In general, spray penetration, autoignition modeling, and modeling of pollutant emissions such as Zeldovich mechanism for NO emissions are some of the submodels that can be considered in thermodynamic models **(Yoshizaki et al, 1993).** Even, these submodels such as representing spray process or chemical models can be coupled with different thermodynamic zones. Even if using multizones have the computational expenditure increased slightly, it is still much cheaper than that of CFD.

In computing emissions especially of NOx, local properties are of great significance, this is because it is plausible that the combustion chamber is represented as multi zones having different thermodynamic properties instead of a single zone. That's why, being investigated physical or chemical processes are not considered in two or three dimensional domain, but multi zones. (see Figure 2.2)

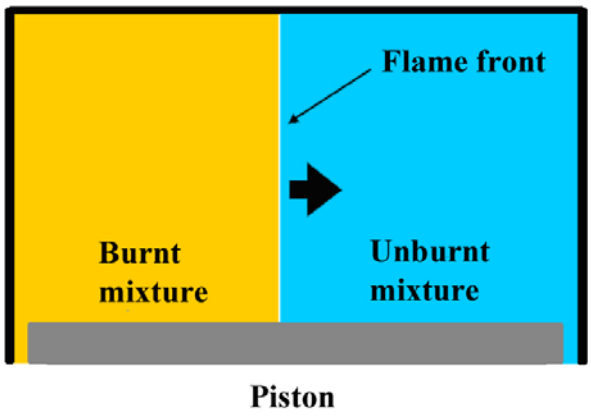

Figure 2.2. Schematic illustration of two zone thermodynamic model

Furthermore, because of this spatial resolution, important subprocesses can be modeled and the prediction of heat release rates and exhaust emissions as a function of characteristic engine parameters becomes possible. In this regard, the more increasing number of zones, the more accurate solution. However, the spatial

resolution is still relatively coarse in these models, and the turbulent flow field inside the engine cylinder is not solved for. Thus, effects of the engine geometry on combustion can hardly be accounted for, and analyses of subscale processes, that would require a higher spatial and temporal resolution, are limited.

In addition, time dependent ordinary differential equations utilized to represent thermodynamic models are much more robust than the partial differential equations (time and space dependent) of multidimensional models with respect to numerical solution.

2.1.2. Multidimensional Models

In multidimensional models, numerical solutions are obtained by the gas phase equations of the conservation laws for time dependent, three dimensional, turbulent, chemically reacting flows of multi-component mixture of ideal gases, coupled to the equations for single component vaporizing fuel sprays. (see, Figure 2.3).The effects due to presence of droplets and chemical reactions are accounted for via appropriate source terms in the gas phase equations. Source terms are derived from the submodels of physical and chemical processes as detailed as possible. Of the most important advantages, turbulent flow field is taken into account in this kind of modeling approach. However, time dependent, moving frame of combustion chamber require a suitable numerical solution approach. This is because, of the most popular codes, KIVA-3V code, based on arbitrary Lagrangian-Eulerian (ALE) finite volume method was selected in this study (**Amsden, 1989**). Due to its being open-source code, it is the outstanding feature to implement new models developed yet. The spray computations are based on a discrete-particle technique treating the spray in a Lagrangian way. Since it does not require the nozzle region to be fully resolved by the computational mesh, it is much more practical and computationally efficient than Eulerian method. Even though computer technology is developing rapidly, computational expenditure and some intricate numerical problems still inhibit Eulerian method requiring resolution of nozzle region. For example, in general, lengths of the cells in the mesh structure are about 1-2 mm, whereas diameter of nozzle orifice is usually as small as 0.130 mm. This is because, parcels, group of identical droplets in Lagrangian method are of zero dimension and do not occupy any space in the domain, they only serve to act as a marker determining the cell in which

liquid/gas exchange takes place. However, these parcels can be assigned many properties as many as desired. Some of them are location, velocity, diameter, mass, temperature and fuel composition. The more parcels, the more accurate representation of the spray.

Another mesh resolution problem arises from the small scales of turbulence, so turbulence effect on micro-mixing in the cell can not be known on a grid level. That's why, in order to correlate the sub grid conditions with those of grid level, the so called EBU (Eddy Break-up) models are widely used.

Briefly, the prominent feature of the multidimensional models is to represent detailed physical and chemical processes of ICEs as much as possible contrary to thermodynamic models. However, these representive mathematical sub models and their numerical solution techniques require improvement because of existing plenty of unknowns in physics. That's why it is necessary to verify the computed results by comparing with those of experimental.

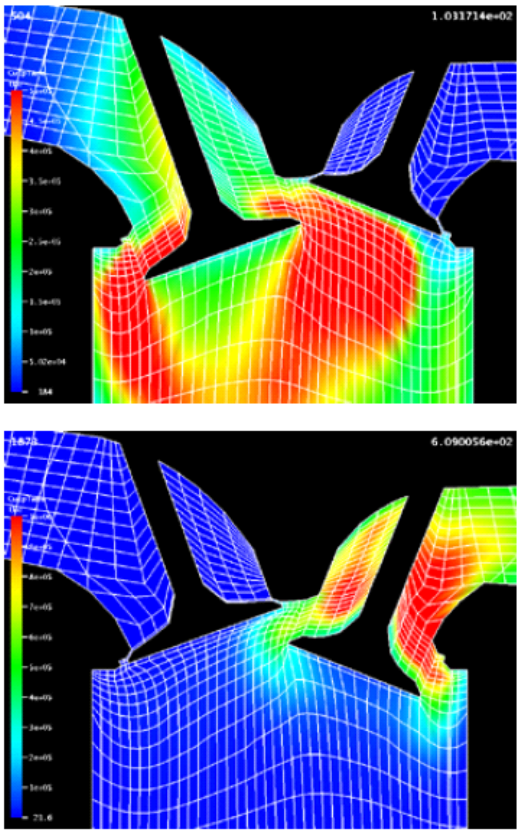

Figure 2.3. An example of multidimensional modeling approach **(Amsden, 1998)**

2.2 Governing Equations in Multidimensional Models

In this section, governing equations (conservation laws of mass, momentum and energy) of both gas (Eulerian) and liquid (Lagrangian) phases will be represented respectively. Because of the coupling between the Eulerian and the Lagrangian approaches, the Eulerian equations have extra source terms to account for the gas and liquid phase interaction. Considering that spray parcels are of zero dimension and do not occupy in the Eulerian frame, the source terms are utilized to transfer of physical and chemical evolution or mass, momentum and energy changes of these spray parcels into flow field equations (the Eulerian).

2.2.1. The Eulerian Equations

In reacting flows, the fluid consists of at least three components. Thus, governing equations have to be derived for multi-component mixtures.

The position and velocity vectors are defined respectively as;

$$\mathbf{x} = xi + y\mathbf{j} + z\mathbf{k} \tag{2.2.1}$$

$$\mathbf{u} = u(x, y, z, t)\mathbf{i} + v(x, y, z, t)\mathbf{j} + w(x, y, z, t)\mathbf{k} \tag{2.2.2}$$

The vector operator is given by

$$\nabla = \mathbf{i}\frac{\partial}{\partial x} + \mathbf{j}\frac{\partial}{\partial y} + \mathbf{k}\frac{\partial}{\partial z} \tag{2.2.3}$$

2.2.1.1. Continuity Equation

The continuity equation for species m is

$$\frac{\partial \rho_m}{\partial t} + \nabla.(\rho_m \mathbf{u}) = \nabla.\left[\rho \mathbf{D} \nabla\left(\frac{\rho_m}{\rho}\right)\right] + \dot{\rho}_m^c + \dot{\rho}^s \delta_{m1} \tag{2.2.4}$$

The terms, at the right side of the equation above, are the diffusion term, chemical source term and spray source term due to evaporation of liquid respectively.

ρ_m: mass density of the species m

ρ: total mass density

$\mathbf{u}$: fluid velocity

$\mathbf{D}$: mass diffusion coefficient (Fick's law) $\mathbf{D} = \mu/(\rho S_c)$

$\dot{\rho}_m^c$: chemical source term

$\dot{\rho}^s$: spray source term

δ_{m1}: Dirac delta function (Dirac delta function is the value of 1 or 0 depending on whether there is fuel or not in the cell.)

By summing Equation (2.2.4) over all species, we obtain the total fluid density equation;

$$\frac{\partial \rho}{\partial t} + \nabla.(\rho \vec{u}) = \dot{\rho}^s \tag{2.2.5}$$

Additionally, mass fraction is defined by

$$Y_m = \frac{\rho_m}{\rho} \tag{2.2.6}$$

2.2.1.2. The Momentum Equation

Momentum equation for the fluid mixture is

$$\frac{\partial}{\partial t}(\rho \mathbf{u}) + \nabla.(\rho \mathbf{u}\mathbf{u}) = -\nabla p - \nabla\left(\frac{2}{3}\rho\kappa\right) + \nabla.\sigma + \mathbf{F}^s + \rho\mathbf{g} \tag{2.2.7}$$

where,

p : the fluid pressure

$\mathbf{F}^s$: the rate of momentum gain/loss per unit volume due to the spray.

σ: the viscous stress tensor

$$\sigma = 2\mu\mathbf{S} + \lambda\nabla.\mathbf{u}\mathbf{I} \tag{2.2.8}$$

$$\mathbf{S} = \frac{1}{2}\left[\nabla\mathbf{u} + (\nabla\mathbf{u})^T\right] \tag{2.2.9}$$

μ and λ are the first and second coefficients of viscosity (including turbulent viscosity)

2.2.1.3. The Energy Equation

The internal energy equation is

$$\frac{\partial}{\partial t}(\rho I) + \nabla.(\rho \mathbf{u} I) = -p\nabla.\mathbf{u} - \nabla.\mathbf{J} + \rho\varepsilon + \dot{Q}^C + \dot{Q}^S \tag{2.2.10}$$

Here,

I : specific internal energy, exclusive of chemical energy

$\dot{Q}^C$: Chemical heat release

$\dot{Q}^S$: Spray interaction

$\mathbf{J}$: the heat flux vector which is the sum of heat conduction and enthalpy diffusion:

$$\mathbf{J} = -K\nabla T - \rho \mathbf{D} \sum_m \left[h_m \nabla \left(\frac{\rho_m}{\rho} \right) \right] \tag{2.2.11}$$

where T is the gas temperature and h_m is the specific enthalpy of species m.

2.2.1.4. The Turbulence Equation

Despite numerous turbulence models available to close the conservation equations, k-ε and its RNG version, widely applied in CFD codes, have been used in this thesis.

k-ε model is given by

$$\frac{\partial(\rho k)}{\partial t} + \nabla.(\rho \mathbf{u} k) = -\frac{2}{3}\rho k \nabla.\mathbf{u} + \sigma : \nabla \mathbf{u} + \nabla.\left[\left(\frac{\mu}{\mathrm{Pr}_k} \right) \nabla k \right] - \rho\varepsilon + \dot{W}^S \tag{2.2.12}$$

and

$$\frac{\partial(\rho\varepsilon)}{\partial t}+\nabla.(\rho\mathbf{u}\varepsilon)=-\left(\frac{2}{3}C_{\varepsilon 1}-C_{\varepsilon 3}\right)\rho\varepsilon\nabla.\mathbf{u}+\nabla.\left[\left(\frac{\mu}{\mathrm{Pr}_{\varepsilon}}\right)\nabla\varepsilon\right] +\frac{\varepsilon}{k}\left[C_{\varepsilon 1}\sigma:\nabla\mathbf{u}-C_{\varepsilon 2}\rho\varepsilon+C_{s}\dot{W}^{s}\right] \tag{2.2.13}$$

$\sigma:\nabla\mathbf{u}=\sigma_{ij}\partial u_i/\partial x_j$ is defined to account for the effects of compressibility. $\dot{W}^{s}$ is the source term arising due to interaction with the spray. The value of C_s=1.5 has been suggested for Diesel sprays by **O'Rourke (1986)**. The other models constants are listed in Table 2.1.

In the RNG k-ε model, only the ε equation is modified as,

$$\frac{\partial(\rho\varepsilon)}{\partial t}+\nabla.(\rho\mathbf{u}\varepsilon)=-\left(\frac{2}{3}C_{\varepsilon 1}-C_{\varepsilon 3}+\frac{2}{3}C_{\mu}C_{\eta}\frac{k}{\varepsilon}\nabla.\mathbf{u}\right)\rho\varepsilon\nabla.\mathbf{u} +\nabla.\left[\left(\frac{\mu}{\mathrm{Pr}_{\varepsilon}}\right)\nabla\varepsilon\right]+\frac{\varepsilon}{k}\left[\left(C_{\varepsilon 1}-C_{\eta}\right)\sigma:\nabla\mathbf{u}-C_{\varepsilon 2}\rho\varepsilon+C_{s}\dot{W}^{s}\right] \tag{2.2.14}$$

where

$$C_{\eta}=\frac{\eta(1-\eta/\eta_0)}{1+\beta\eta^{3}},\quad \eta=S_m\frac{k}{\varepsilon},\quad S_m=\left(2S_{ij}S_{ij}\right)^{1/2}, \qquad \eta_0=4.38,\quad \beta=0.012 \tag{2.2.15}$$

For ideal gases the molecular viscosity, μ_{air}, is related with T^{m} ($\mu_{air}\sim T^{m}$; T is temperature, and m equals to 0.5) $C_{\varepsilon 3}$ is also dependent on the polytropic exponent n. ($n\sim 1.3-1.4$)

$$C_{\varepsilon 3}=\frac{-1+2C_{\varepsilon 1}-3m(n-1)+(-1)^{\delta}\sqrt{6}C_{\mu}C_{\eta}\eta}{3} \tag{2.2.16}$$

$$\delta=\begin{cases}1, & \nabla.\mathbf{u}\le 0\\ 0, & \nabla.\mathbf{u}>0\end{cases} \tag{2.2.17}$$

Standard and RNG k-e turbulence model constants are given in Table 2.1:

Table 2.1. Model constants for standard and RNG k-e turbulence model.

Model	C_η	$C_{\varepsilon 1}$	$C_{\varepsilon 2}$	$C_{\varepsilon 3}$	Pr_k	Pr_ε	C_s
Standard	0.09	1.44	1.92	-1.0	1.0	1.3	1.5
RNG	0.0845	1.42	1.68	Equation(2.2.16)	0.7194	0.7194	1.5

And the transport coefficients

$$\nu = \nu_{air}\left[1+\sqrt{\frac{C_\mu}{\nu_{air}}}\frac{k}{\sqrt{\varepsilon}}\right]^2, \quad \nu = \frac{\mu}{\rho}, \quad \mu_{air} = \frac{A_1 T^{3/2}}{T + A_2}, \quad \lambda = -\frac{2}{3}\mu \tag{2.2.18}$$

$$\kappa = \frac{\mu c_p}{\mathrm{Pr}}, \quad D = \frac{\nu}{Sc} \tag{2.2.19}$$

where the Prandtl and Schmidt numbers are input (itape5 of KIVA-3V) constants and

$A_1 = 1.457\times 10^{-5}, \quad A_2 = 110.0$

2.2.1.5. The Chemistry Equations

The chemical reactions occurring in the system are symbolized by

$$\sum_m a_{mr}\chi_m \Leftrightarrow \sum_m b_{mr}\chi_m \tag{2.2.20}$$

where χ_m represents one mole of species m and a_{mr} and b_{mr} are integral stoichiometric coefficients for reaction r.

Kinetic reaction r proceeds at rate $\dot{\omega}_r$ given by

$$\dot{\omega}_r = k_{fr}\prod_m\left(\frac{\rho_m}{W_m}\right)^{a'_{mr}} - k_{br}\prod_m\left(\frac{\rho_m}{W_m}\right)^{b'_{mr}} \tag{2.2.21}$$

a'_{mr} and b'_{mr} are the empirical reaction orders. k_{fr} and k_{br} are of a generalized Arrhenius form and represent forward and backward reaction rate coefficients.

$$k_{fr} = A_{fr} T^{\xi fr} \exp\left\{-\frac{E_{fr}}{T}\right\} \tag{2.2.22}$$

$$k_{br} = A_{br} T^{\xi br} \exp\left\{-\frac{E_{br}}{T}\right\} \tag{2.2.23}$$

where E_{fr} and E_{br} are the activation temperatures (Kelvin). Having defined the chemical equations, the chemical source term in the species continuity equation can be written as:

$$\dot{\rho}_m^c = W_m \sum_r (b_{mr} - a_{mr}) \dot{\omega}_r \tag{2.2.24}$$

and the chemical heat release term in the energy equation is given by

$$\dot{Q}^c = \sum_r Q_r \dot{\omega}_r \tag{2.2.25}$$

where Q_r is the negative of the heat reaction at absolute zero,

$$Q_r = \sum_m (a_{mr} - b_{mr})(\Delta h_f^0)_m \tag{2.2.26}$$

and $(\Delta h_f^0)_m$ is the heat of formation of species m at absolute zero.

2.2.2. The Lagrangian Equations

The equations of evaporation, motion and energy for the liquid phase will be represented in this section.

2.2.2.1. The Equation of Motion

The Droplet momentum equation (Newton's second law) is given by

$$\mathbf{F} = m_d \frac{\partial \mathbf{u}_d}{\partial t} \tag{2.2.27}$$

md : droplet mass, $\mathbf{u}_d$: droplet velocity, $\mathbf{F}$: force acting on the droplet.

The acting force on the droplet, only considering the drag and gravitational force, is

$$\mathbf{F} = -\frac{\pi D^2}{8}\rho C_D \left|\mathbf{u}_d - \mathbf{u}\right|\left(\mathbf{u}_d - \mathbf{u}\right) + m_d \mathbf{g} \tag{2.2.28}$$

where C_D is the drag coefficient. Suggested expressions of the drag coefficient are below. **(Amsden,1989)**

$$C_D = \begin{cases} \dfrac{24}{\mathrm{Re}_d}\left(1 + \dfrac{1}{6}\mathrm{Re}_d^{2/3}\right) \rightarrow \mathrm{Re} < 1000 \\ 0.424 \ldots\ldots\ldots\ldots\ldots \rightarrow \mathrm{Re} > 1000 \end{cases} \tag{2.2.29}$$

When solving the equation of motion in practice, equations (2.2.27) and (2.2.28) are combined and written as below

$$\frac{\partial \mathbf{u}_d}{\partial t} = -\frac{\mathbf{u}_d - \mathbf{u}}{\tau_u} + \mathbf{g} \tag{2.2.30}$$

where τ_u is given by

$$\tau_u = \frac{8 m_d}{\pi \rho C_D D^2 \left|\mathbf{u}_d - \mathbf{u}\right|} = \frac{4}{3}\frac{\rho_d D}{\rho C_D \left|\mathbf{u}_d - \mathbf{u}\right|} \tag{2.2.31}$$

2.2.2.2. The Droplet Energy Equation

The equation for the heat transfer to the liquid droplet is given by

$$m_d \frac{dh_d}{dt} = \dot{m}_d h_v(T_d) + \pi D \kappa Nu \left(T - T_d\right) f \tag{2.2.32}$$

$$f = \frac{z}{e^z - 1}, \quad z = -\frac{c_{p,v}\dot{m}_d}{\pi D \kappa Nu} \tag{2.2.33}$$

f is a factor which corrects the rate of heat exchange due to the presence of mass transfer. The expression used for Nu number is

$$Nu = 2.0 + 0.6\,\mathrm{Re}^{1/2}\,\mathrm{Pr}^{1/3} \tag{2.2.34}$$

where the Prandtl numer is given by

$$\Pr = \mu \frac{c_p}{\kappa} \tag{2.2.35}$$

All the properties using film temperature can be evaluated by the 1/3 rule

$$T_f = \frac{2T_d + T}{3} \tag{2.2.36}$$

To solve practically Eq.(2.2.32), τ_h can be defined as below

$$\tau_h = \frac{m_d c_{l,d}}{\pi D \kappa Nu} \tag{2.2.37}$$

where $c_{l,d}$ is the specific heat for the liquid.

Rearranging Eq.(2.2.32) with mass transfer equation given below as Eq.(2.2.40), $h_d = c_{l,d}\left(T_d - T_{ref}\right)$ and τ_h yields rate of droplet temperature change

$$\frac{dT_d}{dt} = \frac{T - T_d}{\tau_h} f - \frac{1}{c_{l,d}} \frac{h_v(T_d)}{\tau_e} \tag{2.2.38}$$

where τ_e is defined later in Eq. (2.2.43)

3.2.2.3. The Droplet Mass Equation

Assuming that the droplet is spherical and its evaporation follows the D^2 rule,

$$\frac{dD^2}{dt} = C_{evap} \tag{2.2.39}$$

the rate of evaporation for a single droplet is defined by

$$\frac{dm_d}{dt} = \dot{m}_d = -\pi D \mathbf{D} \rho_v Sh \ln \frac{p - p_{v,\infty}}{p - p_{v,s}} = -\pi D \mathbf{D} \rho_v Sh \ln\left(1 + \frac{X_{v,s} - X_{v,\infty}}{1 - X_{v,s}}\right) \tag{2.2.40}$$

where ρ_v is the density of the fuel vapor close to the surface, **D** is the coefficient of mass diffusion.

$$\rho_v = \frac{p}{R_v T} \tag{2.2.41}$$

Sh represents Sherwood number and it is given by

$$Sh = 2.0 + 0.6\,\mathrm{Re}^{1/2}\,Sc^{1/3} \tag{2.2.42}$$

To solve practically Equation (2.2.40), τ_e is defined below as

$$\tau_e = \frac{m_d}{\pi D \mathbf{D} \mathrm{Sh} \rho_v \ln(1+B)} \tag{2.2.43}$$

$$B = \frac{X_{v,s} - X_{v,\infty}}{1 - X_{v,s}} \tag{2.2.44}$$

Then, the evaporation rate can be given by

$$\frac{dm_d}{dt} = -\frac{m_d}{\tau_e}, \quad \frac{dD}{dt} = -\frac{D}{3\tau_e} \tag{2.2.45}$$

In addition, boiling conditions of the fuel must be taken into account. Because, in the event of the liquid starts to boil, the vapor pressure rises above the ambient pressure, then B tends to infinity. In this case, τ_e tends to zero, causing an infinite evaporation rate. (Infinite evaporation occurs only at the critical point of the liquid.) Therefore, it is unphysical to use Eq. (2.2.40) for the boiling conditions.

Instead, the evaporation rate equation under boiling conditions is derived from Eq.(2.2.32). Since the temperature is constant, left hand side of this equation is zero. Evaporation rate expressions are below

$$\frac{dm_d}{dt} = -\frac{\pi D \kappa Nu}{c_{p,v}} \ln\left(\frac{c_{p,v}}{h_v}\left(T - T_d\right) + 1\right) \tag{2.2.46}$$

$$\frac{dD}{dt} = -\frac{D}{\tau_{boil}} \tag{2.2.47}$$

$$\tau_{boil} = \frac{D^2 \rho_d c_{p,v}}{2\kappa Nu \ln\left(\frac{c_{p,v}}{h_v}\left(T - T_d\right) + 1\right)} \tag{2.2.48}$$

In this way, mass transfer eEq. (2.2.40) is replaced by the Eq. (2.2.46) for boiling conditions in the numerical solution algorithm.

2.3. Spray Formation and Breakup of Drops

In internal combustion engines, it is essential that the mixture formation be improved in order to get better combustion performance. That is to say, to obtain rapid evaporation and combustion, it is important that mixture formation be improved by increasing the surface area between the liquid fuel and surrounding air. For example, disintegrating 2 mm drop into about eight million droplets of 10 μm increases the evaporation rate by a factor of 200 **(Stiesch, 2003).**Thus, the spray is one of the most effective measures to control the combustion process. In addition, the kinetic energy of the spray is the main source for turbulence production within the combustion chamber, and therefore governs the micro-scale air-fuel mixing by turbulent diffusion. Accordingly, it can be said that the spray significantly affects the ignition delay, heat release rate, exhaust emissions, fuel consumption and the noise level. As a consequence, it is necessary that the spray processes be understood as detailed as possible.

2.3.1. The Spray Regimes

Spray regimes are distinguished into several categories as depicted in Figure 2.4. At the nozzle orifice an intact core of the liquid phase can be identified (void fraction, i.e. volume fraction of the gas phase to the liquid phase, $\theta < 0{,}5$). Then, it rapidly disintegrates into ligaments (churning flow) and further into droplets. But, droplets are still denser than the gas phase. This spray regime is generally called as thick or dense spray. It is often assumed that a spray behaves as a thick spray if the void fraction is less than about, $\theta \approx 0{,}9$. **(O'Rourke, 1981)** Due to the conical spray shape and droplet evaporation process, the average spacing between droplets expands further downstream of the nozzle, and the void fraction approaches unity. On the other hand, due to the liquid to gas density ratio, the mass fraction of the liquid phase is still noticeable. (Thin spray regime). The last stage of the spray evolution is called as very thin or dilute spray. In this regime, both volume and mass fractions of the liquid phase are usually ignored.

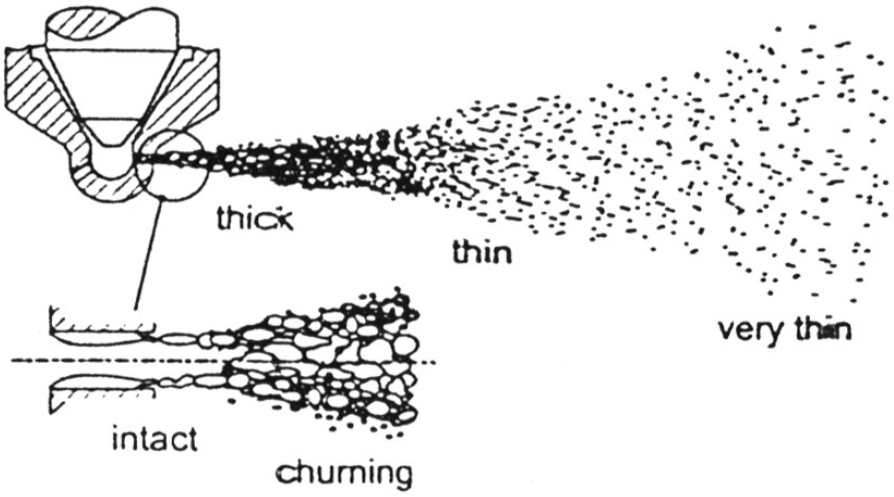

Figure 2.4. Schematic representation of spray regimes. **(Stiesch,2003)**

To distinguish the spray jet into several regimes is of great significance on its mathematical modeling. For example, in the dense spray regime droplet collisions and coalescences are the dominant models or interactions, whereas, the influence of the gas phase is negligible. However, in dilute spray regime collisions between droplets are rare and generally ignored in the modeling. Besides, in the vicinity of the nozzle the governing mechanisms of the intact core regime have still considerable uncertainties. That's why, this regime is ignored in most of the CFD codes.

2.3.2. The Spray Equation

In typical diesel engines, atomization of the fuel jet causes the droplets to disintegrate into a number of up to 100 million with average diameter of 10 μm. Therefore, it is impractical to resolve each single droplet in the numerical simulations with regard to today's computer power. Instead, some statistical averaging techniques are utilized so-called spray equation. **(Williams, 1985)** In this approach, the probable number of drops per unit volume is considered.

$$\frac{probable\ number\ of\ droplets}{unit\ volume} = f\left(\bar{x},\bar{v},\bar{r},T_d,y,\dot{y},t\right)d\bar{v}\ dr\ dT_d\ dy\ d\dot{y} \qquad (2.3.1)$$

where

t : time

$\vec{x}$: position (3)

$\vec{v}$: velocity (3)

r : radius

T_d : temperature

y : distortion from sphericity

$\dot{y}$: temporal rate of change of y

(in total 11 independent variable)

The spray equation formulated by Williams is

$$\frac{\partial f}{\partial t} = -\frac{\partial}{\partial x_i}(fv_i) - \frac{\partial}{\partial v_i}(fF_i) - \frac{\partial}{\partial r}(fR) - \frac{\partial}{\partial T_d}(f\dot{T}_d) - \frac{\partial}{\partial y}(fy) - \frac{\partial}{\partial \dot{y}_i}(f\ddot{y}) + \dot{f}_{coll} + \dot{f}_{bu} \tag{2.3.2}$$

By solving the spray equation, the so-called source terms of the Eulerian equations, that describe the interactions between the liquid and gas phases, are obtained.

The source term accounting for mass evaporation of the liquid droplets is added into mass conservation equation.

$$\dot{\rho}^s = -\int f\rho_d 4\pi r^2 R d\vec{v} dr dT_d dy d\dot{y} \tag{2.3.3}$$

The rate of momentum gain due to droplet drag, body forces and evaporation is

$$\vec{F}^s = -\int f\rho_d \left(\frac{4}{3}\pi r^3 \vec{F}' + 4\pi r^2 R\vec{v}\right) d\vec{v} dr dT_d dy d\dot{y} \tag{2.3.4}$$

Energy transfer between the gas and liquid phase is

$$\dot{Q}^s = -\int f\rho_d \left\{ \begin{array}{l} 4\pi r^2 R\left[I_1(T_f) + \frac{1}{2}(\vec{v}-\vec{u})^2 \right] \\ + \frac{4}{3}\pi r^3 \left[c_1 \dot{T}_d + \vec{F}'.(\vec{v}-\vec{u}-\vec{u}') \right] \end{array} \right\} d\vec{v} dr dT_d dy d\dot{y} \tag{2.3.5}$$

The negative of the rate at which turbulent eddies are doing work in dispersing the spray droplets is

$$\dot{W}^{s} = -\int f\rho_d \frac{4}{3}\pi r^3 \vec{F}'.u' d\vec{v} dr dT_d dy d\dot{y} \tag{2.3.6}$$

Generally speaking, there are two methods commonly used to solve the spray equation: Continuum droplet model (Eulerian-Eulerian) and discrete droplet model (Eulerian-Lagrangian) **(Kuo, 1986).**

In CDM, the spray equation is solved directly with a Eulerian finite difference or finite volume scheme similar to the numerical solution of the gas phase. However, the CDM requires to discretize the droplet probability function f in all eleven independent dimensions. Thus, computational expenditure costs too much. For example, discretizing the problem on a coarse mesh with only ten grid points in each dimension requires 10^{11} grid points.

The DDM, proposed by Dukowicz and used in most of the CFD codes, is more practical approach than the CDM. Finite numbers of groups of particles (parcels) are used to represent the entire spray. For example, 10^3 to 10^4 parcels represent 100 million droplets in this approach. Thus, CPU power demand is decreased significantly. In addition, the motion and transport of representative samples of discrete drops are tracked through the flow field using a Lagrangian formulation, while a Eulerian formulation is used to solve the governing equations for the gas phase. The effect of droplets on the gas phase is taken into account by introducing appropriate source terms in the gas phase conservation equations.

2.3.3. Spray Atomization and Breakup Regimes

The atomization process of Diesel sprays is distinguished into two successive stages. First, the drops and ligaments start to shed from the liquid jet due to the primary jet breakup process. The latter, smaller drops are formed due to secondary breakup around the liquid jet as a result of the liquid-gas interaction and drop collisions. **(Reitz, 1987)**

2.3.3.1. Breakup Regimes

Breakup regimes are typically distinguished into three categories as depicted in Figure 2.5. **(Reitz,1978)** For relatively low injection velocities, Rayleigh regime governs the breakup process. In this regime breakup length is far downstream of the nozzle orifice. (Fig.2.5.a) In the wind induced breakup regime, breakup process is

accelerated by the relative motion of the ambient gas and the jet. (Fig.2.5.b) The atomization regime is the regime of interest to internal combustion engine applications. (Fig.2.5.c) Here the jet forms a diverging cone-shaped spray at the nozzle exit. However, the breakup mechanism for jets in the atomization regime has still uncertainties, whereas the mechanisms controlling the breakup in Rayleigh and wind induced breakup regimes are reasonably well understood. This is partly due to the fact that the spray is optically very dense in the vicinity of the nozzle and thus hardly accessible by optical measuring techniques. But, there is a general agreement for the atomization regime that as the injection pressure increases, the effects of turbulence and cavitation become more and more.

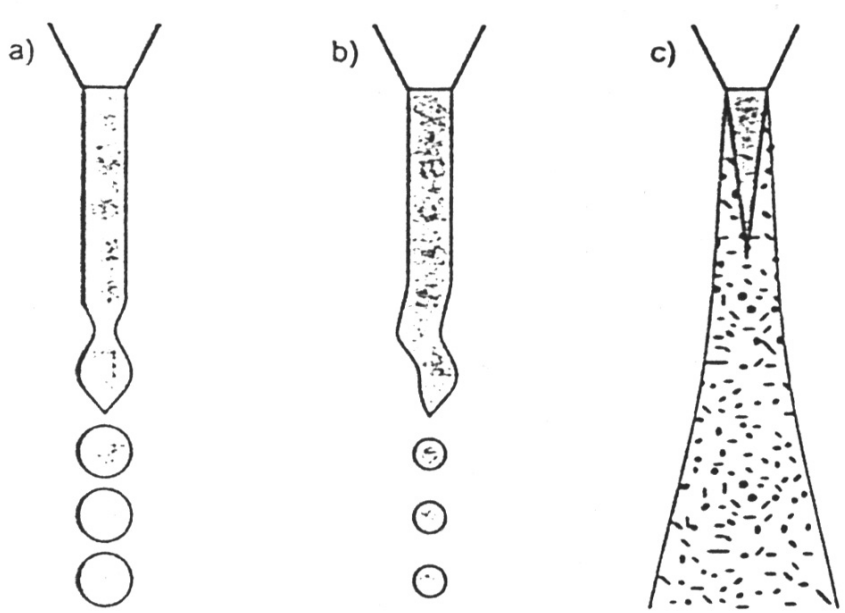

Figure 2.5. Schematic illustration of breakup regimes **(Stiesch,2003)**

2.3.4. Spray Breakup Models

Due to uncertainties in the vicinity of the nozzle, primary breakup model is usually neglected in the CFD applications. In this case, instead of primary breakup model, the initial size and spray angle is specified as constants. However, in the literature, there are several proposed mechanisms controlling primary breakup of high speed diesel jets.

Of widely used primary breakup models, the blob injection model is based on the combination model of KH (Kelvin-Helmholtz) and RT (Rayleigh-Taylor) models, that are usually applied in secondary breakup process of the liquid jet. In this model

it is assumed that during the injection duration there are continuously added large drops (so-called blobs) with a diameter comparable to the size of the nozzle hole. Immediately after injection, the KH instabilities start to grow on the blob surface, subsequently, child droplets are stripped from the parent drop. In addition, it is assumed that the KH instabilities are caused by the effects of the inner nozzle flow, e.g. by turbulence within the liquid phase. (see Figure 2.6)

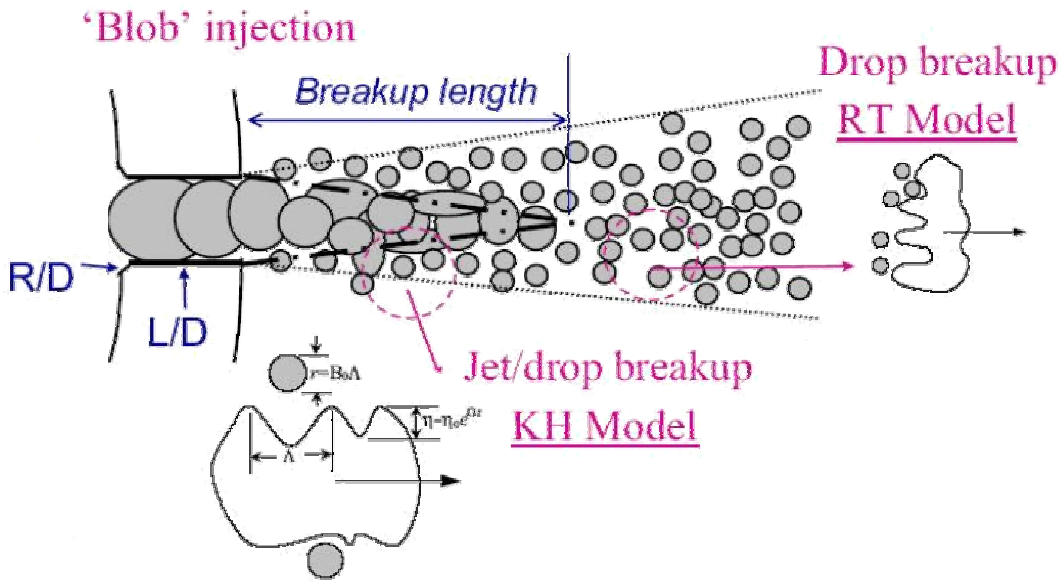

Figure 2.6. Schematic depiction of Blob Injection Model, **(Reitz,1987)**

And, the spray cone angle is specified by assuming that the droplet velocity component perpendicular to the spray direction. Since the influence of the inner nozzle flow on atomization cannot be predicted, this model is calibrated by adjusting empirical constants.

Furthermore, comprehensive studies on this subject show that effects of the inner nozzle flow such as turbulence of liquid phase and cavitation have an increasing influence on primary spray breakup **(Arcoumanis et al, 2000).** A comprehensive two zone primary breakup model, based on turbulence and cavitation, can be seen in Figure 2.7.

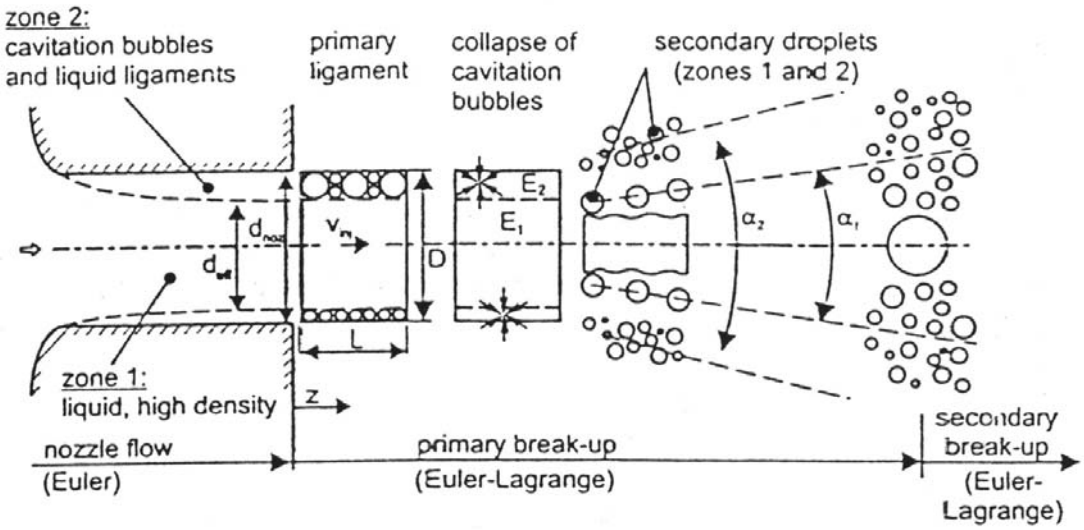

Figure 2.7. Schematic representation of the primary breakup model based on turbulence and cavitation **(Baumgarten et al, 2002)**

The secondary breakup of droplets is determined by Weber number, defined as the ratio of the inertia forces to the surface tension forces. There are a variety of mathematical models for drop breakup proposed in the literature. Most widely known models are the Taylor analogy (TAB), KH and RT breakup models.

In the TAB model, proposed by **O'Rourke and Amsden (1987),** it is assumed that the droplet distortion is described as a one-dimensional spring-mass system. The droplet distortion is characterized by the dimensionless parameter $y = 2x/r$, where x describes the deviation of the droplet equator from its equilibrium position. (Figure 2.8.)

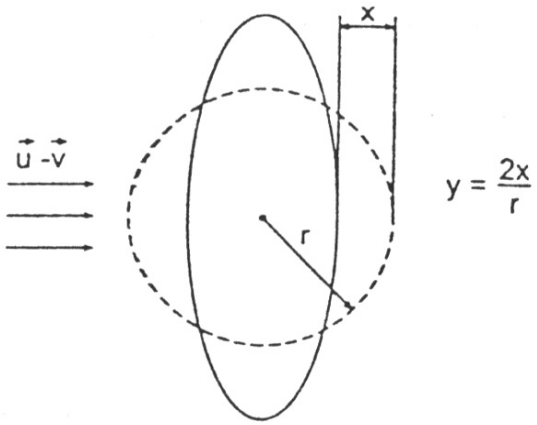

Figure.2.8. Schematic illustration of the distortion parameter, y, in the TAB model. **(O'Rourke and Amsden, 1987)**

Breakup occurs if and only if the distortion parameter y exceeds 1; that is, x becomes greater than half the droplet radius. O'Rourke states that this is the case which is in agreement to critical Weber number for vibrational breakup ~ 6.

Of the most widely used secondary breakup models, KH-RT model is a combination of KH and RT breakup models. **(Reitz,1987)** Model explanation is presented below: The liquid jet is subject to a number of infinitesimal perturbations with an initial amplitude of η_0 and a spectrum of wavelengths λ. It is assumed that initial perturbations are caused by the effects of the inner nozzle flow, e.g. by turbulence within the liquid phase. Their amplitudes will be increased by the liquid gas interactions, e.g. aerodynamic forces. Therefore, immediately after injection, the KH instabilities start to grow on the blob surface, subsequently, child droplets are stripped from the parent drop.

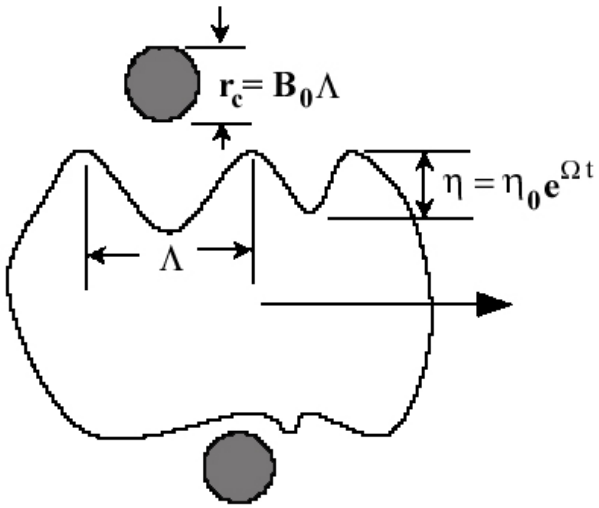

Figure 2.9. Schematic picture of the KH breakup model **(Reitz, 1987)**

By assuming that there is a linear dependency between the child droplets and the wavelength of the most unstable surface perturbation, the child droplets with the size

$$r_c = B_0\Lambda \tag{2.3.7}$$

are stripped from the parent parcel. $B_0 = 0.61$ is suggested model constant. The radius of the parent parcel is reduced according to the rate expression

$$\frac{dr}{dt} = -\frac{r - r_c}{\tau_{kh}}, \quad \tau_{kh} = \frac{3.788 B_1 r}{\Omega \Lambda} \tag{2.3.8}$$

where $B_1 = 10$ is selected and in the literature values ranging 1.73 up to 30 have been used. It was pointed out that B_1 may need to be adjusted to different initial disturbance levels.

To solve the equations governing the parent and child droplet radii above, the maximum growth rate, Ω, and its wavelength, Λ, is necessary. These are defined by Reitz as below

$$\Omega = \frac{0.34 + 0.38 We^{1.5}}{(1 + Oh)(1 + T^{0.6})} \sqrt{\frac{\sigma}{\rho_d r^3}} \tag{2.3.9}$$

$$\Lambda = 9.02 r \frac{(1 + 0.45\sqrt{Oh})(1 + 0.47 T^{0.7})}{(1 + 0.865 We^{1.67})^{0.6}} \tag{2.3.10}$$

where We is defined as the gas phase Weber number,

$$We = \frac{\rho |\mathbf{u}_{rel}|^2 r}{\sigma} \tag{2.3.11}$$

Oh is the Ohnesorge number,

$$Oh = \frac{\sqrt{We_l}}{\mathrm{Re}_l} \tag{2.3.12}$$

and T is the Taylor number,

$$T = Oh\sqrt{We} \tag{2.3.13}$$

We_l is the liquid Weber number, just gas density is replaced by the liquid density.

Re_l is the liquid Reynolds number.

$$\mathrm{Re}_l = \frac{\rho_l |\mathbf{u}_{rel}| r}{\mu_l} \tag{2.3.14}$$

The RT model is based on the considerations of the liquid-gas interface that is subject to aerodynamic forces. RT instabilities develop if the fluid acceleration has an opposite direction to the density gradient. In the event of a liquid droplet is decelerated by drag forces in a gas phase, the RT instabilities may grow unstable at the trailing edge of the droplet. (see Figure 2.10.)

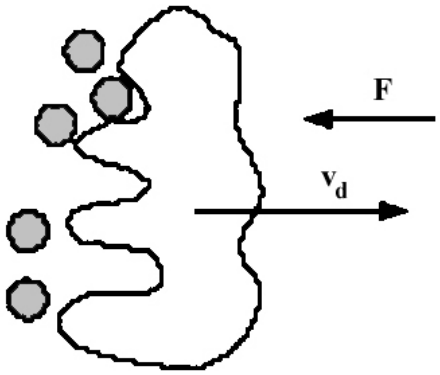

Figure 2.10. Schematic depiction of RT model **(Reitz,1987)**

The RT mode of breakup works in a slightly different way. The size of the new child droplets is calculated depending on RT wavelength, Λ_t, and breakup occurs when Λ_t is less than the diameter of the parent droplet.

$$\Lambda_t = \frac{\pi}{K} \tag{2.3.15}$$

where

$$K = \sqrt{\frac{|g_t(\rho_l - \rho)|}{3\sigma}},\ g_t = \left(\mathbf{g} + \frac{d\mathbf{u}_d}{dt}\right) \cdot \frac{\mathbf{u}_d}{|\mathbf{u}_d|}$$

The breakup time is found as the reciprocal of the frequency of the fastest growing wave, $\tau_t = 1/\Omega_t$

where

$$\Omega_t = \sqrt{\frac{2}{\sqrt{27\sigma}} \frac{|g_t(\rho_l - \rho)|^{3/2}}{\rho_l + \rho}}$$

Typically, the RT breakup model is not utilized as the only method to describe secondary breakup mechanism. Instead, a combined model of KH and RT models are preferred. In this way, close to the injector nozzle where the droplet velocities are highest, the RT mode becomes dominant, whereas the influence of KH mode increases further downstream.

Another important consequence, utilization of this combined model, disintegrating the drops into child and parent droplets, yields more realistic droplet size distribution compared to TAB model.

2.4. Fuel Evaporation

Evaporation of fuel injected into combustion chamber is of great importance with respect to mixture formation and combustion process especially in direct injection internal combustion engines. Because, combustion process occurs if and only if vaporized fuel mixes with air in a combustible ratio. Thus, evaporation rate has direct influence on engine's thermodynamic efficiency and formation of emissions as well. Poor evaporation will typically cause increased soot and unburned hydrocarbon emissions, whereas very rapid evaporation leads to increase the amount of fuel-air mixture accumulated during the ignition delay, and thus, rapid premixed burn causes high temperatures that result the increase in NOx emissions. As a consequence, a thorough understanding of the mechanisms controlling the fuel evaporation is of great significance.

In direct injection engines, the major fraction of the fuel evaporates after the atomization of the spray, i.e. brokenup into small droplets. That's why the droplet evaporation mechanism is the most important part in evaporation modeling. However, the other mechanisms such as wall film evaporation may become important under some certain conditions.

2.4.1. Droplet Evaporation

Evaporation of droplets propagating in the combustion chamber is governed by conductive, convective and radiative heat transfer from the hot gas to the colder droplet and by simultaneous diffusive and convective mass transfer of fuel vapor at the drop surface into the gas environment.

With respect to determine basic principles of evaporation, usually, evaporation of single and ideally spherical droplet is examined. There are several approaches as: infinite-diffusion model that is used as standard in the CFD codes, diffusion limit model by which multi-component fuel evaporation is considered.

In the "infinite-diffusion" model, it is assumed that the droplet interior is well-mixed without spatial gradients at any time and the temperature within the droplet depends on time only. Thus, an infinite mixing and heat transfer are considered in the droplet. (Figure 2.11)

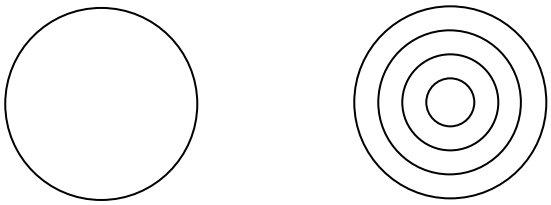

Infinite diffusion	Diffusion-limit
$T = T(t)$ $c_i = c_i(t)$	$T = T(r,t)$ $c_i = c_i(r,t)$

Figure 2.11. Modeling approaches for droplet evaporation

The so-called diffusion-limit model assumes a one-dimensional temperature and, in the case of a multi-component fuel, mass distribution as a function of the droplet radius. Since there exists no circulation within the droplet interior, it can be said that the heat and mass exchange processes inside the droplet are governed by conduction and diffusion, respectively.

In addition, the convective heat transfer of the gas flow is of great importance on the evaporation of droplets. The convective phenomenon increases the heat transfer between the phases, and thus evaporation rate increases as well. Moreover, it influences the evaporation rate by inducing interior circulations or vortices. (see Figure 2.12)

Several researchers investigated the evaporation of a single droplet including the influence of convection. Of these approaches, Ranz-Marshall correlation considers the influence of convection just by adding an empirical term to the ideally-spherical single droplet model. (Equation 2.2.40)

In this study, Ranz-Marshall correlation and infinite diffusion model for single component fuel, that can be viewed as the standard in today's engine simulations, have been used. On the other hand, **Aggarwal (1987)** has stated that the infinite-diffusion model yields results that are markedly different from the others, i.e. diffusion limit and vortex models.

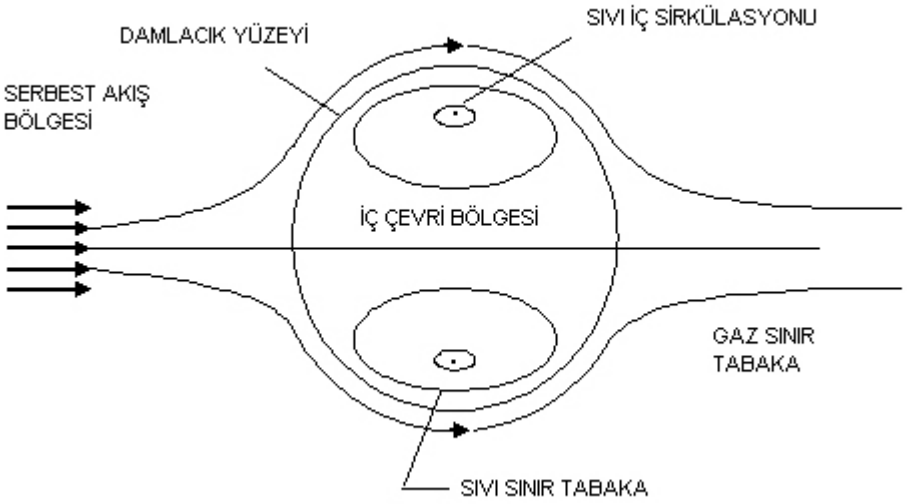

Figure 2.12. Schematic view of the evaporation model of Prakash and Sirignano.

2.5. Ignition Modeling

Ignition process is classified into two groups: (1) thermal explosions, (2) chain reactions. It is widely accepted that the ignition of hydrocarbons fuels can be viewed as a chain branching process. Therefore, ignition delay is extremely dependent on the reaction path.

Formerly, multidimensional simulations of diesel combustion have been carried out based on two main forms: either (1) The assumption is made that a single Arrhenius rate equation adequately describes the entire course of ignition and combustion, or (2) The simplification is imposed that the chemical reaction time is instantaneous relative to turbulence mixing time (e.g. the eddy breakup model is employed). **(Theobald, 1986)**

The first method has proved difficult to implement with a reasonable reaction rate But, these single-step Arrhenius models are easy to use, that's why they have often been employed in the simulations. Usually those models use an empirical reaction

equation to account for the energy release. That is; collision frequency coefficient in the Arrhenius reaction expression is tuned to model both the ignition and the combustion processes as shown below:

$$Fuel + \lambda n_1 O_2 \rightarrow n_2 CO_2 + n_3 H_2 O \tag{2.5.1}$$

$$k = C_f T^{\xi} \exp\left(-\frac{E_a}{RT}\right)[Fuel]^a [Oxidant]^b \tag{2.5.2}$$

E_a: activation energy

Usually C_f represents kinetic collision frequency of reactant atoms. Under most IC engine operating conditions the flame is turbulent and the single-step global kinetics model does not account for the turbulence interactions. Therefore the pre-exponentional factor C_f becomes very much an empirical constant which needs to be adjusted from case to case so that the calculated data provides sufficient agreement with experimental measurements. **(Lu et al, 1993)**

The second description also is not sufficient, particularly for very cold starting conditions when ignition delay apparently becomes much longer than the mixing time. The use of separate chemical reaction descriptions for autoignition and main combustion may ultimately resolve these conflicts.

Hence, in both cases, it is difficult to tune single step models in order to describe the entire course of both ignition and combustion. Therefore, at least a multi-step kinetics model such as Shell and IFP ignition models **(Kong, 1996)** to simulate ignition and a turbulence-chemistry interaction model for main combustion process are required.

Moreover, the more computer power, the more detailed multi-step kinetics that represent both considering low and high temperature cases. So, in recent years, detailed chemistry approach is widely utilized in CFD codes.

One of the goals of this study is to develop a predictive combustion model for direct injection diesel engines. Therefore, Diesel fuel surrogate chemistry model, proposed by **Golovitchev et al (2002),** has been considered in order to model both low temperature (autoignition) and high temperature cases, as well as soot and NOx emissions.

2.5.1. Diesel Fuel Surrogate Model

Practical Diesel fuels comprises a great number of aliphatic and aromatic compounds, and their combustion is too much complex to be modeled using comprehensive chemical mechanism. Instead, surrogate fuel models are used in numerical simulations.

Aliphatic components can be represented by long chain hydrocarbons such as n-heptane, n-dodecane, of which cetane number ~ 56, similar to conventional diesel fuel. Aromatic components significantly contribute to soot formation.

Golovitchev assumed the diesel fuel surrogate model to comprise 70/30% mixture of n-heptane, C_7H_{15}, and toluene, C_7H_8. In the simulation, the physical properties of the model fuel have been considered as the same as those of the real diesel oil#2.

The mechanism consists of 68 species and 279 reactions and its validation through autoignition is shown in Figure 2.13 and 2.14.

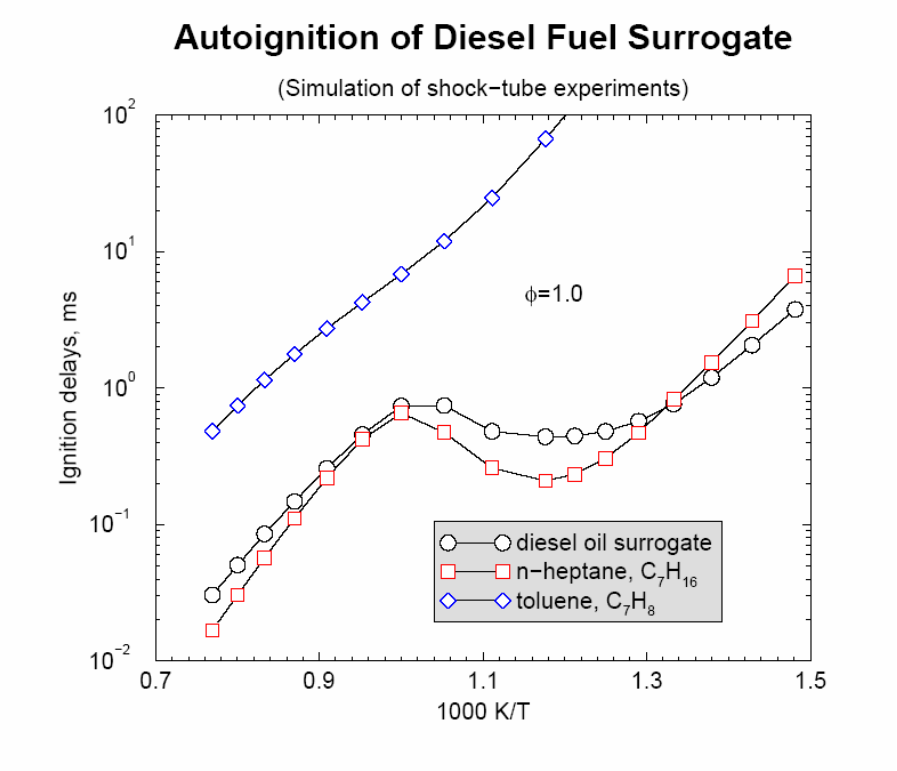

Figure 2.13. Calculated ignition delays for fuel surrogate. P_0 =41 bar and ϕ=1 for all compounds. **(Golovitchev et al, 2003)**

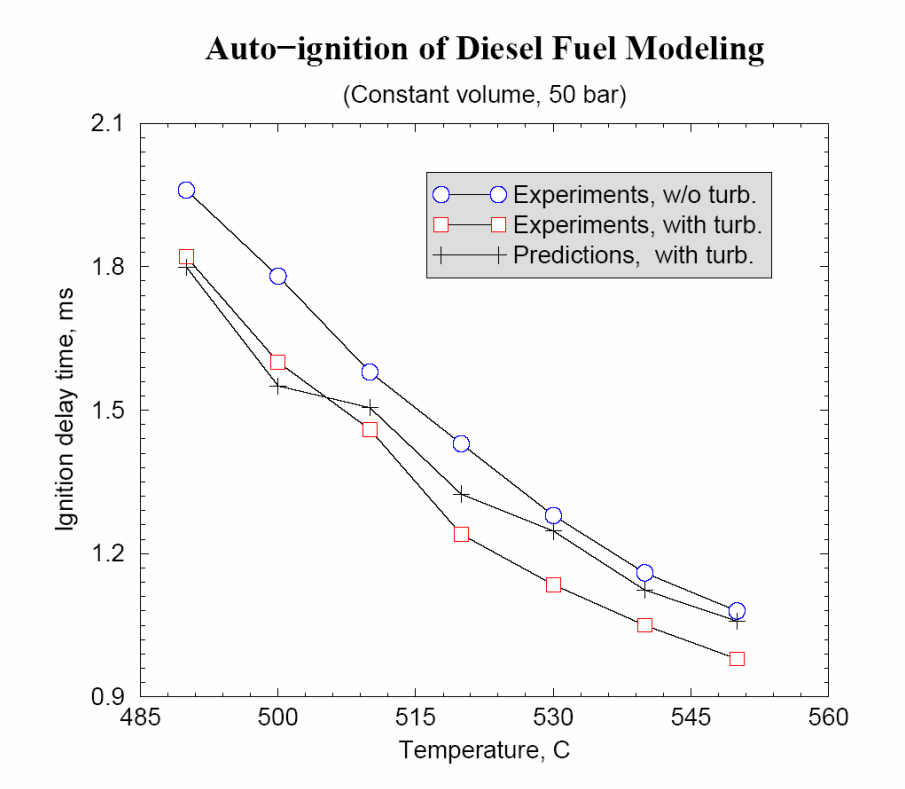

Figure 2.14. Calculated ignition delays for diesel fuel surrogate vs. experimental data on auto ignition of real diesel oil in the constant volume combustion chamber with the turbulence generator: P_0=50.0 bar, T_0=800 K, m_{inj}=6 mg, τ_{inj}=1.28 ms. **Golovitchev et al, 2003)**

2.5. Mixing Controlled Combustion

As noted in the previous sections, the mixture formation of evaporated fuel droplet and surrounding air plays a significant role on combustion process. Since the flow field in the internal combustion engines is highly turbulent, turbulence has direct influence on the mixture formation and thus combustion process. Therefore, an interaction model of turbulence and chemistry must be considered.

In order to describe this intricate process, there are numerous turbulent combustion models in the literature. With the introduction of the Eddy Break-Up model by Magnussen and Hjertager, it became possible to treat turbulent diffusion combustion in a successful manner. **(Magnussen,1976)**. Due to its simplicity and the lack of any other developed models, it is used widespread in most of the CFD codes. Actually, there are other models, have been derived, such as Flamelet Model, PDF (Probability Density Function), Lagrangian Approach and some modified versions of the Eddy Break-Up model. When it is necessary to use detailed chemistry approach, only the Lagrangian approach is convenient. Flamelet model assumes that the chemical time

scale is much smaller than turbulent time scale. Thus, turbulence and chemical reactions are separated via laminar flow approach; solution is tried to be reached in this manner. This approach is not applicable to diesel fuel spray, in which both fast and slow chemistry is of importance. Although, the PDF, theoretically, is the most correct approach, the intricacy of the model makes it untreatable in three dimensional applications with complex geometry.

The Partially Stirred Reactor concept, utilized in this study, is an extension of the eddy-break-up model. With this model, application to diesel fuel spray and complex chemistry becomes suitable.

From the viewpoint of numerical application of the turbulent combustion models, one must find out the chemical source term in the species continuity equation. Therefore, in the next sections, a special technique, so-called the Reference Species Technique as a standard in the KIVA code, will be presented to compute both the reaction rate and the characteristic chemical time. Then, the implementation of the PaSR model to the KIVA code will be dealt.

2.5.1. Reference Species Technique

In this method, the reactions are solved in a sequential manner and the species concentrations are updated after each reaction. The most important advantage of this method is applying the same algorithm to the whole reaction set without checking each reaction whether it is fast or slow. On the other hand, there is a risk of being driven to negative of the species. So, the most risky one in the reaction is determined and the computations based on this reference specie are carried out.

Let the elementary reactions be in the form of,

$$\nu_1 c_1 + \nu_2 c_2 \overset{k_f, k_b}{\Leftrightarrow} \nu_3 c_3 + \nu_4 c_4 \tag{2.5.1}$$

where ν_i is the stoichiometric reaction coefficient and c_i is the molar concentration. For simplicity, $\nu_i = 1$. (In detailed chemistry approach, it is usually 1.)

The rate equation of this reaction,

$$\frac{dc_1}{dt} = \frac{dc_2}{dt} = -\dot{\omega}, \quad \frac{dc_3}{dt} = \frac{dc_4}{dt} = \dot{\omega} \tag{2.5.2}$$

and the discretization of the forward reaction yields,

$$\frac{c_1^{n+1} - c_1^n}{\tau} = -\dot{\omega}^x \quad \Rightarrow \quad c_1^{n+1} = c_1^n - \tau\dot{\omega}^x \tag{2.5.3}$$

where x in the term, $\dot{\omega}^x$, determines the time level, i.e. x = n, n+1 or (n+1)/2

If x=n (c_1^n and $\dot{\omega}^n$ is known) and τ (timestep) is sufficiently large, it is obvious that the term, c_1^{n+1},in the Eq.(3.5.2) becomes negative. But, in the case of sufficiently large τ, $\dot{\omega}$ should tend to zero; that is, the concentrations will lead to achieve the equilibrium values.

$$c_1^{eq} = \left(\frac{k_b c_3 c_4}{k_f c_2} \right)^{eq} \tag{2.5.4}$$

Thus, at the x=n time level, there is no solution. To overcome this deficiency, the reaction is discretized in a semi-implicit manner. In this case, x=n+1 time level is used.

Differentiating $\dot{\omega}$ with respect to time yields

$$\frac{d\dot{\omega}}{dt} = k_f \left(\frac{dc_1}{dt} c_2 + c_1 \frac{dc_2}{dt} \right) - k_b \left(\frac{dc_3}{dt} c_4 + c_3 \frac{dc_4}{dt} \right) \tag{2.5.5}$$

Combining the equation (2.5.2) with equation above, one can get

$$\frac{d\dot{\omega}}{dt} = -\left(k_f \left(c_2 + c_1 \right) + k_b \left(c_4 + c_3 \right) \right) \dot{\omega} = -\alpha\dot{\omega} \tag{2.5.6}$$

$$\alpha = k_f \left(c_2 + c_1 \right) + k_b \left(c_4 + c_3 \right) \tag{2.5.7}$$

Discretizing equation (2.5.5) in a semi implicit manner gives

$$\frac{\dot{\omega}^{n+1} - \dot{\omega}^n}{\tau} = -\alpha^n \dot{\omega}^{n+1} \Rightarrow \dot{\omega}^{n+1} = \frac{\dot{\omega}^n}{1 + \alpha^n \tau} \tag{2.5.8}$$

If $\dot{\omega}^{n+1}$ is placed into the equation (2.5.2), new concentration is found as below:

$$c_1^{n+1} = c_1^n - \tau \frac{\dot{\omega}^n}{1+\alpha^n \tau} \quad \overset{\tau \to \infty}{\longrightarrow}$$
$$c_1^n - \frac{\dot{\omega}_n}{\alpha_n} = c_1^n - \left(\frac{k_f c_1 c_2 - k_b c_3 c_4}{k_f (c_1 + c_2) + k_b (c_3 + c_4)} \right)^n \tag{2.5.9}$$

When the timestep, τ, is sufficiently large to reach equilibrium, this new concentration equation does not satisfy with the equation (2.5.4), giving equilibrium concentration. In this case, the reference species is defined as the species most in danger of being driven negative.

Thus, it is the species which is being consumed by the reaction and has the lowest concentration.

Let the reference species (c_r) be c_1, then $c_2 > c_1$. Assuming the term, $k_f c_2$, is larger than the other terms gives

$$k_f c_1 << k_f c_2,\ k_b c_3,\ k_b c_4 \qquad \Rightarrow \qquad \alpha^n \approx (k_f c_2)^n \tag{2.5.10}$$

When the new expression for α^n is evaluated in Eq.(2.5.7), and in the case of sufficiently large timestep, equilibrium concentrations can be achieved.

$$c_1^{n+1} = c_1^n - \tau \frac{\dot{\omega}^n}{1+\alpha^n \tau} \quad \overset{\tau \to \infty}{\longrightarrow}$$
$$c_1^n - \frac{\dot{\omega}_n}{\alpha_n} = c_1^n - \left(\frac{k_f c_1 c_2 - k_b c_3 c_4}{k_f c_2} \right)^n = \left(\frac{k_b c_3 c_4}{k_f c_2} \right)^n \tag{2.5.11}$$

In this way, the equilibrium condition for each reaction can be ensured with the same algorithm.

Moreover, the reference species technique can be utilized to determine the characteristic chemical time, which is of great importance in the modeling of turbulence-chemistry interaction, e.g. PaSR, and the other extensions of the EBU models.

The chemical reaction times are formally defined as characteristic times of the destruction rates, if the species chemical production rates are presented as a sum of creation and destruction terms. Thus, destruction rates can be expressed as

$-k_f c_i c_k \approx -c_i / \tau_{c,i} \approx -c_k / \tau_{c,k}$ where i,k represent species indices. If the reference specie is determined, characteristic chemical time can be determined by using this specie.

Let the source term in the species continuity equation be expressed as:

$$\begin{aligned} f_m(c) &= \sum_{r=1}^{Nr} (\vartheta''_{mr} - \vartheta'_{mr}) \left(k_f^r \prod_{s=1}^{Ns} c_s^{\vartheta'_{sr}} - k_b^r \prod_{s=1}^{Ns} c_s^{\vartheta''_{sr}} \right) \\ &= M_m \sum_{r=1}^{Nr} \left(\vartheta''_{mr} k_f^r \prod_{s=1}^{Ns} c_s^{\vartheta'_{sr}} + \vartheta'_{mr} k_b^r \prod_{s=1}^{Ns} c_s^{\vartheta''_{sr}} \right) \\ &- M_m \sum_{r=1}^{Nr} \left(\vartheta''_{mr} k_b^r \prod_{s=1}^{Ns} c_s^{\vartheta''_{sr}} + \vartheta'_{mr} k_f^r \prod_{s=1}^{Ns} c_s^{\vartheta'_{sr}} \right) \\ &= \sum_{r=1}^{Nr} \left(\xi_1^r - \xi_2^r \right) = term1 - term2 \end{aligned} \tag{2.5.12}$$

Linearizing the equation above around c_r gives,

$$f_m(c) = term1^0 - term2^0 \frac{c_r^1}{c_{r0}} \tag{2.5.13}$$

$term1^0 \; and \; term2^0$ are held constant. Differentiating the Eq.(2.5.12) with respect to time yields

$$\frac{df_m(c)}{dt} = -\frac{(term2)^0}{c_r^0} \frac{dc_r}{dt} = -\frac{(term2)^0}{c_r^0} f_m(c) \tag{2.5.14}$$

Discretizing in a semi-implicit manner gives

$$\frac{df_m(c)}{dt} = \frac{f^1 - f^0}{\tau} = -\frac{(term2)^0}{c_r^0} f^1 \tag{2.5.15}$$

After some manipulations, both the reaction rate at the next time step and chemical time can be found.

$$f^1 = \frac{f^0}{c_r^0 + (term2)^0 \tau} c_r^0 = -\frac{1}{\tau_c} c_r^0, \quad \tau_c = -\frac{c_r^0 + (term2)^0 \tau}{f^0} \tag{2.5.16}$$

By using this reference species technique, one can utilize the findings above, i.e. chemical source term, reaction rates and chemical time, just in the case of laminar chemistry. Therefore, it is not suitable in the internal combustion engines, in which, a high level of turbulence is available. In the next section, of the turbulence/chemistry interaction model, the implementation of the Partially Stirred Reactor model will be presented.

2.5.2. Partially Stirred Reactor Model

In this model, each computational cell is divided into two zones. One of these zones is considered as a perfectly stirred reactor, and thus all the reactions occur within this zone, whereas, there is no reaction in the other zone.

Three molar concentrations are considered in this model. (see Figure 2.15)

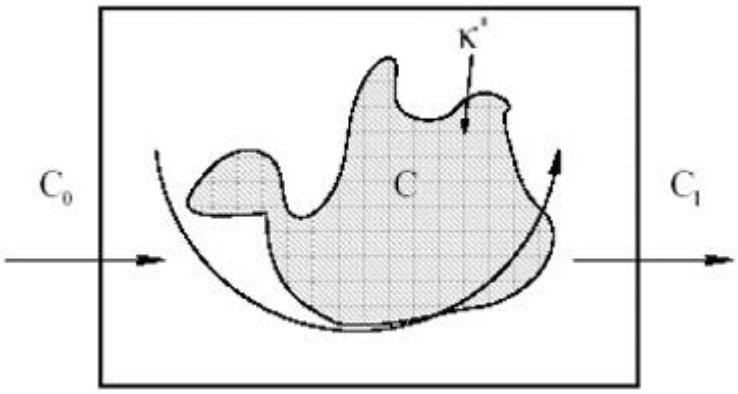

Figure 2.15. Schematic illustration of the PaSR model

c_0: initial average concentration

c: unknown concentration at the reactive zone

c_1: time averaged value of reactor exit concentration

$c_0(1-\kappa^*)$ represents the concentration in the non-reactive zone, and the concentration in the reactive zone can be expressed as $c\kappa^*$ .Thus, Reactor exit concentration can be calculated via conservation of mass in the following manner.

$$c_1 = \kappa * c + (1 - \kappa *) c_0 \tag{2.5.17}$$

where κ^* is the volume fraction of the reacting mixture. The relationship between these processes can be examined by a model based on linear interpolation. (see, Figure.2.16)

Because, the combustion process in the reactor proceeds in parallel; that is, reaction and mixing processes realizes in the same time. So, one can write,

$$\frac{c_1 - c_0}{\tau} = \frac{c - c_1}{\tau_{mix}} = f_m(c) = -\frac{c}{\tau_c} \tag{2.5.18}$$

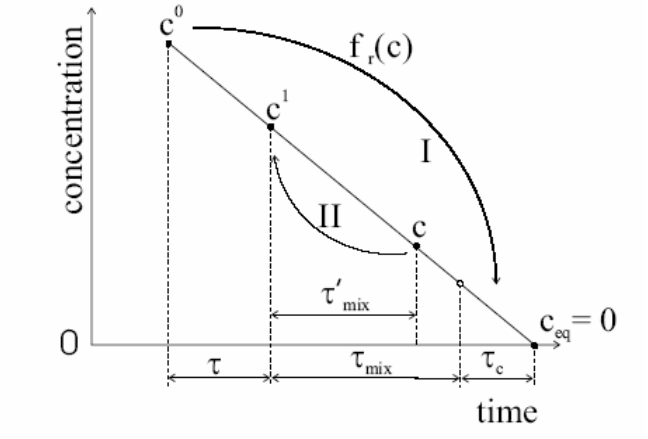

Figure 2.16. Reaction and mixing processes

By using Eq.(2.5.17) and (2.5.18), κ^* is obtained.

$$c_1 = \kappa * c + (1 - \kappa *) c_0, \qquad \kappa * = \frac{\tau}{\tau + \tau_{mix}} \tag{2.5.19}$$

Now, term c is required to use in calculation of c_1. Using Taylor expansion yields

$$f_m(c) = f_m(c_1) + \frac{\partial f_m}{\partial c}(c - c_1) + \frac{1}{2}\frac{\partial^2 f}{\partial c^2}(c - c_1)^2 \tag{2.5.20}$$

Assuming that the dominant term is $\partial f_m / \partial c_r$ and ignoring the higher order derivatives, i.e. $\partial^2 f / \partial c^2 = 0$, chemical time is calculated by the following formula: (using reference species technique, Section 2.5.1)

$$\frac{1}{\tau_c} = -\frac{\partial f_m}{\partial c_r} \tag{2.5.21}$$

Thus, Equation (2.5.20) turns into:

$$f_m(c) = f_m(c_1) - \frac{c - c_1}{\tau_c} \tag{2.5.22}$$

Eliminating the term, c, with Eq.(2.5.19) and after some manipulations,

$$\frac{c_1 - c_0}{\tau} = f_m(c) = f_m(c_1) - \frac{1}{\tau_c}\left[\left(\frac{c_1}{\kappa^*} - \frac{1-\kappa^*}{\kappa^*}c_0\right) - c_1\right] \tag{2.5.23}$$

$$\begin{aligned}\frac{c_1 - c_0}{\tau} = f_m(c) &= f_m(c_1) - \frac{1}{\tau_c \kappa^*}\left(c_1 - \kappa^* c_1 - (1-\kappa^*)c_0\right) \\ &= f_m(c_1) - \frac{1-\kappa^*}{\tau_c \kappa^*}(c_1 - c_0)\end{aligned} \tag{2.5.24}$$

$$\left(\frac{1}{\tau} + \frac{1-\kappa^*}{\tau_c \kappa^*}\right)(c_1 - c_0) = f_m(c_1) \tag{2.5.25}$$

$$\left(\frac{1}{\tau} + \frac{1-\kappa^*}{\tau_c \kappa^*}\right)(c_1 - c_0) = \frac{c_1 - c_0}{\tau}\frac{\tau_c + \tau_{mix}}{\tau_c} = f_m(c_1) \tag{2.5.26}$$

we obtain the expression below:

$$\frac{c_1 - c_0}{\tau} = \kappa\ f_m(c_1), \qquad \kappa = \frac{\tau_c}{\tau_c + \tau_{mix}} \tag{2.5.27}$$

And final result can be summarized as:

$$f_m(c) = \kappa\ f_m(c_1) \tag{2.5.28}$$

In this way, the influence of the turbulence on the micro-mixing process has been coupled with the chemical source term.

In implementing this PaSR concept to the modeling software, KIVA, a relationship is required between the solution technique of KIVA and the PaSR model. Let's

consider the Eq. (2.5.16), obtained in the section 2.5.1, explaining the Reference Species Technique.

$$\frac{c^1 - c^0}{\tau} = f_m(c^1) = \frac{f^0 c_r^0}{c_r^0 + (terim2)^0 \tau}, \qquad \tau_c = -\frac{c_r^0 + (term2)^0 \tau}{f^0} \tag{2.5.29}$$

When the expressions above, τ_c and $f_m(c^1)$, are substituted with the values in the equation below:

$$\frac{c^1 - c^0}{\tau} = \kappa\, f_m(c^1) = \frac{\tau_c}{\tau_c + \tau_{mix}} f_m(c^1) = \frac{f^0 c_r^0}{c_r^0 + (terim2)^0 (\tau + \tau_{mix})} \tag{2.5.30}$$

By comparing the Eq. (2.5.29) and (2.5.30), it can be said that they coincide with each other. In the first one, the whole cell can be considered as a well-stirred reactor, and thus total combustion time is τ. The latter is the case of including the mixing effects of the turbulence to the chemistry. So, this time, total combustion time is $\tau + \tau_{mix}$.

There is a wide range of scales in turbulent flows, from the largest eddies down to the molecular level, and in order to account for all these different scales, using only one characteristic value is a great simplification. Therefore, the correct definition of the micro-mixing time is a matter of importance for any EBU models.

In a study by Kjäldman, three different options for definition of τ_{mix} were investigated. They were related to:

Kolmogorov time scale:

$$\tau_k \sim (\nu / \varepsilon)^{1/2} \tag{2.5.31}$$

Taylor time scale:

$$\tau_t \sim k / \varepsilon \tag{2.5.32}$$

and a geometric mean of Kolmogorov and Taylor scales:

$$\tau_{kc} \sim \sqrt{\tau_t \tau_k} \tag{2.5.33}$$

Kjäldman also reported that best results were obtained using the Taylor scale. **(Kjäldman,2000)**

Furthermore, a generalized micro-mixing time definition, proposed by Golovitchev, is given below:

$$\tau_{mix} = \left(\frac{k}{\varepsilon}\right) \cdot \left(\frac{c_\mu}{\mathrm{Re}_t}\right)^{\frac{1-\alpha}{2}} \tag{2.5.34}$$

where $\alpha = \frac{3(D-3)}{1+D}$.

In this equation, a typical $\mathrm{Re}_t = 10^3$ case, $c_\mu = 0.09$ (k-ε turbulence model coefficient) are selected. Thus, in the case of D=3, the generalized equation gives Kolmogorov time scale ($\tau_{mix} \sim 0.001\, k/\varepsilon$). When D=5 is chosen, the generalized equation corresponds to Taylor time scale ($\tau_{mix} \sim k/\varepsilon$).

If the RNG k-ε turbulence model is employed, the micro-mixing time is defined as below:

$$\tau_{mix} = \left(2\sqrt{c_\mu}\,\frac{k}{\varepsilon}\,\tau_k\right)^{1/2} \tag{2.5.35}$$

Golovitchev states that the above expression formally corresponds to D=3.8 ($\tau_{mix} \sim 0.1\, k/\varepsilon$) in the generalized equation giving only a provisional value for τ_{mix} that must be refined in comparisons with experiments. **(Golovitchev,2003)**

Another approach developed is based on the usage of Kolmogorov expression ($\tau_k \sim (\nu/\varepsilon)^{1/2}$) for the micro-mixing time with the molecular viscosity replaced by a fraction of the effective viscosity assumed to be responsible for micro-mixing. For example, in terms of the k-ε model, the micro-mixing time is defined as

$$\tau_{mix} = (\nu_{eff} / \varepsilon)^{1/2} = \left(c_\mu k^2 / \varepsilon \cdot \varepsilon\right)^{1/2} = 0.3\, k / \varepsilon \qquad (2.5.36)$$

Therefore, it is seen that the model constant, C_{mix} ($\tau_{mix} = C_{mix} \frac{k}{\varepsilon}$), varies between 0.001-0.3, depending on the flow. In this study, RNG k-ε turbulence model and $\tau_{mix} \sim 0.1\, k / \varepsilon$ case have been employed.

2.7. Pollutant Emission Modeling

In the ideal case, the complete combustion of a hydrocarbon fuel with stoichiometric air yields carbon dioxide (CO_2), water (H_2O) and molecular nitrogen (N_2). In internal combustion engines, all chemical reactions are bidirectional, occur with finite rate and complete combustion can never be realized. Thus, at least a small amount of reactants will remain in the product side. However, in the combustion chamber, mixture distribution, temperature and turbulence level are often non-homogeneous or not ideal. Therefore, those may lead flame extinction and subsequent unburned and partially burned species, or the formation of compounds such as soot, NOx etc.

As a consequence, in the exhaust gases of combustion engines, there always exist additional compounds compared to the complete combustion case. Some of the major compounds are carbon monoxide, unburned hydrocarbons, nitrogen oxides and soot.

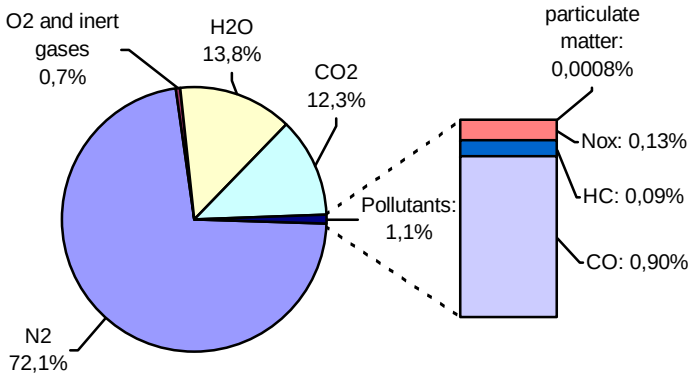

(a)

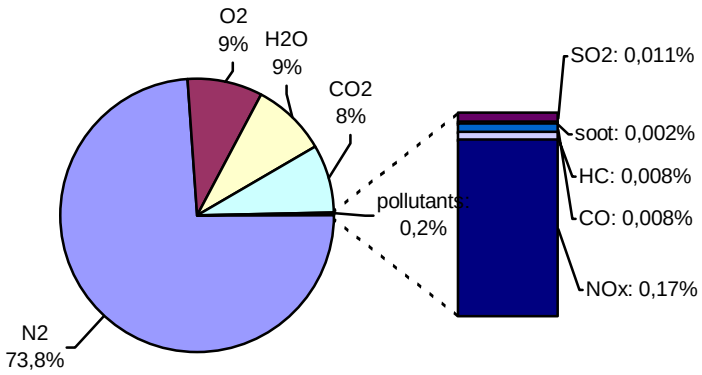

(b)

Figure 2.17 Engine-out exhaust emissions (volume fractions). a) SI engine, b) Diesel engine **(Stiesch, 2003)**

Typical exhaust emissions of both SI and Diesel engines are depicted in Figure 2.17, above. In SI engines, the volume fraction of the pollutants are around %1 and in Diesel engines it is even less. Thus, from the viewpoint of thermodynamics, they do not have a noticeable effect on the total amount of heat released. As for human health and environmental concerns, even small concentrations in the ppm range can be of great significance.

As pollutants of SI engine (see Figure 2.17) are considered, it is seen that the major compounds are CO,HC and NOx. A three way catalyic converter can be used efficiently as an exhaust aftertreatment method. As to the diesel engine, NOx and soot are the major challenges. SCR (Selective Catalytic converter) and DPF (Diesel Particle Filter) can be utilized to reduce NOx and soot levels respectively.

From the point of view of mathematical modeling, in general, NOx and soot mechanisms are great of importance. In the next sections, these pollutants will be dealt.

2.7.1. Formation of Nitric Oxides

Scientific findings state that NOx is a major contributor of photochemical smog and ozone in the urban air. Furthermore, NOx participates in a chain reaction that removes ozone from the stratosphere because of increased ultraviolet radiation reaching the earth's surface. **(Warnatz, 1996)** Considering its negative effect on human health and environment, minimization of NOx production becomes one of the most important topics in combustion.

Four different mechanisms are considered in the formation of NOx: thermal NO, prompt NO, N_2O intermediate, fuel NO.

2.7.1.1. Thermal NO

Thermal NO or Zeldovich NO is formed by the elementary reactions: **(Miller&Bowman, 1989)**

$$N + NO \rightarrow O + N_2 \qquad k_{1f} = 3.3x10^{12}\ T^{0.3} \qquad (2.7.1)$$

$$N + O_2 \rightarrow NO + O \qquad k_{2f} = 6.4x10^{9}\ T \exp(-3160/T) \qquad (2.7.2)$$

$$N + OH \rightarrow NO + H \qquad k_{3f} = 3.8x10^{13} \qquad (2.7.3)$$

The name thermal is used, because the reaction (2.7.1) has a very high activation energy due to strong triple bond in the N_2 molecule, and is thus sufficiently fast only at high temperatures. Because of its small rate, the reaction (2.7.1) is the rate limiting step of the thermal NO formation.

2.7.1.2. Prompt NO

The mechanism of prompt or Fenimore NO was postulated by C.P.Fenimore. Prompt NO is formed directly within the reaction zone. The additional mechanism that is promptly producing NO at the flame front is more complicated than thermal NO, because the prompt NO results from the radical CH, which was previously considered to be an unimportant transient species that is generated through a complex reaction scheme

2.7.1.3. NO Generated via Nitrous Oxide

The nitrous oxide mechanism is analogous to the thermal mechanism in that O atom attacks molecular nitrogen. However, with the presence of a third molecule M, the outcome of this reaction is N_2O

$$N_2+O+M->N_2O+M \qquad (2.7.4)$$

The N_2O may subsequently react with O atoms to form NO

$$N_2O+O->NO+NO \qquad (2.7.5)$$

This reaction has been overlooked since it usually is a insignificant contributor to the total NO. However, lean conditions can suppress the formation of CH, hence lead to less Fenimore NO, and low temperatures can suppress the Zeldovich-NO. What

remains is NO generated via N_2O, which is promoted at high pressures because of the three body reaction ad typical for three body reactions, has a low activation energy so that low temperatures do not penalize this reaction as much as they do the Zeldovich-NO reaction. All of these circumstances lead to the N_2O route being the major source of NO in lean premixed combustion in turbines.

2.7.1.4. Conversion of Fuel Nitrogen into NO

The conversion of fuel-nitrogen into NO is mainly observed in coal combustion. The nitrogen-containing compounds evaporate during the gasification process and lead to NO formation in the gas phase.

2.7.2. Formation of Soot

It is widely accepted that the formation of soot is leaded by the further growth of the PAH (Polycyclic aromatic hydrocarbon). In the next sections; first, the formation of PAH is considered, then phenomenology of soot is given. The latter is about modeling considerations.

2.7.2.1. PAH Formation:

In the case of no extinction, the fuel is completely broken down to C_1- and C_2-hydrocarbons. Thus, higher hydrocarbons have to be formed from these smaller hydrocarbon fragments.

With respect to soot formation, the most important class of higher hydrocarbons is that of PAH. These are usually formed under fuel-rich conditions. However, acetylene (C_2H_2), which is formed in high amounts under rich conditions, is the most important precursor of higher hydrocarbons.

The first aromatic ring is formed by the reaction of CH or CH_2 with C_2H_2 to C_3H_3. Two C_3H_3 radicals may then perform a self reaction and, after rearrangement of H_2 atoms, lead to the first aromatic ring (C_6H_6).

After the initial formation of single aromatic rings, the so-called HACA sequence (H abstraction, C_2H_2 addition) leads to the growth of the PAH molecule. (see Figure 2.18) In addition, single aromatic rings can directly combine to form more complex aromatic structures.

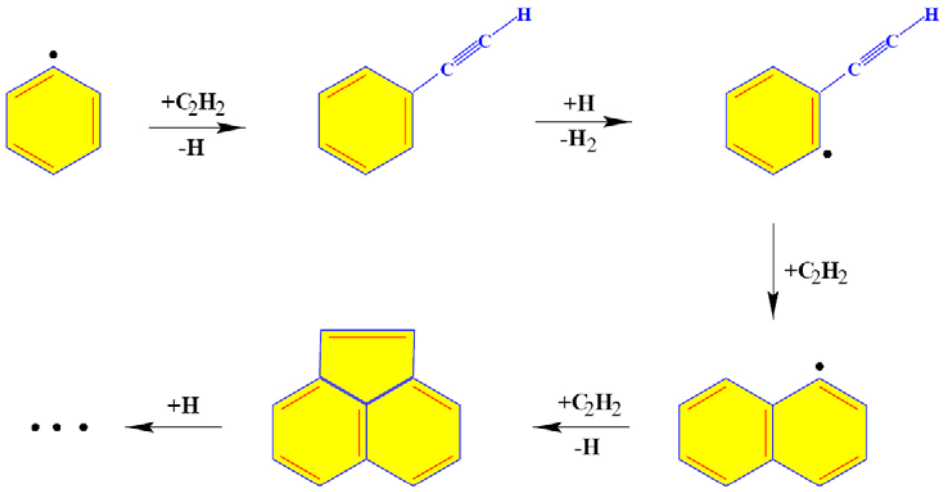

Figure 2.18. PAH growth by the HACA sequence: H abstraction and acetylene addition

2.7.2.3. Phenomenology of soot

Formation of soot includes a number of processes: The first step is the growth of the PAH. Typically, they are called as PAH as long as the molecules are arranged in a two dimensional structure. Once they extend into three dimensional space, they are referred to as particles (particle inception or nucleation). The particles are then subject to surface growth by addition of mainly acetylene, and they further increase in size by coagulation. During the entire process hydrogen is continuously abstracted, thus the resulting soot particles have a very high carbon fraction.

Typical of soot formation is the bell-shaped temperature dependence which is caused by two facts: Soot formation needs radicalic precursors (like C_3H_3) and, thus does not occur at low temperatures. Furthermore, soot precursors are pyrolized and oxidized at elevated temperatures so that the soot formation is limited to a temperature range between 1000 K and 2000 K.

Typically, at least 90% and often up to 99% of the formed soot is oxidized, thus, in the exhaust gas, soot concentration occupies only a small fraction. This represents a numerical problem in computing engine-out soot emissions. Since soot concentration is the difference of two models, i.e. formation and oxidation, relative error becomes significant.

2.7.2.4. Semi-Global Mechanisms:

The simplest approach to model soot formation and oxidation is based on two global steps by Hiroyasu. Change of the soot mass or the soot mass balance is given by:

$$\frac{dm_s}{dt} = \frac{dm_{s,f}}{dt} - \frac{dm_{s,ox}}{dt} \tag{2.7.6}$$

where the first term and the second term on the right hand side denote the rates of soot formation and oxidation, respectively.

$$\frac{dm_{s,f}}{dt} = A_f m_{f,v} p^{0.5} \exp\left[-\frac{E_{s,f}}{RT}\right] \tag{2.7.7}$$

$$\frac{dm_{s,ox}}{dt} = A_{ox} m_s \frac{p_{02}}{p} p^{1.8} \exp\left[-\frac{E_{s,ox}}{RT}\right] \tag{2.7.8}$$

Here; $m_{f,v}$ denotes mass of vaporized fuel, m_s is the soot mass. $E_{s,f} = 52{,}335\ kJ/kmol$ and $E_{s,ox} = 58{,}615\ kJ/kmol$. A_f and A_{ox} need to be adjusted in order to reproduce experimentally determined soot emissions of a particular engine.

In many engine studies to estimate soot emissions, the soot balance and formation equations (Eq.(2.7.6). and (2.7.7)) are used, but the oxidation rate is replaced by an approach suggested by Nagle and Strickland-Constable.

A more detailed but still quasi-global mechanism, proposed by **Fusco (1994)**, is composed of eight reaction steps. Methodology is: (Depicted in Figure 2.19) Vaporized fuel can be converted by pyrolysis into either a generic precursor radical species (1) or into a surface growth species (2), which is assumed to by C_2H_2 . Both intermediate species can either be oxidized directly. (3,4), or they can contribute to the formation of soot. Inception of soot particles occur from the precursor radicals (5), and the growth species leads to an increase in the size of individual particles (6). Finally, the existing soot particle are either oxidized into inert products again (7), or they are subject to coagulation. (8)

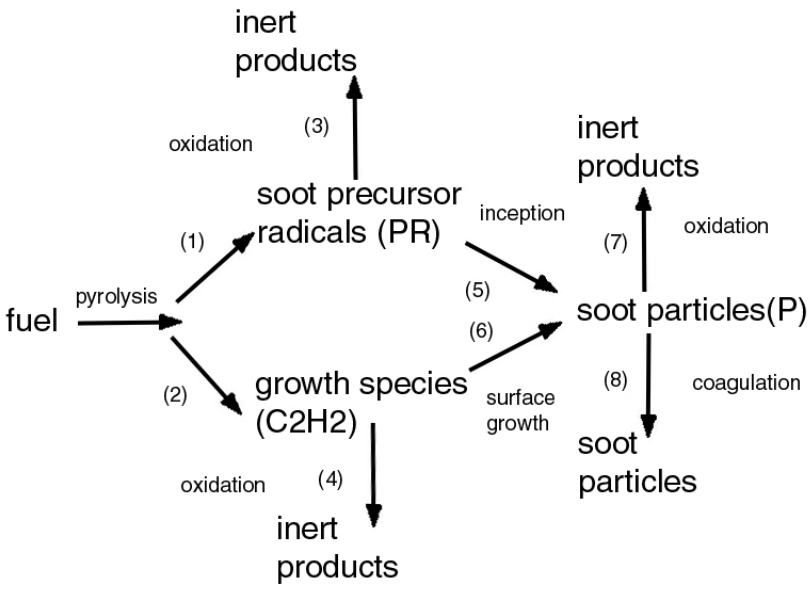

Figure 2.19. Schematic illustration of the 8 step soot mechanism**. (Fusco,1994)**

In this study, detailed chemistry approach has been utilized to consider soot formation and oxidation modeling. Proposed mechanism **(by Golovitchev,2000)** consists of the formation of main sooting agent acetylene and other generic soot precursors, such as polyynes and PAH. The soot formation mechanism consists of series of elementary reaction steps leading from acetylene and hydrogen to the formation of the first aromatic ring, A_1. Reaction steps leading to the formation of the phenyl, $\dot{A}_1$, radical and the first aromatic ring are followed by the successive stages of H abstraction, C_2H_2 addition (see, HACA sequence), thus, yielding a chain of aromatic rings. When this HACA sequence is included in the mechanism, it is possible to describe higher order PAHs. Reaction paths to higher rings are similar as below:

$$A_i + H \rightarrow \dot{A}_i + H_2$$
$$\dot{A}_i + C_2H_2 \rightarrow \dot{A}_iC_2H_2$$
$$\dot{A}_iC_2H_2 + H \rightarrow \dot{A}_iC_2H + H_2$$
$$\dot{A}_iC_2H + C_2H_2 \rightarrow A_{i+1}$$

where A_{i+1} is a higher ring, dot sign labels the corresponding radical.

The incipient soot was formed from long-chain acetylene C_4H_2, and acenaphtylene due to graphitization processes.

$$C_6H_2 \rightarrow H_2 + 6C(s)$$
$$A_2R_5 \rightarrow 4H_2 + 12C(s)$$

Oxidation rates of soot are similar to those of the Nagle-Strickland-Constable approach. Since the contribution of O_2 to the oxidation of soot is not sufficient, in the proposed mechanism there also exist soot oxidation by the OH and HO_2 radicals and NO molecule. The details of the mechanism development and validation can be found in **Gustavsson and Golovitchev (2003).**

CHAPTER 3

COMPUTATIONS

3.1. An overview of modeling software

The KIVA-3V computer program solves numerically the conservation laws for unsteady, three dimensional, turbulent, chemically reacting flows of multi-component mixture of ideal gases, coupled to the equations for single component vaporizing fuel sprays. The effects due to presence of droplets and chemical reactions are accounted for via appropriate source terms in the gas-phase equations.

Turbulence modeling is based on the RNG k-ε turbulence model which can be reduced to conventional and grid sub-scale (SGS) sub-models modified to include the effects of droplets.

The gas-phase solution procedure is based on the arbitrary Lagrangian-Eulerian (ALE) finite volume method which offers the flexibility to combine computations in a moving frame of reference with the solution procedure for a fixed mesh volume. A generalized mesh of the ALE type provides a great deal of geometrical flexibility. It allows a convenient direct representation of curved and moving boundaries, such as moving cupped piston. In general, the cells need not to be square or rectangle, so a variety of different geometries can be represented.

The valves are treated as solid objects that move through the mesh using a method, so-called the snapper technique used for piston motion as well.

The spray computations are based on a Monte Carlo based discrete-particle technique, in which each computational particle represents some number of droplets of identical size, velocity, temperature, and surface deformation rate. Besides the particle-turbulent gas interactions, the effects of droplet collisions, breakups and evaporation are accounted for.

The spray source terms are constructed by integrating the rates of change of mass, momentum and energy over all droplets at given position and time. The droplet evolution is governed by the probability density function which describes the volume specific droplet number density in a specific parameter space characterized by droplet coordinates, velocity, radius, temperature, droplet distortion and rate of distortion from a spherical shape.

Collision between two parcels occurs when they occupy the same computational cell and the probability for the collision is higher than a threshold value based on collision frequency.

The droplet breakup due to the aerodynamic forces is governed by the droplet distortion parameters which follow the Taylor analogy breakup model, TAB.

The change in the droplet radius due to evaporation is described by the quasi d^2- law. The initial droplet radii follow either a mono-disperse or a χ-squared distribution governed by the Sauter mean radius.

Chemical reactions are treated by a procedure that distinguishes between slow reactions, which proceed kinetically, and fast reactions, which are assumed to be in equilibrium. Chemical rate expressions for the kinetic reactions are evaluated by the reference species technique. The rate coefficients are assumed to be of a generalized Arrhenius form. The equilibrium reactions are solved iteratively. To take into account the turbulence-chemistry interaction, M-H (Magnussen-Hijertager) model is optional as well.

3.1.1. Numerical Scheme of KIVA

KIVA3V uses arbitrary hexahedrons to divide the main volume into sub-volumes and solves the equations via finite volume method. The equations are discretized both in time and space. In Figure 3.1, a typical cell is shown.

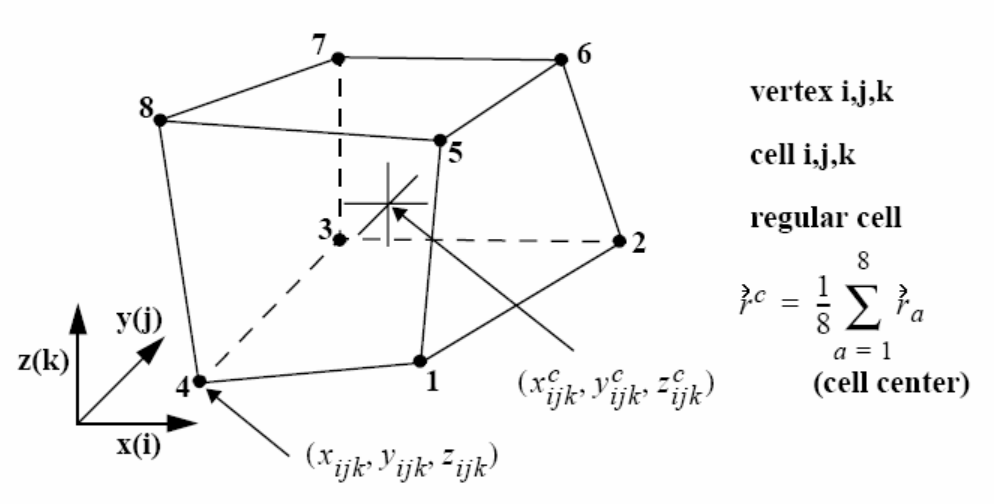

Figure 3.1. Typical cell layout in KIVA-3V

The spray and the fluid phase equations are solved in three phases respectively: A, B and C. The three phases are summarized in Table 3.1.

Phase A

In this phase; spray droplet collision and oscillation/break-up terms ($\dot{f}_{coll}$, $\dot{f}_{bu}$) and, mass and energy source terms due to the chemistry and spray ($\dot{\rho}_m^c, \dot{\rho}^s, \vec{F}^s, \dot{Q}^c \text{ and } \dot{Q}^s$) are calculated.

Phase B

In Phase B, KIVA3V solves the governing equations in a coupled, implicit fashion with individual equations solved by the conjugate residual method. In general the procedure is very similar to the SIMPLE scheme. Δt is determined on accuracy, not stability. Acoustic mode terms (namely the pressure gradient in the momentum equations and velocity dilatation terms in mass and energy equations), the spray momentum source term, diffusion terms (mass, momentum, energy) and the remaining source terms in the turbulence equations are calculated in this phase.

Phase C

The flow field is frozen and rezoned or remapped onto a new computational mesh. The connective transport associated with the moving mesh relative to the fluid. Convective terms are calculated by QSOU (Quasi Second Order Upwind) or PDC (Partial Donor Cell) methods. This is accomplished in a sub-cycled, fully explicit fashion. Δt_c is determined based on stability.

Table 3.1. Three phases overview including the sub-routines used

Initialization	Read input data Grid generation Calculate gas viscosity Initialize time step, piston velocity	begin.f, rinput.f, setup.f, timstp.f, newcyc.f
Phase A	Spray modeling (fuel injection, drop breakup, collision, evaporation…) Combustion chemistry Emission modeling Mass and energy contribution due to spray and combustion	inject.f, pmovtv.f, atomize.f, colide.f, evap.f, lawall.f, chem.f, pmom.f, pcoupl.f, repack.f
Phase B	Fluid phase calculation, Mass, momentum, velocity, temperature, pressure, turbulence properties (Implicit solver, iterations) Update droplet velocity	ysolve.f, exdif.f, vsolve.f, tsolve.f, psolve.f, pgrad.f, kesolve.f, paccel.f
Phase C	Rezoning grids Remapping fluid properties to new grids Update cell properties	Rezone.f, volume.f, ccflux.f, momflux.f, chop.f, state.f

3.1.2. Physical boundary Condition of KIVA

Options of KIVA to determine physical boundary conditions are listed below in Table 3.2.

Table 3.2. Boundary conditions in KIVA3V

(1)- Physical Boundary Conditions:
(I) Rigid Wall (a) No-slip
(b) Free-slip
(c) L-O-W
(d) Fixed Temperature
(e) Adiabatic
(II) Periodic
(III) Spray Injector
(2) Boundary/Initial Conditions for the Spray Equation
(For the spray droplets and the walls)
(3) Numerical Boundary Conditions:
(I) Velocity Inflow/Outflow
(II) Pressure Inflow/Outflow

3.1.3 Modifications to KIVA 3-V rel.2

An accurate spray model is crucial for diesel engine modeling. The spray model to simulate the atomization and breakup processes in standard KIVA-3V is the Taylor Analogy Breakup (TAB) model. An alternative model is that of Reitz, which considers the unstable growth of Kelvin-Helmholtz waves on a liquid surface to describe the breakup details of the injected liquid blobs. The KHRT spray model has been used to replace the TAB model in KIVA-3V for diesel spray modeling. (See Section 2.3.4)

In the standard KIVA code, the kinetic reactions are constituted by one global reaction and extended Zeldovich reactions. The equilibrium reactions are as below:

$$H_2 \Leftrightarrow 2H$$
$$O_2 \Leftrightarrow 2O$$
$$N_2 \Leftrightarrow 2N$$
$$O_2 + H_2 \Leftrightarrow 2OH$$
$$O_2 + 2H_2O \Leftrightarrow 4OH$$
$$O_2 + 2CO \Leftrightarrow 2CO_2$$

And, turbulence chemistry interaction is modeled by Magnussen-Hijertager EBU model, which is only applicable to global reactions.

Diesel fuel surrogate model, which comprises reduced mechanism of n-heptane and toluene mixture with the ratio of 70/30% respectively, has been replaced to single step global reaction set of standard KIVA. This complex chemistry approach, accounting tri-molecular reactions and third body influence, has been used both ignition modeling and combustion process. For turbulence chemistry interaction, PaSR model of the Chalmers University of Technology, applicable to the whole reaction set, has been utilized in the code.

3.2. The Specifications of Ford-Otosan Ecotorq Engine

Ford Otosan has developed a new heavy-duty Diesel engine, Ecotorq, for the new Ford Cargo Trucks (See Figure 3.2). In this work, they improved Dovertech, the predecessor of this engine, and replaced with the new one, named Ecotorq, to comply with the market demands with respect to higher power, higher durability, lower cost of ownership and lower noise level, to meet future emission limits and to offer a competitive product. **(San et al, 2004).**

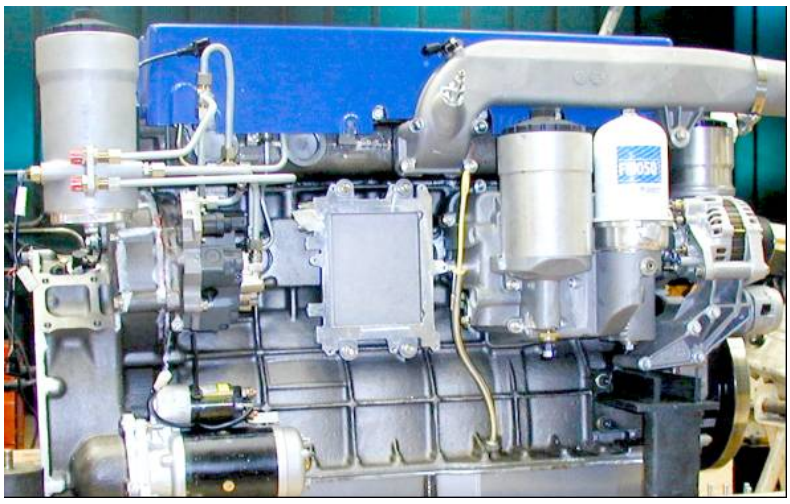

Figure.3.2. Photogragh of Ford Ecotorq engine

The engine is 7.3 liters, 6-cylinder in-line, with common rail fuel injection system and overhead cam shaft design with 4 valves per cylinder. The main specifications of the engine is given in Table 3.3.

Table.3.3.. The main specifications of Ford Ecotorq engine

No of cylinders	6	Idle rpm	600 rpm
Bore	112 mm	Max. rpm	3150 rpm
Stroke	124 mm	Injection Sys.	Common Rail
Displacement	7330 cm^3	Inlet Valve Open	280 BTDC
Comp. Ratio	17,4:1	Inlet Valve Close	420 ABDC
Max. Power	220,7 kW (2200 rpm)	Exhaust Valve Open	590 BBDC
Max. Torque	750 Nm (1495 rpm)	Exhaust Valve Close	270 ATDC

One of the most important part of the engine is the piston geometry, which plays a crucial role in generating air motions and strongly drives subsequent fuel-air mixing process. In Figure 3.3. (a and b), technical drawing of the piston geometry is shown.

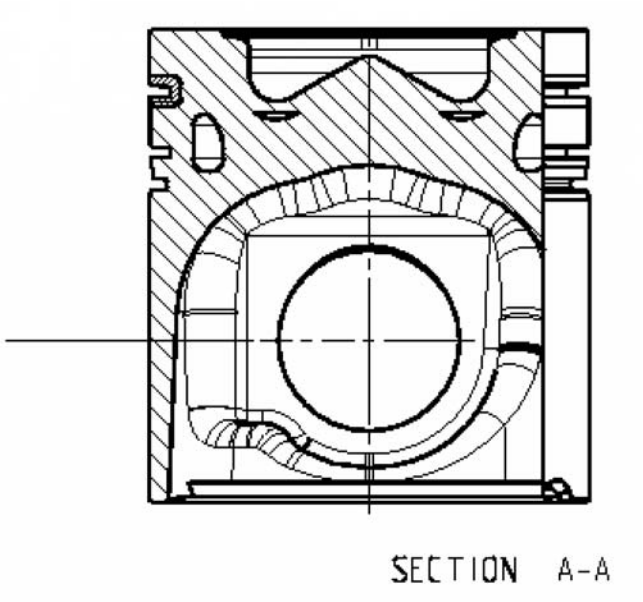

(a)

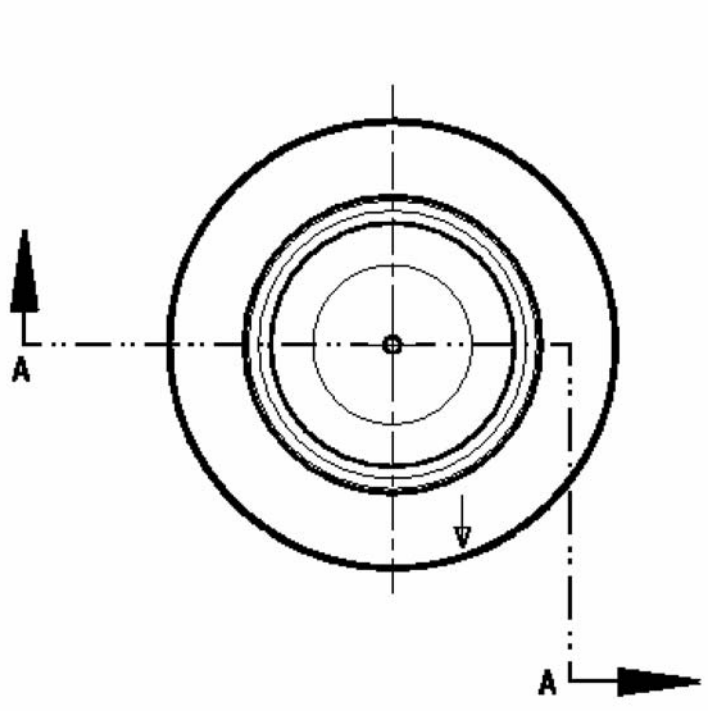

(b)

Figure 3.3 (a),(b) Technical drawing of the piston geometry.

3.3. Modeling Inputs

Since the simulation starts at inlet valve closure and ends at exhaust valve open, i.e. the case both valves are closed, only in-cylinder volume is considered to build computational mesh. Moreover, it is advantageous to utilize sector mesh in computations due to the symmetry of the multiple hole injector with respect to computational expenditure. In this way, sector mesh of the geometry corresponds to only one nozzle of the injector.

Two possible ways of generating mesh: One is using standard preprocessor of KIVA software, so-called k3prep. The latter is using commercial software as ICEM-CFD. Procedure is described as:

The piston profile, shown in Figure 3.3, has been drawn by means of I-DEAS, afterwards, it has been exported into ICEM-CFD, and finally itape17, input file for kiva3v, has been created via this grid generation software. (See Appendix C for explanation and structure of the code.) Some grids, created by ICEM-CFD are demonstrated in Figure 3.4 (a) and (b) below:

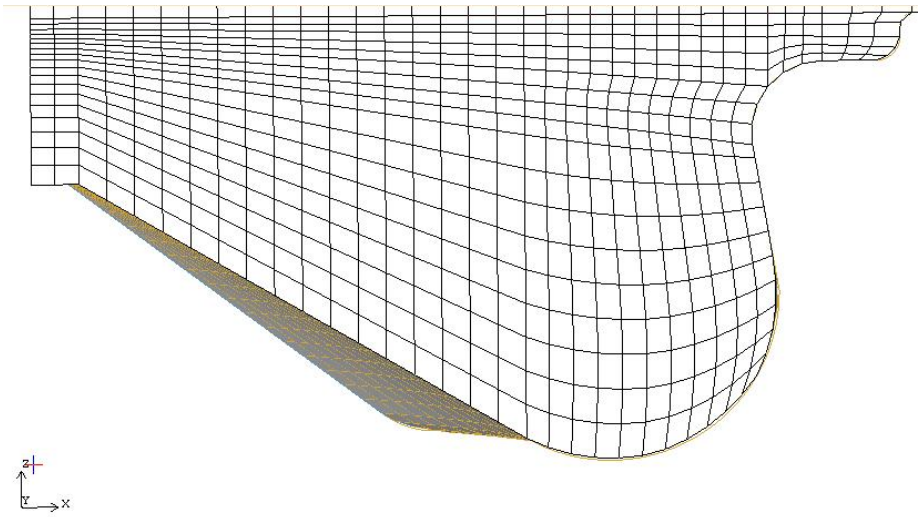

(a)

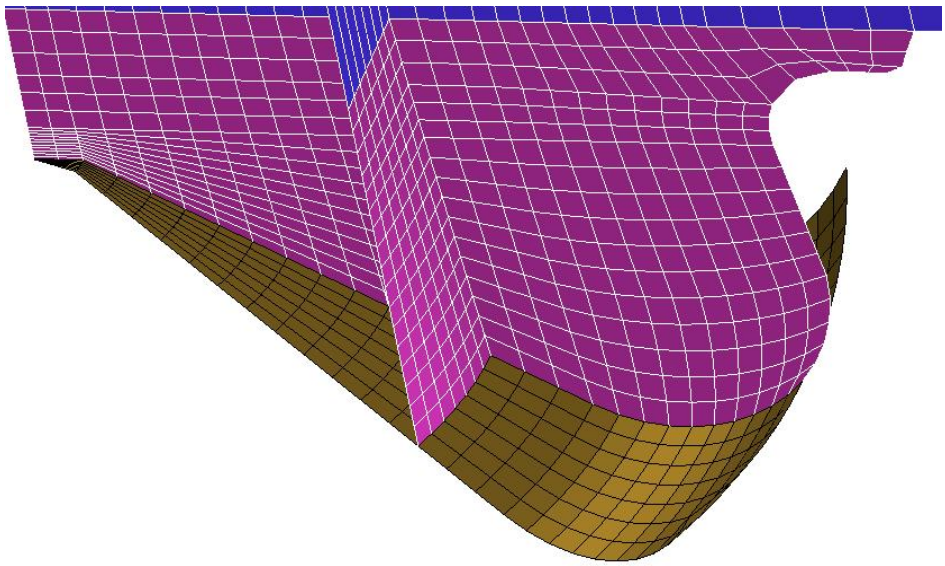

(b)

Figure.3.4. (a),(b) Demonstration of some created meshes via ICEM-CFD

In our simulations, 45 ^{o} sector mesh, (29x15x16 in the bowl region, 37x15x30 in the squish region and a total of 27717 cells) created by k3prep, has been employed. (see Figure 3.5)

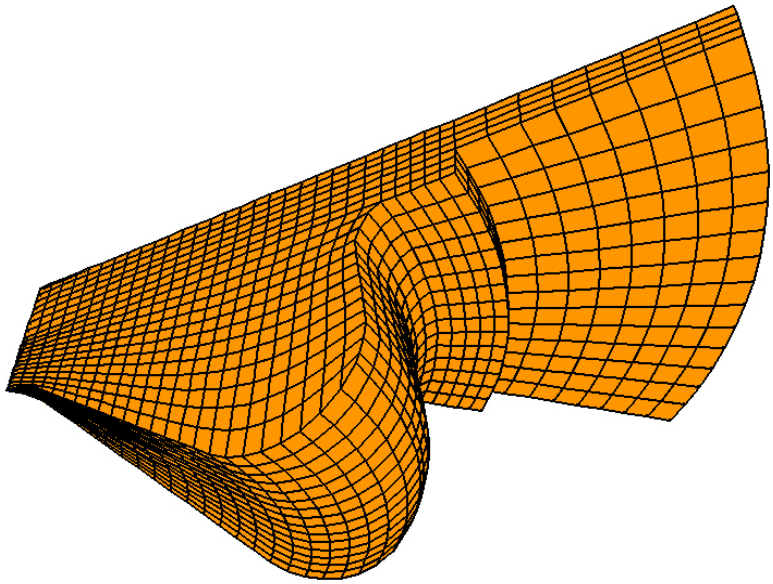

Figure 3.5. Computational mesh used in the simulations

In the computational model, 0^o CAD represents the time when piston is at top dead center. -138^o CAD, the beginning flag of the simulation, corresponds to the time at inlet valve closure. Compression ratio is not an input, instead, 'squish' value is used. That is, when the computed bowl volume and the real one are slightly different, 'squish' value is usually adjusted to obtain the exact compression ratio of the real engine (Table 3.4). It is plausible, because some volumes above the piston rings and below the inlet and exhaust valves were not taken into account in this modeling approach. From this point of view, 'squish' value of this model has been calculated as 0.238 cm.

Table 3.4. Comparisons of the real bowl volume and the computed ones

Bowl volume of the ECOTORQ engine	50.69 ± 0.4 cm^3
Bowl volume obtained via I-DEAS	50.3 cm^3
Computed volume of the bowl mesh by means of KIVA	50.29 cm^3

In the computations, swirl is also taken into account. The simplest model assumes that the swirl velocity has a wheel-flow profile, but this is not usually a realistic assumption (see Figure 3.6). Because, boundaries make the swirl decrease in the wall region. From experimental observation, a Bessel function profile may represent more

accurate flow. The quantity α (input as 'swipro') is a dimensionless constant that defines the initial azimuthal velocity profile and lies between 0.0 (the wheel flow limit) and 3.83 (zero velocity at the wall). For typical engine applications, it is suggested 3.11. **(Amsden,1989).** Experimentally obtained swirl ratio is between 1.45~ 1.50.

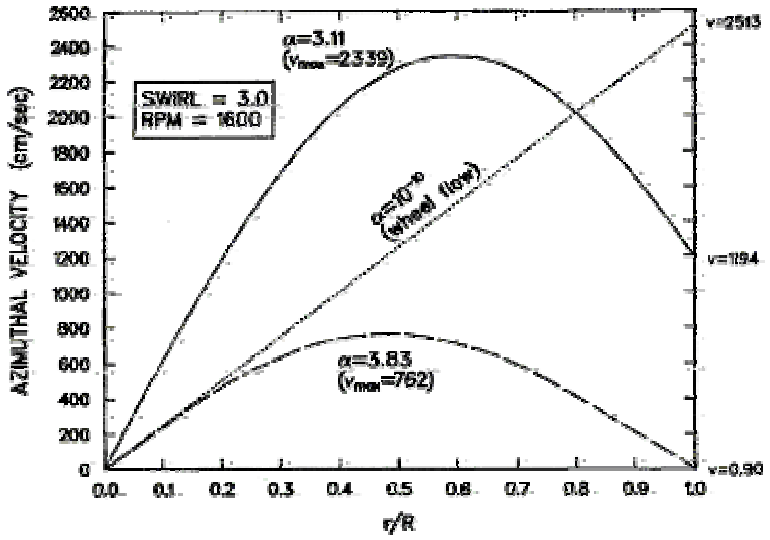

Figure 3.6. Bessel function swirl velocity profile provided in KIVA setup. **(Amsden,1989)**

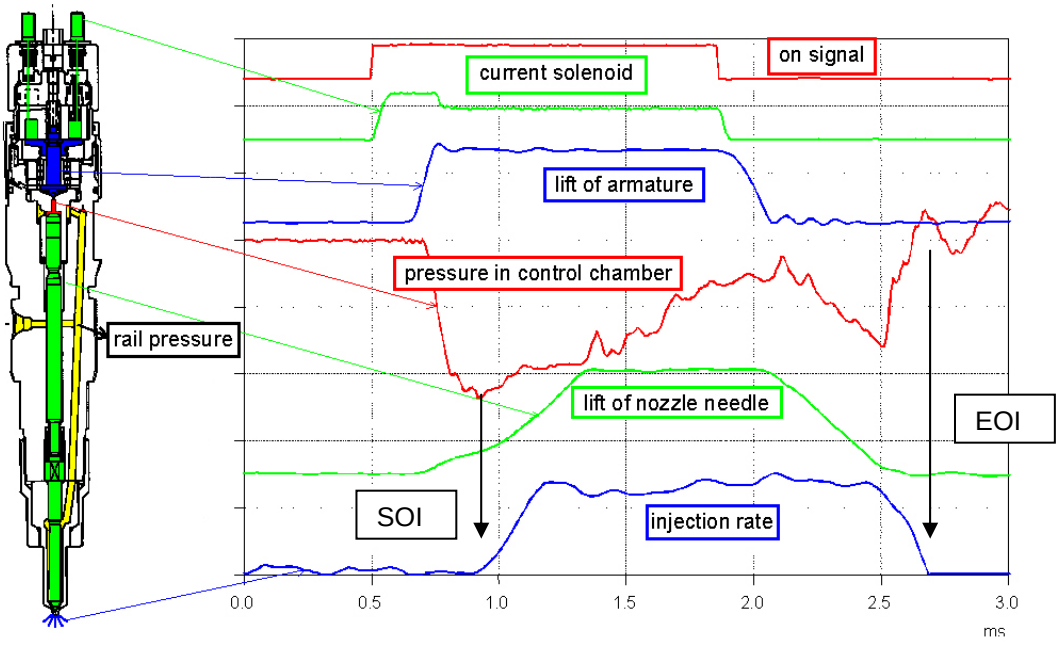

Figure 3.7. Comparison between the Prail signal and the injection rate.

It should be pointed out that the SOI (start of injection) corresponds to the beginning of the current pulses (i.e. see pressure in control chamber) and not to the actual start of the fuel injection, which is delayed by the electric, hydraulic and mechanical transient phenomena of the system. (see Figure 3.7) Similarly, for injection stop (EOI), there exists close response time. **(Su et al, 2001)**

Because of not having the measured injection rate profiles, solenoid current information has been utilized to predict the beginning and duration of injection. In this study, a constant delay of about 300 μs for SOI and close response time 450 μs have been estimated.

3.4. Cycle modeling

In cycle modeling process (both ignition and combustion), it is essential that both chemical mechanism and turbulence-chemistry interaction model be controlled. Because, $\tau_{mix} \approx k/\varepsilon$ might not always yield the best results, depending on the flow situation, as well as the chemical mechanism.

As mentioned before, it is difficult to tune single step models in order to describe the entire course of both ignition and combustion. Therefore, at least a multi-step kinetics model, e.g. Shell and IFP ignition models, to simulate ignition and a turbulence-chemistry interaction model for main combustion process are required. Therefore, in this study, detailed chemistry approach has been utilized. The mechanism, consisting of 68 species and 279 reactions, considers the ignition process as that of n-heptane of which cetane number ~ 56, similar to conventional diesel fuel. (See Appendix D for the reaction set) PaSR model has been used to account the effects of turbulence on mean reaction rate.

3.4.1. An Example Calculation

In this section, an example of how cycle modeling of Ecotorq engine is modeled will be given. In the Table 3.5, some of the measurement parameters of the engine, at operating conditon of 1780 rpm and 100% load, are given.

Table 3.5. Some results of the Ecotorq engine (@1780 rpm, 100% load)

Engine speed	1780 rpm
Engine load	100%
Quantity of injected fuel in a cycle	125 mg/stroke
Start of injection (solenoid current)	6 CAD BTDC
Duration of injection (solenoid current)	1995 μs
Rail pressure	1150 bar
Measured in-cylinder pressure at inlet valve closure	3,01 bar
Air Temperature	22,56 ^{o}C
Fuel Temperature	31,1 ^{o}C
Water Temperature	88,2 ^{o}C
Oil Temperature	107,2 ^{o}C
Swirl ratio	1,4 – 1,5
Power	197,05 kWh
Specific Fuel Consumption	203,40 g/kWh
Exhaust-out NOx emission in a cycle	1115 ppm, 8,73 g/kW-h
Exhaust-out soot emission in a cycle	0,13 FSN

The next step is to prepare the datasheet for KIVA input, itape5 file which represents engine operating conditions. Some important parameters are given in Table 3.6.

Table.3.6. Datasheet for KIVA inputs

Bore	11,2 cm
Stroke	12,4 cm
Squish	0,238 cm
Connecting rod	22,2 cm
Injector nozzle diameter	0,130 mm
Engine speed	1780 rpm
Injection timing	5 CAD BTDC
Injection period	24 CAD
Injection mode	Velocity table (defined below)
Injected mass/stroke	0,125 gr
Injection velocity	~400 m/s
Initial in-cylinder pressure	3,01 bar
Initial in-cylinder temp	340 K
Inclination angle of spray	75 deg
Spray cone ½ angle	10~12,5 deg
Initial droplet temperature	350 K
Cylinder head temperature	523 K
Piston temperature	553 K
Wall temperature	500 K
Swirl ratio	1.45

In KIVA, the injection rate is an input in the unit of cm/s. Therefore, if the injection rate is considered as square wave shape, one can estimate the average velocity, that is

helpful to check whether KIVA may compute wrong or not. A method is given below:

$$\dot{m} = \frac{(tspmass) * rpm * 360}{(cadinj) * (\#holes) * 60}$$

$$\dot{m} = \frac{0{,}125 * 1780 * 360}{24 * 8 * 60} 6{,}953 \; g / hole - \sec$$

$$velinj = \frac{\dot{m}}{(rhop) * anoz}$$

$$velinj = \frac{6{,}953}{0{,}840 * 2{,}06 * 10^{-4}} = 40182 \; cm / s$$

$\dot{m}$: quantity of fuel per hole per second [g/hole-sec]

tspmass: total sprayed mass [gram]

cadinj: duration of injection in CAD

rhop: density of fuel [g/cm^3]

#holes: injector hole number

anoz: nozzle area [cm^2]

velinj: injection velocity [cm/s]

Afterwards, profile of the injection law, acquired from Ford OTOSAN, digitalized as shown in Figure 3.8:

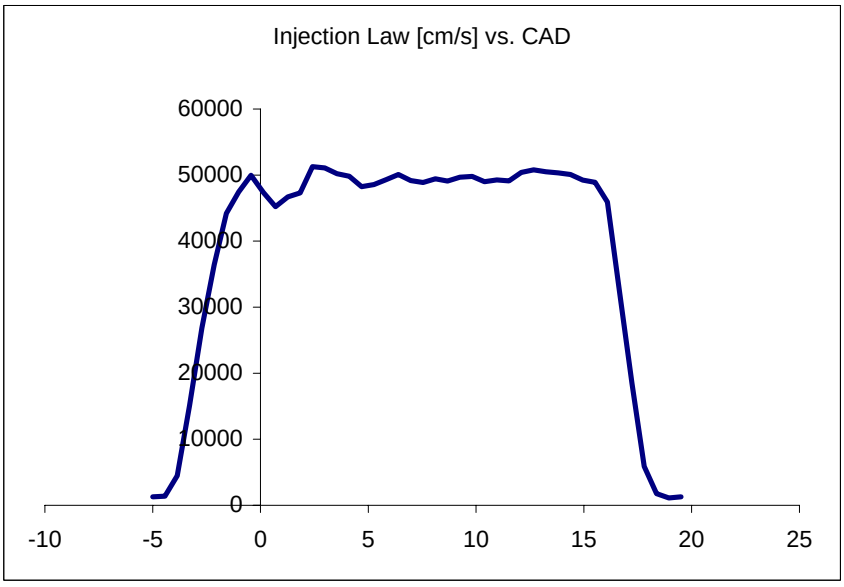

Figure 3.8. Injection velocity profile used in the simulations

Having prepared necessary input files of KIVA, i.e. itape5, itape17, chem.dat (see the explanations of the file structure of KIVA in Appendix C) and having run the code, computed results are post-processed by means of various softwares, e.g. MS Excel™, Amtec Tecplot™, CEI Ensight™, GMV™ etc. Some results are demonstrated below: (see, Figure 3.9,10,11)

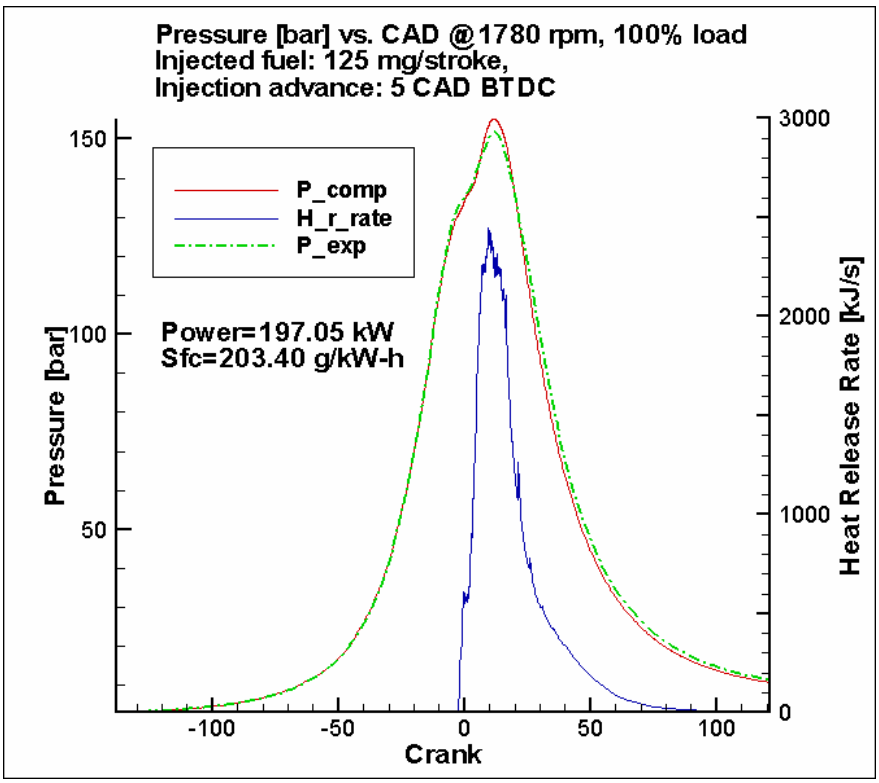

Figure 3.9. Comparison of in-cylinder pressure with respect to experimental and computational results

It is seen that the traces of computed pressure are in good agreement with those of measured values. A typical heat release rate curve of diesel engines comprises two evident stages representing premixed burn, a steep increase in heat release, and a gradual diffusion burn. In the figure above, premixed burn fraction of the heat release rate curve has a steep rise and is much more than that of diffusion burn as expected. Because, high pressure common rail injection system gives possibility of increased quality of mixture formation relatively in a short time in comparison with the conventional injection systems. Therefore, homogeneous mixture fraction increases during the ignition delay, that leads to consume most of the fuel in the premixed burn stage causing less soot emissions.

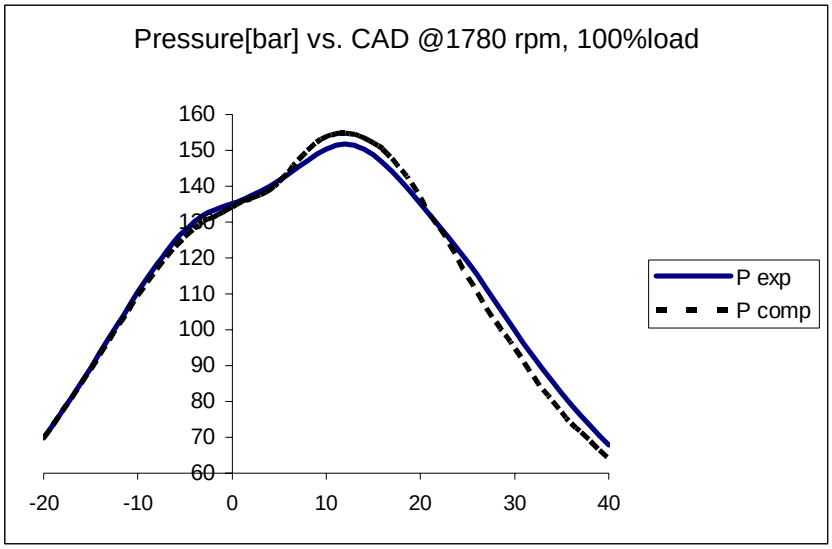

Figure 3.10. Experimental and computational results of in-cylinder pressure in a zoomed view

In the figures below, NOx and soot emissions of this operating condition are shown. Soot curve is like typical bell-shaped as seen in Diesel engines. But, exhaust-out soot concentration has been predicted extremely small when compared to measurements. NOx history demonstrates the typical history seen in Diesel engines where the realistic NO concentration does not follow its equilibrium value, instead, freezes in the expansion stroke.

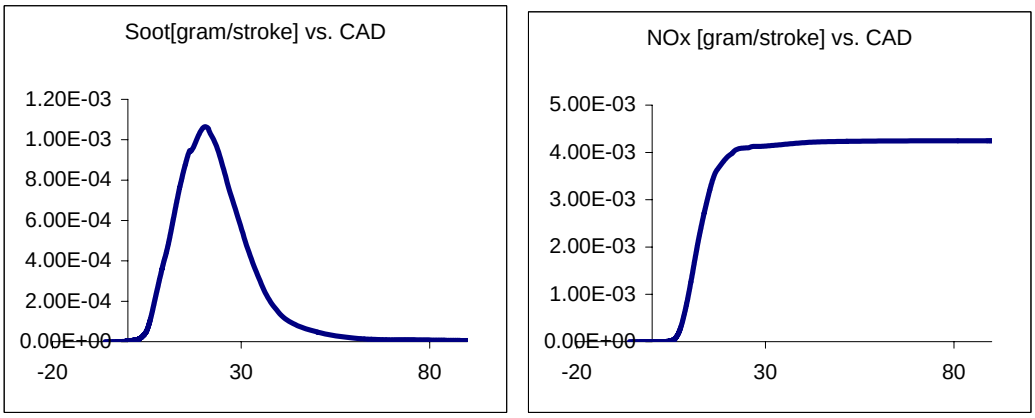

Figure 3.11. Computed histories of NOx and soot emissions in gram

In table 3.7, a comparison between experimental and calculated exhaust-out emissions are listed. As mentioned above, since soot emissions are predicted too small, a calibration factor of 10 has been chosen to achieve typical engine-out raw soot levels.

Table 3.7. Comparison of exhaust-out emissions @ 1780 rpm, 100% load

@ 1780 rpm, 100% load, SOI=5 BTDC, injected mass=125 mg	**Measured NOx [ppm]**	**Measured Smoke [FSN]**	**Computed NOx [ppm]**	**Computed Soot x 10 [g/kW-h]**
	1115	0,13	1074	0,038

In all simulations, no tuning in the KIVA code has been done. In order to verify the model, in different cases (operating conditions), computational and experimental pressure histories have been compared. (see Appendix A). Since pressure is tightly coupled with the heat release rate, correct predicting of pressure is essential for engine modeling.

In Appendix A, quite successful results are observed except low load cases, e.g. lower cases than 45% , when compared with those of experiments. In that case, a clear discrepancy between computed and measured results, that is related with autoignition, is seen. Both simulations have been run at similar conditions, e.g. 1780 rpm and 45% load, fuel is injected at the same time, 3.5 CAD BTDC. Only difference is sourced by influence of turbocharger. Generally speaking, since boost pressure is decreased when engine load decreases, initial pressure, temperature and turbulence levels of the simulation inputs might be adjusted as accurate as possible. This is because, an intake stroke modeling accounting influence of turbocharge may be necessary to estimate correct ignition delay time. In addition, at low load cases injection parameters may need adjusting.

Appendix B deals with how adding a reasonable amount of swirl influenced the spray jet and spatial distribution of temperature. From the figures, it is observed that high temperature combustion zone travelled clockwise. That makes for more oxygen to be available for soot oxidation.

Figure 3.12 (a) and (b) shows the spray penetration and temperature distribution of TAB and KHRT spray models respectively. When TAB model, standard in KIVA code, is used, spray penetration decreases due to rapid breakup of spray jet into smaller droplets leading evaporation rate increase. Hence, in the vicinity of the nozzle, ignition commenced out. In addition, the less spray penetration, the more soot emission out. Because, a longer spray penetration might have more oxygen to be available for soot oxidation.

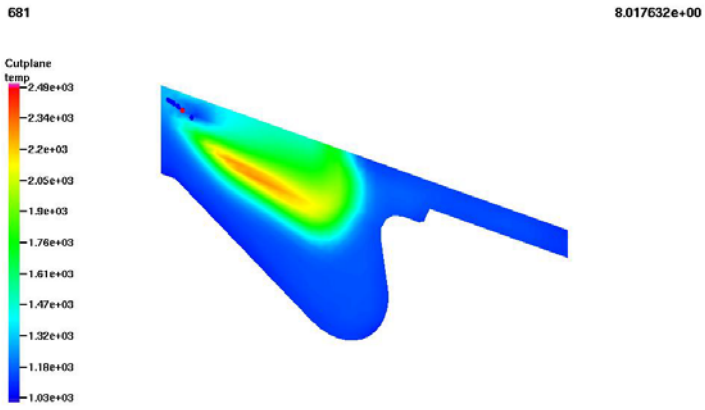

(a)

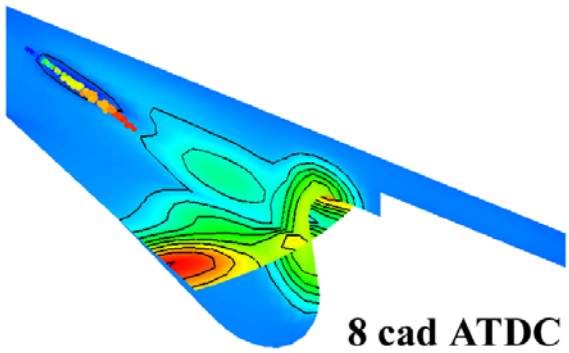

(b)

Figure 3.12 Comparison of spray models with respect to spray penetration and temperature distribution: (a) TAB model, (b) KHRT model

It must also be pointed out that TAB model hasn't been adapted to get better results. As to be in KHRT model, it has adjustable model constants for case to case as well. In this study, KHRT model has been replaced with TAB model because of having parent and child droplets after drop disintegration.

Having said before, two different turbulence model have been tested, namely Standard k-ε and RNG k-ε models which differ in adding an extra term to dissipation equation, yielding a dynamic mean strain rate. This results in more accurate predictions of flows with rapid distortion and anisotropic large scale eddies. Implementation of the RNG k-ε turbulence model is given by Han and Reitz, 1995.

When compared with the standard one, RNG model predicts shorter spray penetration and increased mixing. In Figure 3.13, it is seen that computed in-cylinder pressure of RNG model is in much better agreement with the measured data than that of standard model. It is considered that lower turbulent viscosity and therefore lower

thermal diffusivity play important role. Because predicting lower turbulent diffusivity of RNG model, flow structures and local temperature distribution are significantly influenced. That means emissions, especially those of NO which is sensitive to temperature above 2000 K, will be afffected substantially.

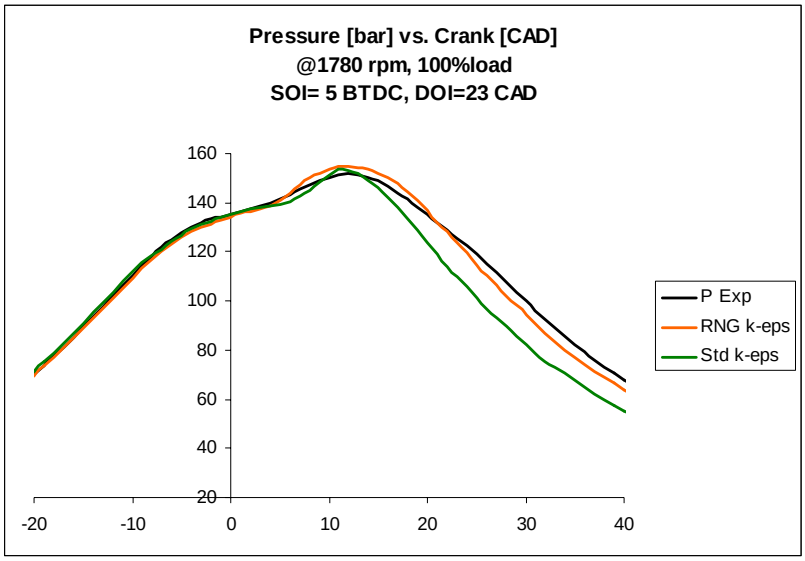

Figure 3.13 Comparison of standard k-ε and its RNG version with respect to in-cylinder pressure traces

Because of its better performance, RNG k-ε model has been used, unless otherwise stated.

3.5 Influence of Injection Advance on Engine Performance and Emissions

With the introduce of Common Rail high pressure injection systems, it is possible to provide for better mixing of fuel and surrounding air. Since the smaller fuel droplet, the faster mixture formation of fuel and air, smaller injection holes can be utilized for the same fuel injection rate. That means shorter ignition delay can be achieved with this high pressure injection system. Hence, this advantage of having better ignition capability gives possibility of retarding the fuel injection, even after TDC. In the case of retarded injection, NOx emissions are reduced significantly by reducing peak cylinder temperatures and pressures, thus reducing the rate of NOx formation. But, it must be pointed out that thermodynamic efficiency of the engine is decreased and soot emissions are increased. **(Heywood,1988)**

From the Figures below (3.14,15,16) and Table(3.8), it can be concluded that the injection advance is of great significance on the engine performance and NOx-soot

trade off. When the fuel injection is retarded, engine power decreases and specific fuel consumption increases. On the other hand, NOx emissions decrease, but those of soot increase.

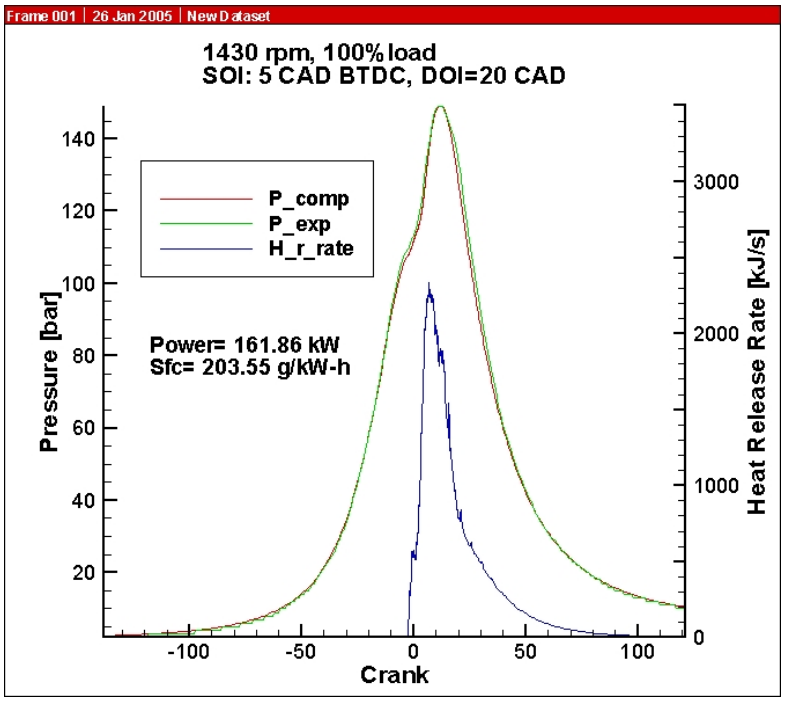

Figure 3.14 Influence of injection advance: 5 CAD BTDC, Engine power:161,86 kWh, Specific fuel consumption: 203,55 g/kWh

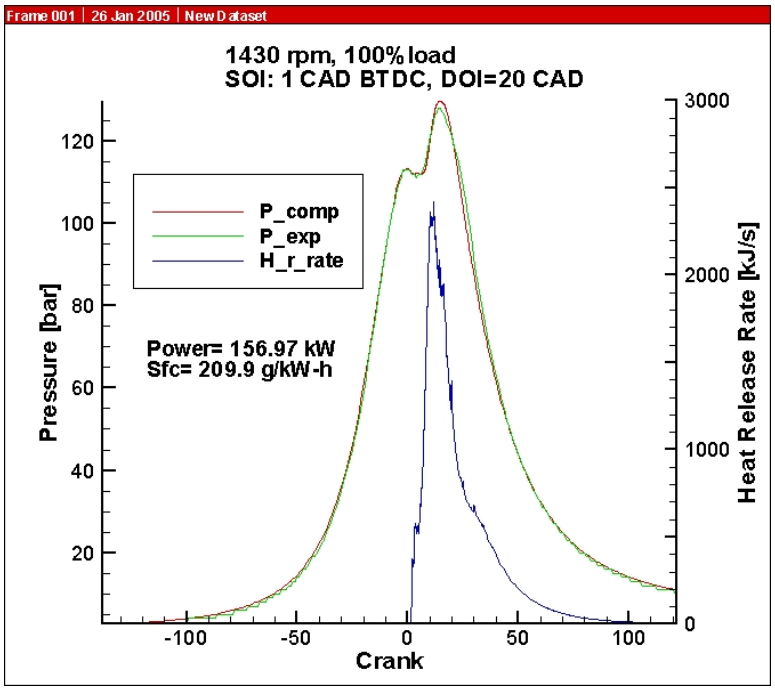

Figure 3.15 Influence of injection advance: 1 CAD ATDC Engine power:156,97 kWh, Specific fuel consumption: 209,90 g/kWh

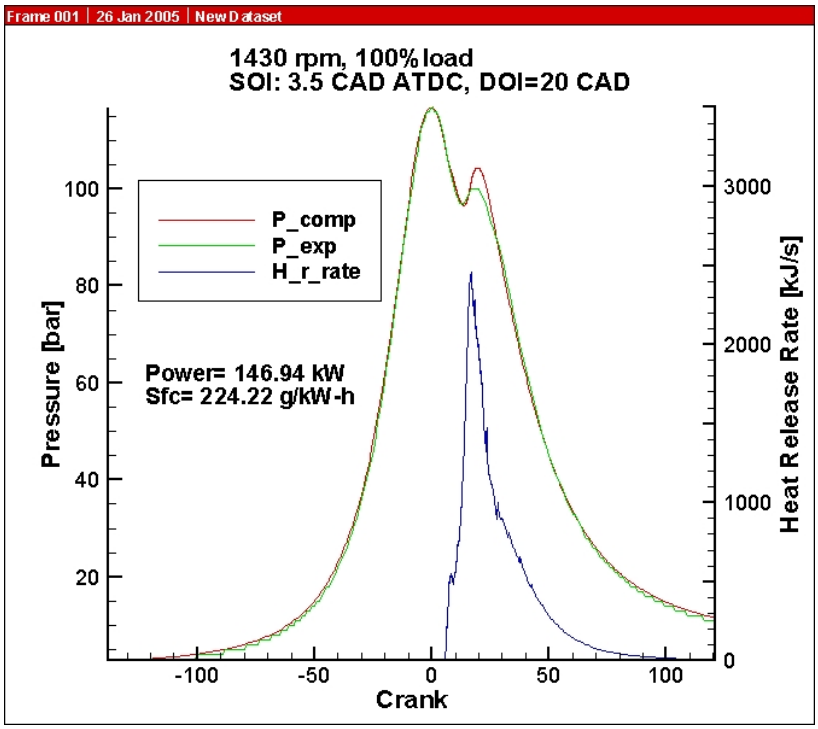

Figure 3.16 Influence of injection advance: 3.5 CAD ATDC Engine power:146,94 kWh, Specific fuel consumption: 224,22 g/kWh

Table 3.8. Influence of injection advance on engine performance and NOx-soot dilemma

@1430 rpm 100% load	**5 CAD BTDC**		**1 CAD ATDC**		**3,5 CAD ATDC**	
	NOx	**Soot**	**NOx**	**Soot**	**NOx**	**Soot**
Comp.	1360 ppm	0,041 gr/kWh	1007 ppm	0,052 gr/kWh	711 ppm	0,076 gr/kWh
Exp.	1249 ppm	0,22 FSN	1072 ppm	0,25 FSN	821 ppm	0,29 FSN
Comp. Power	161,86 kW		156,97 kW		146,94 kW	
Exp. Power	161,76 kW		158,69 kW		148,36 kW	
Comp Sfc	203,55 g/kWh		209,90 g/kWh		224,22 g/kWh	
Exp. Sfc	203,67 g/kWh		207,50 g/kWh		218,29 g/kWh	

As mentioned before, since soot emissions are predicted extremely small, a calibration factor of 10 has been chosen to obtain usual engine-out raw soot levels.

To conclude, it can be said that calculated in-cylinder pressure histories and exhaust-out emissions of NOx results is in good agreement with the experimental data

obtained by Ford-Otosan, whereas soot emission level has been predicted extremely small. But, it is plausible to say that soot trend has been predicted in a good level when injection is retarded.

3.6 Effect of Split Injection on NOx and Soot Emissions:

Split injection is an electronically controlled injection procedure in order to achieve both NOx and soot reduction by means of splitting the injection sequence two events. In the case of the amount of injected fuel in the first pulse is less than that of the latter, this scheme is called as pilot injection. If it is higher than that of the second pulse, then it is called as the post injection scheme.

The pilot injection is used to shorten ignition delay and to control rapid pressure rise. Reducing ignition delay reduces the quantity of premixed burn as well. Since most NOx is believed to be formed in the premixed burn, it can be said that pilot injection scheme is effective on NOx emission control.

The case of diffusion burn is controlled by air mixing with the outer edges of the fuel jet. Fuel in the interior of the spray jet is exposed to high temperatures and pressures but is starved for oxygen, then the rich zone leads to soot production. According to experiments, soot is formed and accumulates in the tip region of the spray jet as described in **Dec, 1987.**

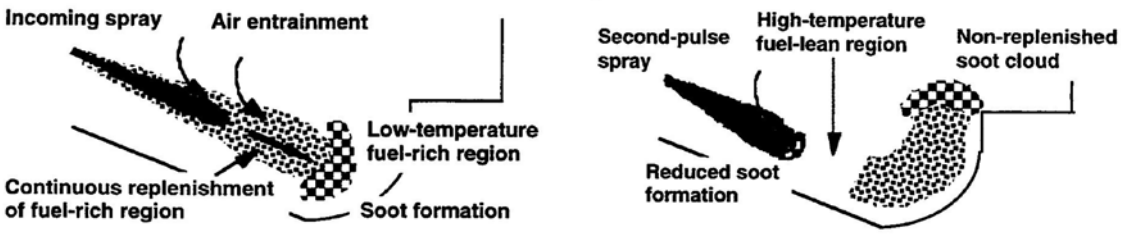

Figure 3.17 Illustration of soot reduction mechanism of split injection cases.
(Han et al., 1996)

In the split injection case, the second pulse spray penetrates into a relatively fuel lean and high temperature region which arises from the first pulse (see Figure 3.17). Hence, soot formation is significantly reduced because the dwell between the pulses prevents continuous replenishment of fuel-rich region and prepares a suitable combustion condition for the second pulse. As a result, the net production of soot in the split injection scheme can be reduced significantly. In addition, there is an optimum dwell time between the pulses. It must be long enough to prevent

replenishment of fuel-rich region, leading soot, and short enough to get better combustion conditions, that is to say, rapid combustion leads relatively less soot.

In this study, it is shown that the significant soot reduction without NOx penalty could be obtained by means of split injection. In addition, that the NOx reduction mechanism of split injection is similar to that of single and retarded injection, is found from the computations.

Labeling scheme of split injection strategy (eg. 25-75-8) is described as: The former represents the injected fuel of the first pulse, the next one shows that of the second pulse, and the latter is just for the dwell time between two pulses. Injection scheme is shown in the next figures:

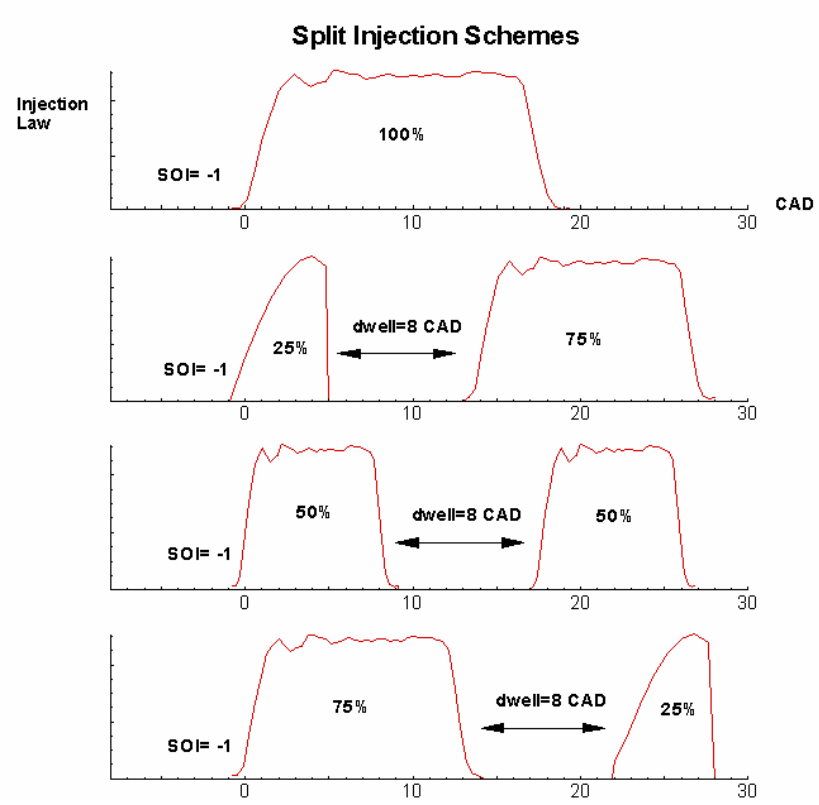

Figure 3.18 Split injection schemes used in the simulations when fuel injection begins at 1 BTDC.

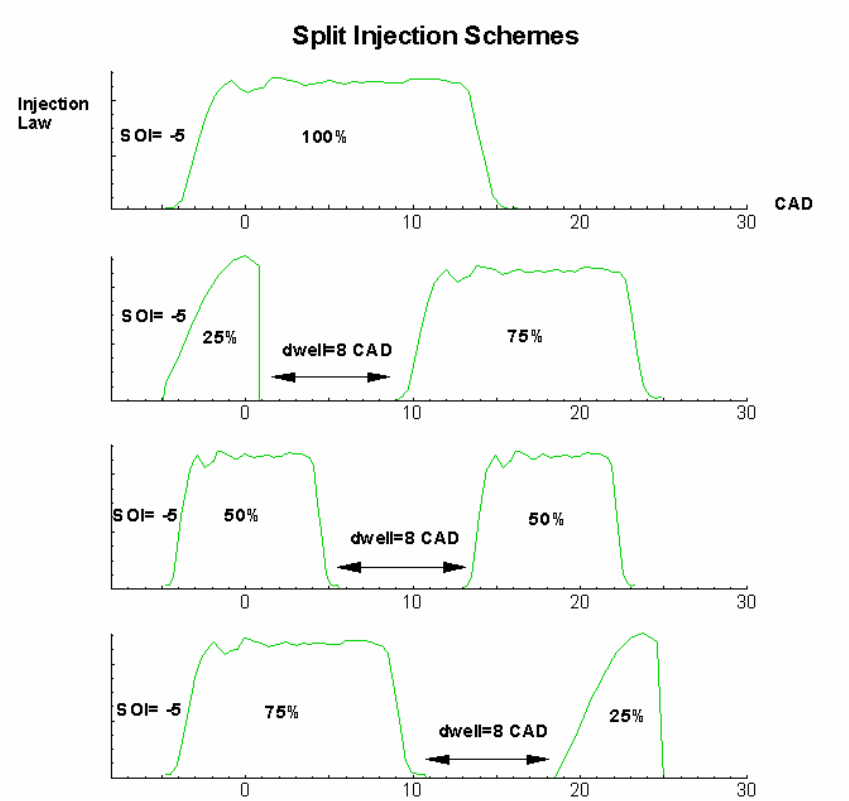

Figure 3.19 Split injection schemes used in the simulations when fuel injection begins at 5 BTDC.

In the table below, injection strategies and results are shown:

Table 3.9 Comparisons of single injection and split injection schemes.

	Start of Injection	**Measured Nox [g/kW-h]**	**Measured Soot [FSN]**	**Predicted Nox [g/kW-h]**	**Predicted Soot*10 [g/kW-h]**	**SFC [g/kW-h]**	**Power kW**
Single inj.	5 BTDC	7.93	0.22	7.12	0.041	203.55	161.86
Single inj.	1 BTDC	7.15	0.25	5.64	0.052	209.9	156.97
Single inj.	3.5 ATDC	6.09	0.29	4.37	0.076	224.22	146.94
25-75-8	5 BTDC	-	-	4.88	0.033	224.65	146.66
50-50-8	5 BTDC	-	-	7.14	0.019	208.52	158.01
75-25-8	5 BTDC	-	-	7.31	0.023	206.01	159.93
25-75-8	1 BTDC	-	-	3.10	0.054	243.65	135.09
50-50-8	1 BTDC	-	-	5.32	0.022	219.09	150.38
75-25-8	1 BTDC	-	-	5.99	0.027	211.75	155.59

At full load, when single injection (SOI = 5 BTDC) and split injection cases (50-50-8) are compared, it is seen that soot is reduced nearly by a factor of two with no increase in NOx and only a 2.5% increase in specific fuel consumption.

An important parameter is the amount of injected fuel in the first pulse. When this amount is increased, NOx level also increases, however, it is seen that soot level has an optimum value in the case of 50% of fuel injected in the first pulse. This prediction is in a good agreement with the findings of **Pierpont et al., 1995**.

Experimentally findings show that with split injections, the soot-NOx trade off curves of a diesel engine can be shifted closer to the origin that those with single-pulse injections, that means both soot and NOx emission reduces significantly. **(Nehmer and Reitz, 1994)**

In the figure below, the predictions show that 50-50-8 cases reduces soot significantly with no increase in NOx when compared with the related single injection scheme.

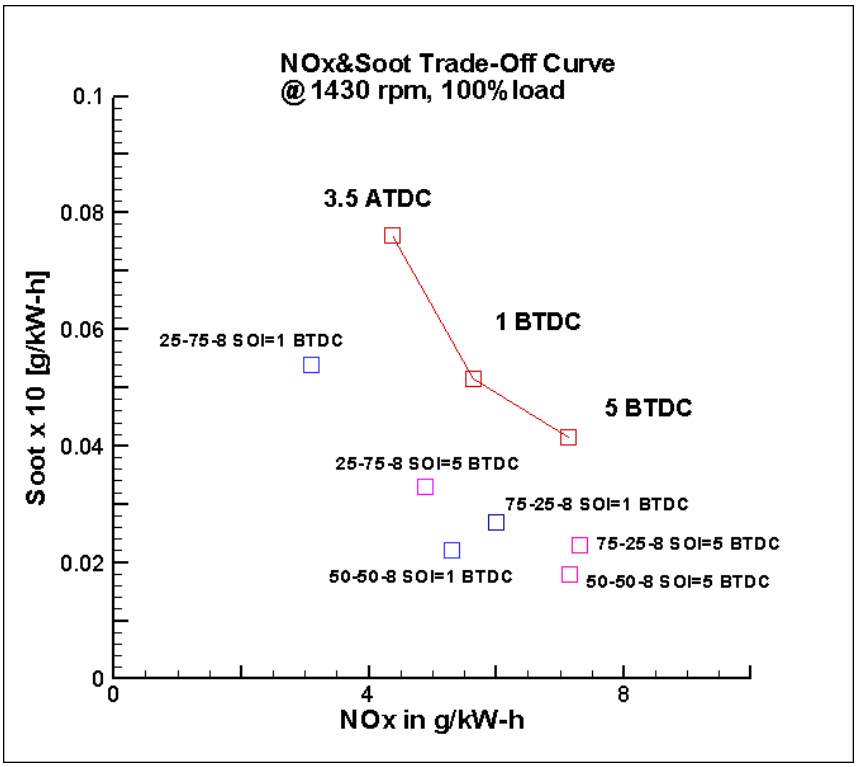

Figure 3.20 NOx & Soot trade of curve when single and split injection strategies are considered.

CHAPTER 4

CONCLUSION

In this study, multidimensional modeling concept was considered to investigate mixture formation and combustion process in Diesel engines. This modeling approach was carried out by means of a modified KIVA-3V code in order to get better performance and less pollutant emissions. At first stage, numerical simulation results were compared with those of experimentally obtained from Ford-Otosan Ecotorq engine. The latter is to carry out parametric analysis such as influence of retarded injection and split injection schemes on engine performance and pollutant emissions.

It was shown that spray modeling is of great importance in modeling approach. An alternative spray model, so-called KHRT, and its influence on mixture formation and combustion process was dealt. Although a good agreement is found with measured cylinder pressure and heat release rate data, improvements are needed for this model.

Turbulence modeling is also important for engine modeling considerations. Standard k-ε and RNG k-ε models which differ in adding an extra term to dissipation equation tested. Higher local temperatures compared to standard model were predicted with the use of RNG k-ε model. It is seen that computed in-cylinder pressure of RNG model is in much better agreement with the measured data than that of standard model.

One of the goals of this study is to develop a predictive combustion model for direct injection diesel engines. Therefore, Diesel fuel surrogate chemistry model, proposed by **Golovitchev et al (2002)**, has been considered in order to model both low temperature (autoignition) and high temperature cases, as well as soot and NOx emissions.

Satisfactory results were obtained except too low load cases due to relatively long ignition delay. It is considered that initial conditions relying on turbocharger are effective on ignition process. From the point of view of modeling approach, more accurate initial conditions can only be obtained by intake stroke modeling.

To account turbulence/chemistry interactions in the computations, the Partially Stirred Reactor concept **(Golovitchev et al., 2000)**, utilized in this study, as an extension of the eddy-break-up model. Due to its suitable coupling with KIVA solution method, application to diesel fuel spray and complex chemistry becomes handy.

Finally, parametric study of injection strategies were done. From the computations, it can be concluded that the injection advance is of great significance on the engine performance and NOx-soot trade off. When the fuel injection is retarded, engine power decreases and specific fuel consumption increases. On the other hand, NOx emissions decrease, but those of soot increase. Predicted NO emission levels, relying on mainly thermal NO, gave successful results due to its relatively well-known mechanism, whereas soot emissions were predicted extremely small, thus a calibration factor of 10 has been chosen to obtain usual engine-out raw soot levels. However, it is plausible to say that soot trend has been predicted in a good level when injection is retarded.

In addition, it was shown that the significant soot reduction without NOx penalty could be obtained by means of split injection. Moreover, it was found from the computations that NOx reduction mechanism of pilot injection strategy is similar to that of single and retarded injection

To conclude, relatively successful computational results obtained show that multidimensional modeling approach is an invaluable and promising tool for engine combustion development. Nevertheless, it must be pointed out that no matter how good results are obtained with calibrating model constants, further improvements are still necessary in both spray and combustion models.

REFERENCES

Aggarwal, S.K., 1987. Modeling of a Dilute Vaporizing Multi-component Fuel Spray, *Int. J. Heat Mass Transfer*, vol30, no9, pp 1949-1961.

Amsden, A.A., O'Rourke, P.J. ve Butler,T.D., 1989, "KIVA-II: A Computer Program for Chemically Reacting Flows with Sprays, Los Alamos National Laboratory", New Mexico.

Amsden, A.A., 1993. KIVA-3: A KIVA Program with Block Struvtured Mesh for Complex Geometries, Los Alamos National Laboratory, New Mexico.

Amsden, A.A., 1997. KIVA-3V: A Block Structured KIVA Program for Engines with Vertical or Canted Valves, Los Alamos National Laboratory, New Mexico.

Arcoumanis, C., Flora, H., Gavaises, M., Badami, M. 2000. Cavitation in Real-Size Multi-Hole Diesel Injector Nozzles, SAE Paper 2000-01-1249

Baumgarten, C., Stegemann, J., Merker, G.P. 2002. A New Model for Cavitation Induced Primary Breakup of Diesel Sprays. *Proc. 18th ILASS Europe Conf.* pp 15-20, Zaragoza, Spain

Dec, J.E., 1987. A Conceptual Model of DI Diesel Combustion Based on Laser-Sheet Imaging, SAE Paper 970873.

Dohle, U., Kampmann, S., Hammer, J., Wintrich, T., Hinrichsen, C., 2004. Advanced Diesel Common Rail Systems for Future Emission Legislation, *Proc. from ICAT 2004*, pp 109-113.

Fusco, A., Knox-Kelecy AL, Foster D.E., 1994. Application of a Phenomenological Soot Model to Diesel Engine Combustion. *3rd Int. Symp. COMODIA 94.* pp 315-324.

Golovitchev, V.I., Atarashiya, K., Tanaka, K., and Yamada, S., 2003. Towards Universal EDC-Based Combustion Model for Compression Ignited Engine Simulations, SAE Paper 2003-01-1849.

Golovitchev, V.I., Nordin, N., Jarnacki, R. ve Chomiak, J., 2000. 3-D Spray Simulations Using a New Detailed Chemistry Turbulent Combustion Model, SAE Paper 2000-01-1891.

Gustavsson, J. and Golovitchev, V.I., 2003. Spray Combustion Simulation Based on Detailed Chemistry Approach for Diesel Fuel Surrogate Model, SAE paper 2003-01-137.

Han, Z. and Reitz, R.D., 1995. Turbulence Modeling of Internal Combustion Engines Using RNG k-ε Models, *Combustion Science and Technology*, vol. 106(4-6) pp 267-295.

Han,Z., Uludogan, A.,Hampson, G.J., Reitz, R.D., 1996.Mechanism of Soot and Nox emission Reduction Using Multiple Injection in a Diesel Engine, SAE 960633.

Heywood, J.B., 1988. Internal Combustion Engine Fundamentals, McGraw-Hill Publishing Company, NewYork.

Kjäldman, L., A. Brink, A. and Hupa, M., 2000**.** Micro mixing time in the eddy dissipation concept, *Combust. Sci. and Tech*, vol. 154, pp 207.

Kong, S.C., and Reitz, R.D., 1993. Multidimensional Modeling of Diesel Ignition and Combustion Using A Multistep Kinetics Models, *ASME Transactions, Journal of Engineering for Gas Turbines and Power*, vol. 115, No. 4, pp 781-789.

Kong, S.C., Han, Z., Reitz, R.D., 1995. The Development and Application of a Diesel Ignition and Combustion Model for Multidimensional Engine Simulation, SAE paper 950278.

Kuo, K., 1986. Principles of Combustion, John Wiley&Sons Inc., New York.

Lu, J., Gupta, A.K., Keating, E.L., 1993. Effect of IC engine Operating Conditions on Combustion and Emission Characteristics Transactions of the ASME Journal of Fluids Engineering Vol,115

Magnussen, B.F., Hjertager, B.H., 1976. On Mathematical Modeling of Turbulent Combustion with Special Emphasis on Soot Formation and Combustion, *The 16th Symposium (International) on Combustion the Combustion Institute*.

Miller, J.A., Bowman, C.T., 1989. Mechanism and Modeling of Nitrogen Chemistry in Combustion, *Prog. Energy Combust Sci.* vol 15, pp 287-338.

Nagle, J., Strickland-Constable RF, 1962. Oxidation of Carbon between 1000-2000^{o}C. *Proc. 5th Conf on Carbon*, vol 1 pp154-164, Pergamon Press, London UK.

Nehmer, D.A., Reitz,R.D., 1994. Measurement of the Effect of Injection Rate and Split Injections on Diesel Engine Soot and Nox Emissions, SAE 940668.

Nordin, N., 2000. "Complex Chemistry Modeling of Diesel Spray Combustion", PhD thesis, Chalmers University of Technology.

O'Rourke, P.J., 1981. Collective Drop Effects on Vaporizing Liquid Sprays, PhD thesis, Princeton University.

O'Rourke, P.J., Amsden, A.A., 1987. The TAB Method for Numerical Calculation of Spray Droplet Breakup, SAE paper 872089.

Penny, I.J., Whelan, S., Jackson, N.S., Cooper, B.G., 2004. Future Emissions Trends and Technologies to Meet Them, *Proc. from ICAT 2004*, pp 97-108.

Pierpont, D.A., Montgomery, D.T.,Reitz, R.D., 1995. Reducing Particulate and NOx Using Multiple Injections and EGR in a D.I. Diesel Engines, SAE 950217.

Ranz and Marshall Part I and II

Reitz, R.D., 1978. Atomization and Other Breakup Regimes of Liquid Jet, PhD Thesis, Princeton University.

Reitz, R.D., 1987. Modeling Atomization Process in High Pressure Vaporizing Sprays, *Atomization and Spray Technology*, vol.3, pp 309-337.

San, D., Gurarslan, E., Ergen, O.R., Kanar, K., 2004. The Development of the New Ford Heavy Duty Truck Engine, SAE paper 2004-01-2688.

Sirignano, W.A., 1978. Theory of Multicomponent Fuel Droplet Vaporization, *Archieves of Thermodynamics and Combustion*, vol.9, 2, 231.

Soruşbay, C., 2002. **"**İçten Yanmalı Motorlarda Karışım Oluşumu" ders notları, İTÜ Makine Fakültesi, İstanbul.

Stiesch, G., 2003. Modeling Engine Spray and Combustion Processes, Springer, Berlin.

Stumpp, G., Ricco, M. 1996. Common Rail - An Attractive Fuel Injection System for Passenger Car DI Diesel Engines, SAE paper 960870.

Su, W., Wang, Y., Lin, T., Xie, H. and Rei, Y. 2001. A Study of Effects of Design Parameters on Transient Response and Injection Rate Shaping for a Common Rail Injector System, SAE paper 2001-01-3506.

Theobald, M. and Cheng, W.K.1987. A Numerical Study of Diesel Ignition, ASME paper No:87-FE-2 .

Yoshizaki, T., Nishida, K., Hiroyasu, H., 1993. Approach to Low NOx and Smoke Emission Engines by Using Phenomenological Simulation, SAE Paper 930612.

Warnatz, J., Maas, U. and Dibble, R.W. 1996. Combustion: Physical and Chemical Fundamentals, Modeling and simulation, Experiments, Pollutant Formation, Springer, Berlin.

Westbrook, C.K. And Dryer, F.L., 1981, Simplified Reaction Mechanisms for Oxidation of Hydrocarbon Fuels in Flame, *Combustion Science and Technology*, vol. 27, pp 31-43.

Williams, F.A., 1985. Combustion Theory, 2nd edn, Benjamin/Cummings, Menlo Park CA.

APPENDIX A

In different load and rpms, computational and experimental pressure histories have been compared.

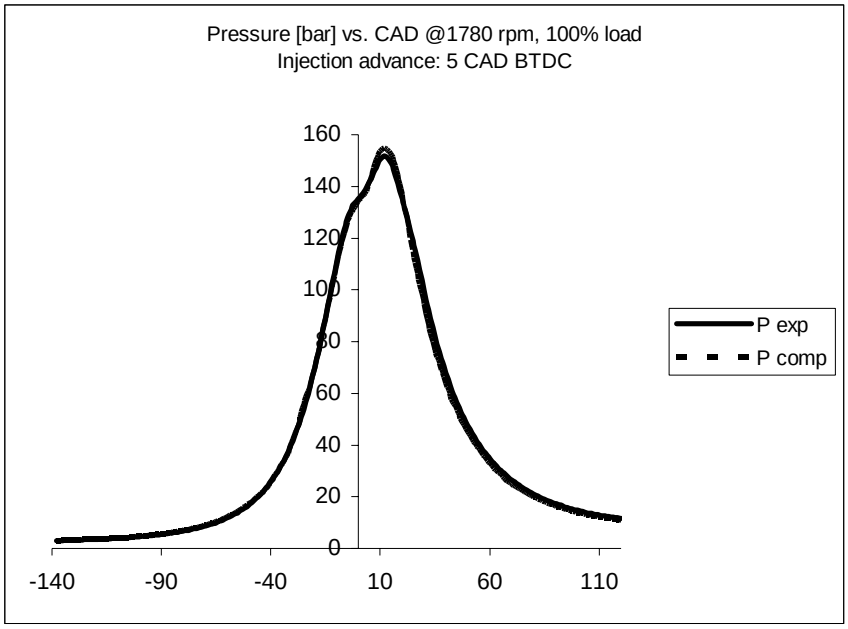

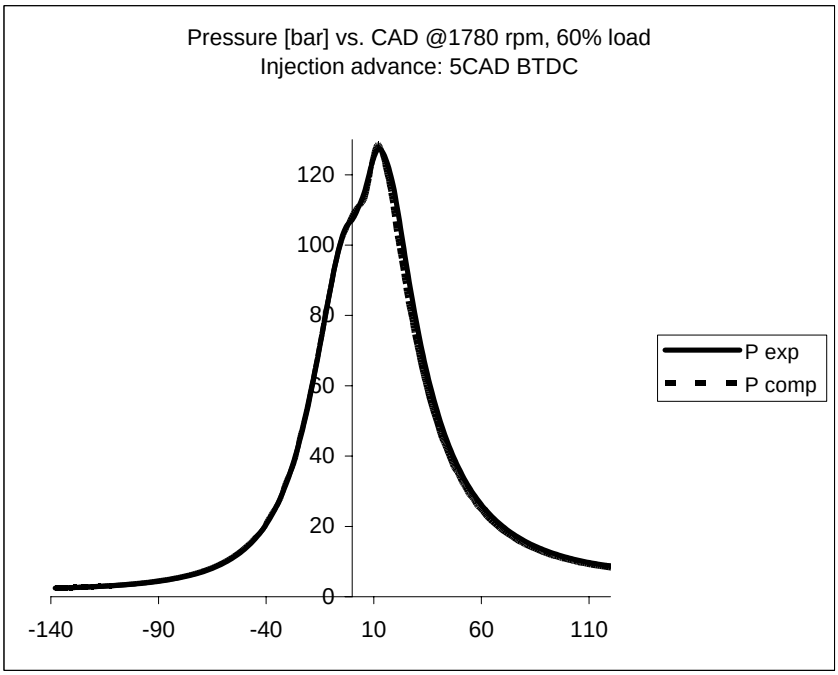

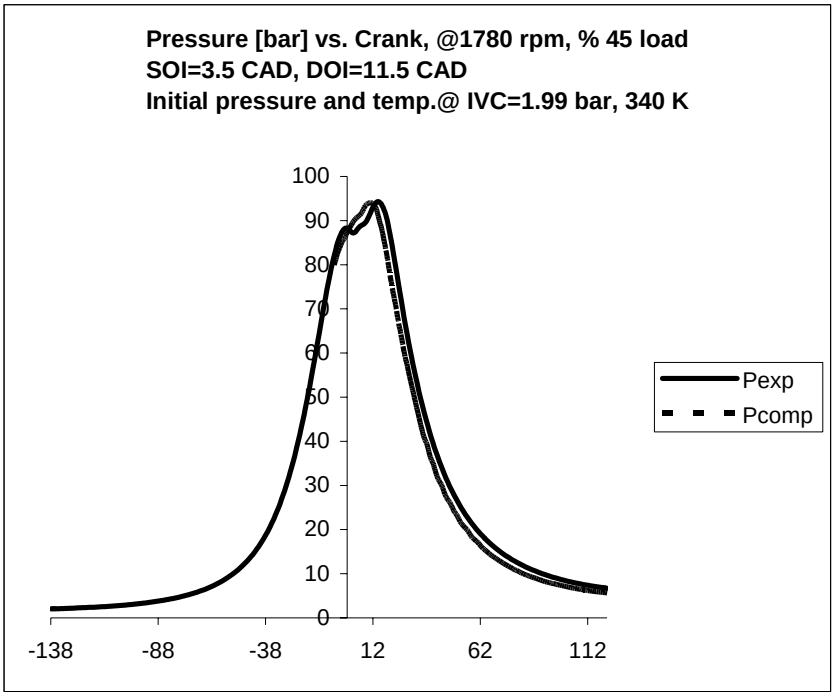
Pressure [bar] vs. Crank, @1780 rpm, % 45 load
SOI=3.5 CAD, DOI=11.5 CAD
Initial pressure and temp.@ IVC=1.99 bar, 340 K
100
90
80
70
60
50
40
30
20
10
0
-138
-88
-38
12
62
112
Pexp
Pcomp

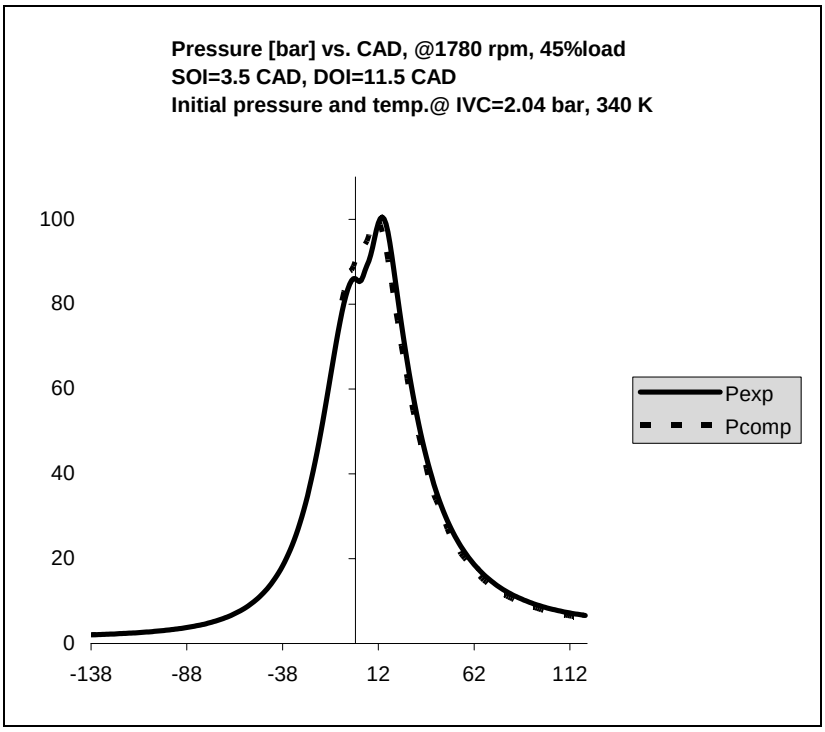
Pressure [bar] vs. CAD, @1780 rpm, 45%load
SOI=3.5 CAD, DOI=11.5 CAD
Initial pressure and temp.@ IVC=2.04 bar, 340 K
100
80
60
40
20
0
-138
-88
-38
12
62
112
Pexp
Pcomp

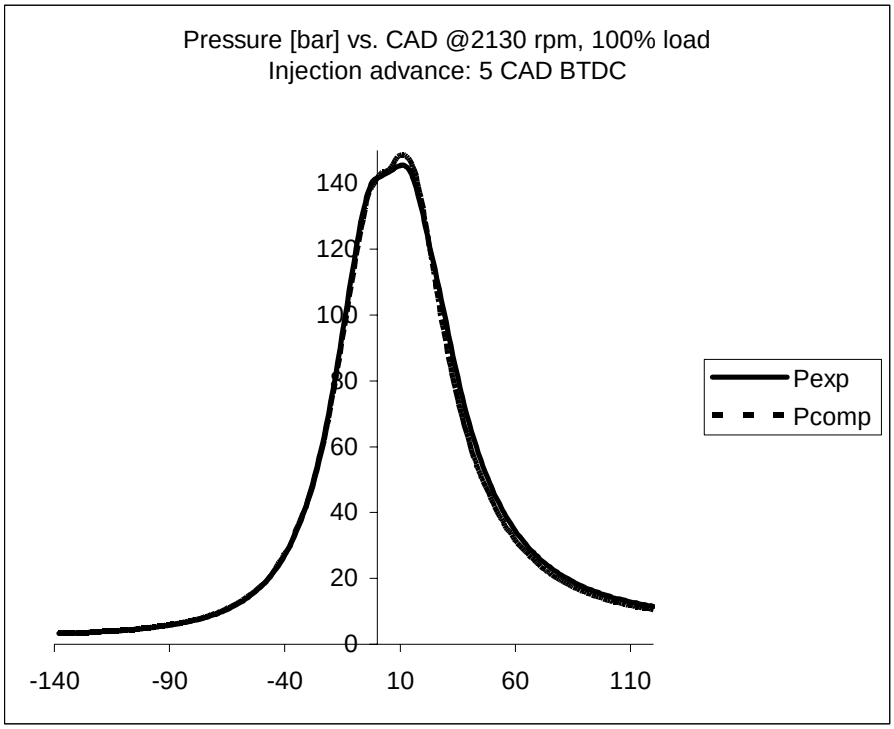
Pressure [bar] vs. CAD @2130 rpm, 100% load
Injection advance: 5 CAD BTDC
140
120
100
80
60
40
20
0
-140
-90
-40
10
60
110
Pexp
Pcomp

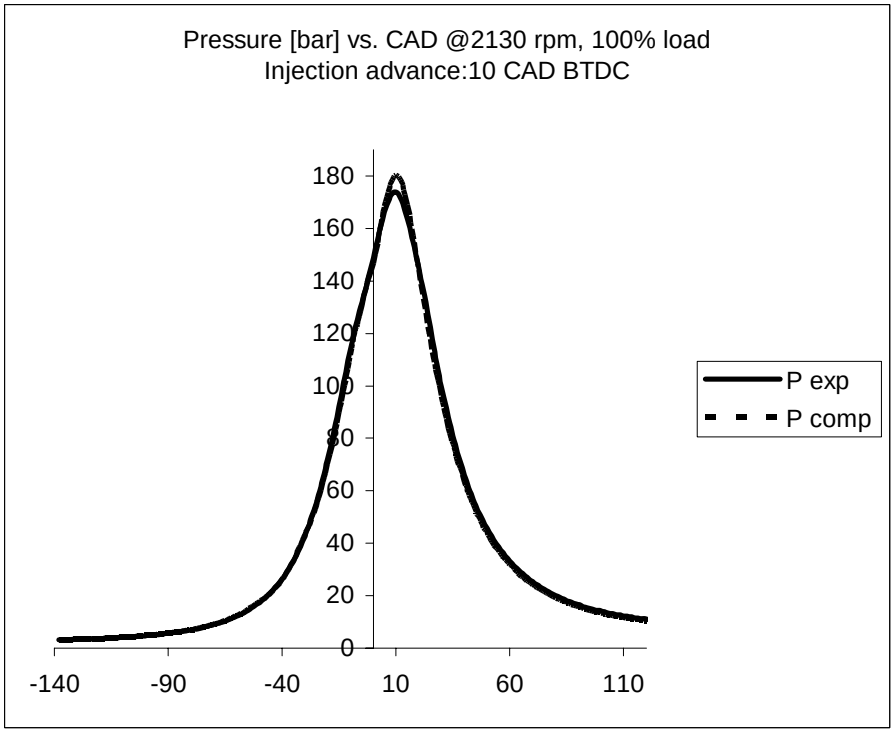
Pressure [bar] vs. CAD @2130 rpm, 100% load
Injection advance:10 CAD BTDC
180
160
140
120
100
80
60
40
20
0
-140
-90
-40
10
60
110
P exp
P comp

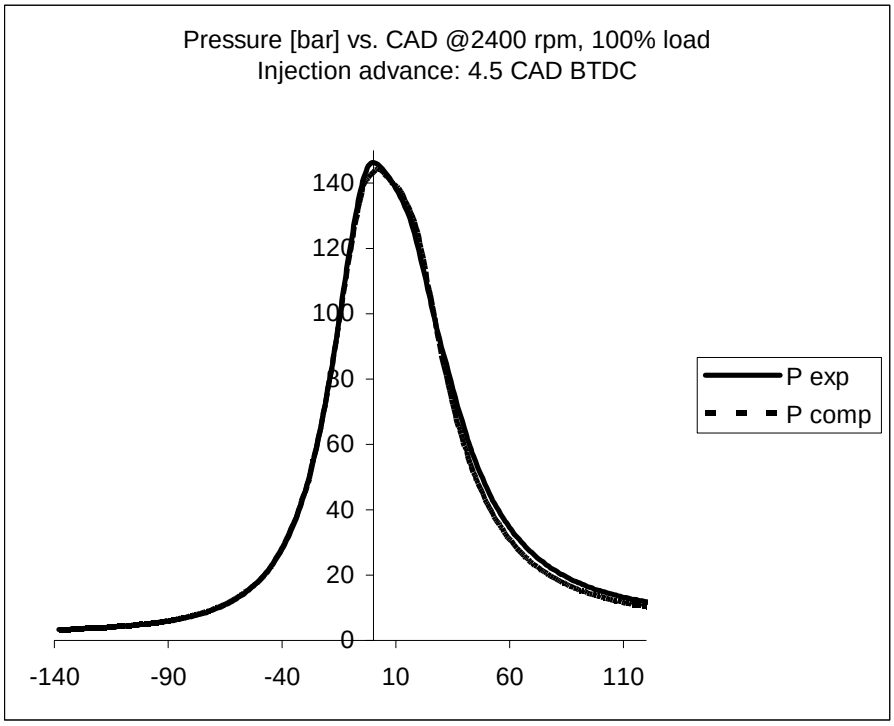
Pressure [bar] vs. CAD @2400 rpm, 100% load
Injection advance: 4.5 CAD BTDC
140
120
100
80
60
40
20
0
-140
-90
-40
10
60
110
P exp
P comp

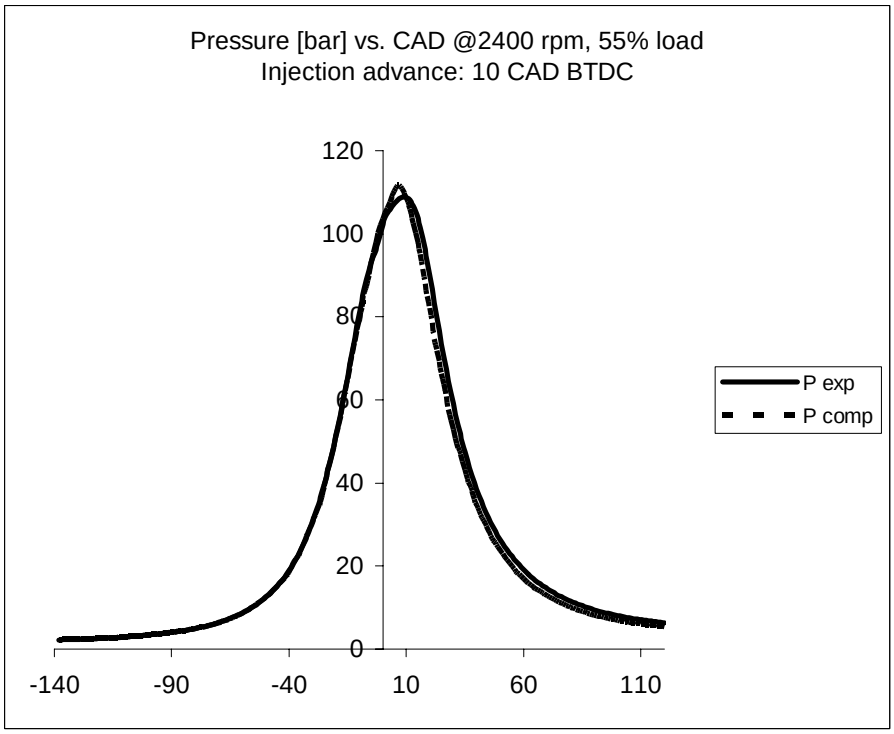
Pressure [bar] vs. CAD @2400 rpm, 55% load
Injection advance: 10 CAD BTDC
120
100
80
60
40
20
0
-140
-90
-40
10
60
110
P exp
P comp

APPENDIX B

KIVA-3V engine predictions of temperature development on 2 perpendicular planes. Engine is 100% loaded and at 1780 rpm. Injection begins at 5 cad BTDC. The fuel spray droplets are magnified and displayed as colored spheres. Swirl ratio is 1.45. The effect of adding a reasonable amount of swirl in the computations can be seen in the figures below, where the center of the flame ball, represented by temperature contours, travels clockwise.

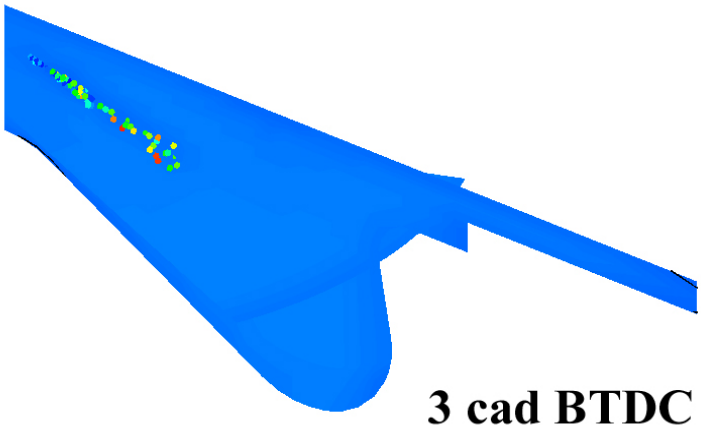

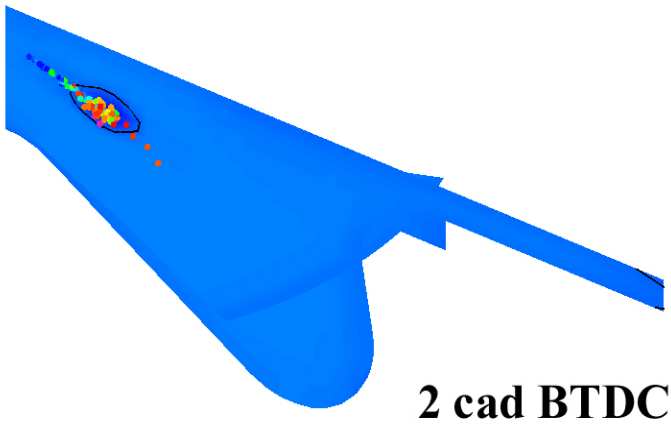

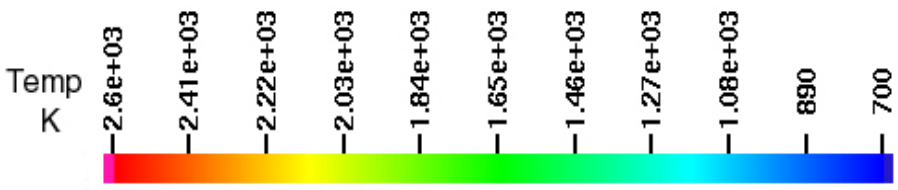

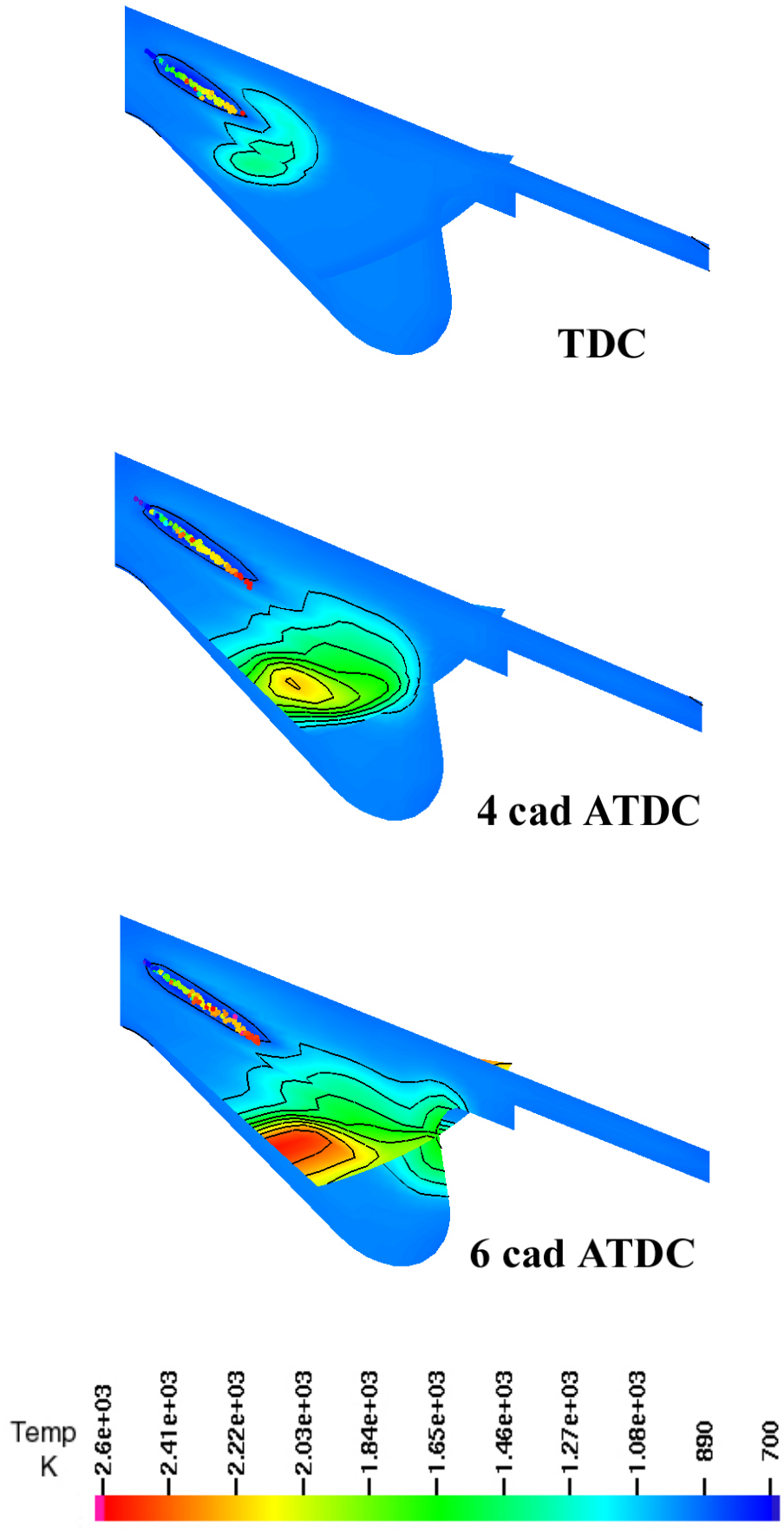
TDC
4 cad ATDC
6 cad ATDC
Temp
K
2.6e+03
2.41e+03
2.22e+03
2.03e+03
1.84e+03
1.65e+03
1.46e+03
1.27e+03
1.08e+03
890
700

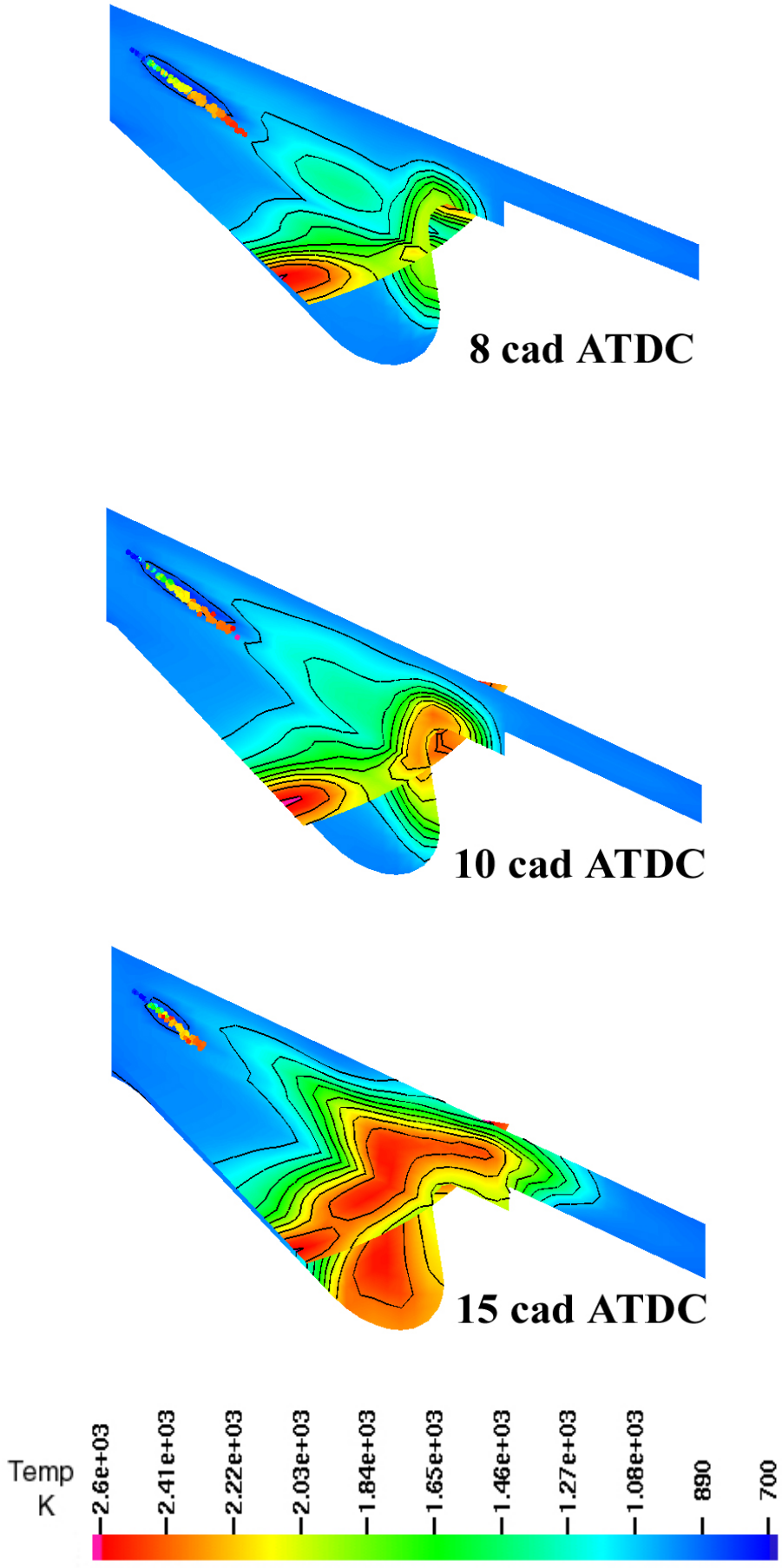
8 cad ATDC
10 cad ATDC
15 cad ATDC
Temp
K
2.6e+03
2.41e+03
2.22e+03
2.03e+03
1.84e+03
1.65e+03
1.46e+03
1.27e+03
1.08e+03
890
700

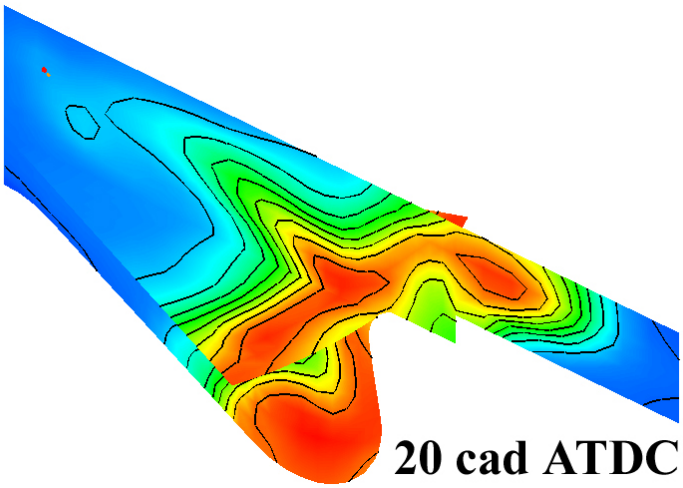
20 cad ATDC

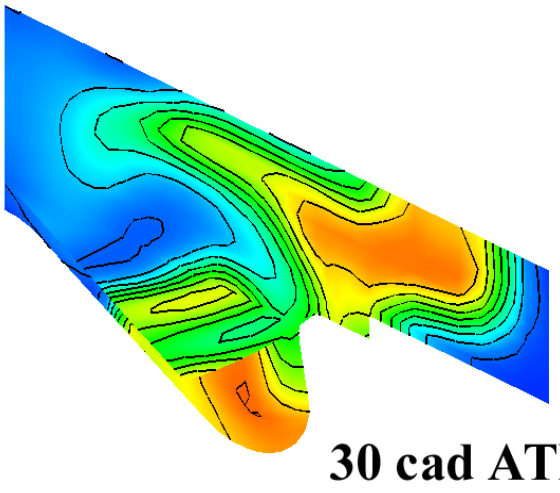
30 cad ATDC

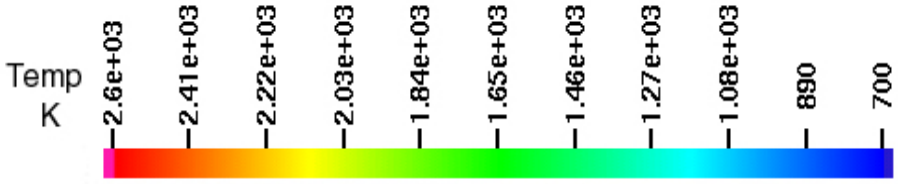
Temp
K
2.6e+03
2.41e+03
2.22e+03
2.03e+03
1.84e+03
1.65e+03
1.46e+03
1.27e+03
1.08e+03
890
700

APPENDIX C

STRUCTURE OF COMPUTER CODE

KIVA3V has been written in FORTRAN programming language. Standard version comprises three independent programs for pre-processing (k3prep), processing (kiva3v) and post-processing (k3post). Since k3post supports only some sorts of Unix based workstations, that are compatible to CGS (Cray Graphics System) library, GMV (General Mesh Viewer) and Ensight software have been preferred, though k3post library may be superimposed into a Linux based or Windows NT PC. The flow chart below summarizes KIVA3V, used in this study.

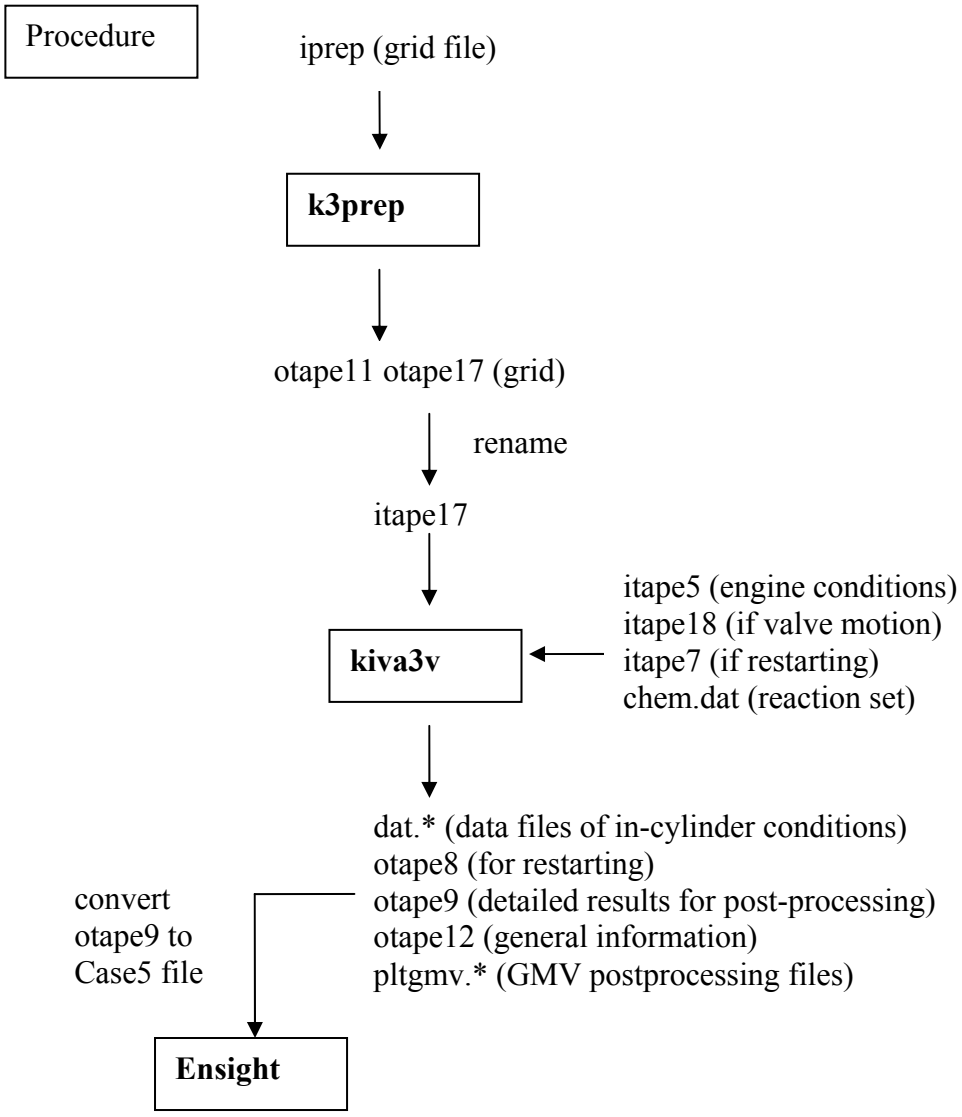

P.S. Rename otape8 as itape7 and increase the value of the parameter irest by one in itape5.

APPENDIX D

REACTION	A_f^r	n_f^r	$E_{a\_f}^r$
! ->Global reactions of fuel decomposition			
C14H28 + O2 = C7H7OH + H2O	5.000E+12	0.0	28000.0
C14H28 + H2O = C7H16 + O2	5.000E+12	0.0	28000.0
C7H16 + O2 = HCO + H2O	5.000E+11	0.0	29300.0
!<-			
!-> Graphatization sub mechanism			
C4H2 = C(S) + H2	2.000E+06	0.0	0.0
A2R5 = C(S) + H2	2.000E+04	0.0	0.0
! <-			
! ->n-heptane sub mechanism			
C7H16 + O2 = C7H15-1 + HO2	4.500E+13	0.0	48810.0
C7H16 + O2 = C7H15-2 + HO2	3.000E+14	0.0	47380.0
C7H16 + H = C7H15-1 + H2	5.600E+07	2.0	7667.0
C7H16 + H = C7H15-2 + H2	4.380E+07	2.0	4750.0
C7H16 + OH = C7H15-1 + H2O	8.610E+09	1.1	1815.0
C7H16 + OH = C7H15-2 + H2O	7.800E+09	1.3	690.5
C7H16 + HO2 = C7H15-1 + H2O2	8.000E+12	0.0	19300.0
C7H16 + HO2 = C7H15-2 + H2O2	1.000E+13	0.0	16950.0
C7H16 = C4H9 + C3H7	3.400E+16	0.0	80710.0
C7H15-1 + O2 = C7H15O2	2.000E+12	0.0	0.0
C7H15-2 + O2 = C7H15O2	2.500E+12	0.0	0.0
C7H15O2 = C7H14O2H	6.000E+11	0.0	20380.0
C7H14O2H+ O2 = C7H14O4H	4.000E+11	0.0	0.0
C7H14O4H = C7KET21 + OH	2.965E+13	0.0	26700.0
C7KET21 = C5H11CO + CH2O + OH	1.050E+16	0.0	4.240E+4
C5H11CHO+ O2 = C5H11CO + HO2	2.000E+13	0.5	4.220E+4
C5H11CHO+ OH = C5H11CO + H2O	1.000E+13	0.0	0.000E+0
C5H11CHO+ H = C5H11CO + H2	4.000E+13	0.0	4.200E+3
C5H11CHO+ O = C5H11CO + OH	5.000E+12	0.0	1.790E+3
C5H11CHO+ HO2 = C5H11CO + H2O2	2.800E+12	0.0	1.360E+4
C5H11CHO+ CH3 = C5H11CO + CH4	1.700E+12	0.0	8.440E+3
C5H11CHO+ CH3O2 = C5H11CO + CH4O2	1.000E+12	0.0	9.500E+3
C5H11CO = C5H11 + CO	1.000E+11	0.0	9.600E+3
C5H11 = C2H5 + C3H6	3.200E+13	0.0	28300.0
C7H15-1 = C2H4 + C5H11	2.500E+13	0.0	28810.0
C7H15-2 = CH3 + C6H12	3.000E+13	0.0	29800.0
C6H12 = C3H7 + C3H5	1.000E+16	0.0	68000.0
C6H12 = C3H6 + C3H6	1.000E+16	0.0	68000.0
C7H15-2 = C4H9 + C3H6	1.500E+13	0.0	28600.0
C7H15-1 = C7H15-2	2.000E+11	0.0	18050.0
C4H9 = C3H6 + CH3	2.232E+17	-1.40	30830.0
C4H9 = C2H5 + C2H4	2.500E+13	0.0	28810.0
C3H7 = C2H4 + CH3	9.600E+13	0.0	30950.0
C3H7 = C3H6 + H	1.250E+14	0.0	36900.0
C3H7 + CH3 = C2H5 + C2H5	1.900E+13	-0.3	0.0
C3H7 + O2 = C3H6 + HO2	1.000E+12	0.0	4980.0
C3H7 + H = CH3 + C2H5	4.060E+06	2.19	890.0
C3H6 = C2H3 + CH3	6.250E+15	0.0	85500.0
C3H6 + H = C3H5 + H2	5.000E+12	0.0	1500.0
C3H6 + CH3 = C3H5 + CH4	9.000E+12	0.0	8480.0
C3H6 + O2 = C3H5 + HO2	4.000E+12	0.0	39900.0
C3H5 + HO2 = C2H3 + CH2O + OH	1.000E+12	0.0	0.0
C3H5 + H = C3H4 + H2	1.000E+13	0.0	0.0
C3H5 + O2 = CH3 + CH2O + CO	4.000E+12	0.0	0.0
C3H4 + OH = C2H3 + CH2O	1.000E+12	0.0	0.0
C3H4 + OH = C2H4 + HCO	1.000E+12	0.0	0.0
C3H4 + O2 = C3H3 + HO2	4.000E+13	0.0	39160.0
CH3O + CO = CH3 + CO2	1.570E+14	0.00	11800.0
CH3O + H = CH2O + H2	2.000E+13	0.00	0.0
CH3O + H = CH3 + OH	1.000E+14	0.00	0.0
CH3O + OH = CH2O + H2O	5.000E+12	0.00	0.0
CH3O + O = CH2O + OH	1.000E+13	0.00	0.0
CH3O + O2 = CH2O + HO2	4.280E-13	7.60	-3530.0
CH3O = CH2O + H	3.000E+12	0.00	27420.0
CH3O2 + CH3 = CH3O + CH3O	2.410E+13	0.0	0.0
CH3O2 + O = CH3O + O2	3.610E+13	0.0	0.0
CH3O2 + H = CH3O + OH	9.640E+13	0.0	0.0
CH3O2 + CH2O = CH4O2 + HCO	1.000E+12	0.0	11665.0
CH3O2 + C2H6 = CH4O2 + C2H5	2.950E+11	0.0	14944.0
CH3O2 + CH3O2 = CH3O + CH3O + O2	2.800E+11	0.0	-780.0

CH3O2	+ H2O2		= CH4O2	+ HO2		2.400E+12	0.0	10000.0
CH4O2			= CH3O	+ OH		3.000E+16	0.0	42920.0
CH3O2	+ C2H4		= C2H3	+ CH4O2		7.100E+11	0.0	17110.0
CH4O2	+ OH		= CH3O2	+ H2O		1.000E+13	0.0	-258.0
CH4O2	+ O		= CH3O2	+ OH		2.000E+13	0.0	4750.0
CO	+ O	+ M	= CO2	+ M		6.170E+14	0.0	3000.0
CO	+ OH		= CO2	+ H		3.510E+07	1.3	70.0
CO	+ O2		= CO2	+ O		1.600E+13	0.0	41000.0
CO	+ HO2		= CO2	+ OH		6.500E+13	0.0	23650.0
H2	+ O2		= OH	+ OH		1.700E+13	0.00	47780.0
H2	+ OH		= H2O	+ H		1.170E+09	1.30	3626.0
O	+ OH		= O2	+ H		4.000E+14	-0.50	0.0
O	+ H2		= OH	+ H		5.060E+04	2.70	6290.0
H	+ HO2		= O	+ H2O		3.100E+10	0.00	3590.0
O	+ OH	+ M	= HO2	+ M		1.000E+16	0.00	0.0
H	+ O2	+ M	= HO2	+ M		3.610E+17	-0.70	0.0
OH	+ HO2		= H2O	+ O2		7.500E+12	0.00	0.0
H	+ HO2		= OH	+ OH		1.700E+14	0.00	874.0
O	+ HO2		= O2	+ OH		1.400E+13	0.00	1073.0
OH	+ OH		= O	+ H2O		6.000E+08	1.30	0.0
H	+ H	+ M1	= H2	+ M1		1.000E+18	-1.00	0.0
H	+ H	+ H2	= H2	+ H2		9.200E+16	-0.60	0.0
H	+ H	+ H2O	= H2	+ H2O		6.000E+19	-1.30	0.0
H	+ H	+ CO2	= H2	+ CO2		5.490E+20	-2.00	0.0
H	+ OH	+ M	= H2O	+ M		1.600E+22	-2.00	0.0
H	+ O	+ M	= OH	+ M		6.200E+16	-0.60	0.0
O	+ O	+ M	= O2	+ M		1.890E+13	0.0	-1788.0
H	+ HO2		= H2	+ O2		1.250E+13	0.00	0.0
HO2	+ HO2		= H2O2	+ O2		2.020E+12	0.00	0.0
H2O2	+ M		= OH	+ OH	+ M	4.300E+16	0.00	45500.0
H2O2	+ H		= HO2	+ H2		1.600E+12	0.00	3800.0
H2O2	+ OH		= H2O	+ HO2		1.000E+13	0.00	1800.0
H2O2	+ H		= H2O	+ OH		1.000E+13	0.00	3590.0
H2O2	+ O		= H2O	+ O2		8.400E+11	0.00	4260.0
H2O2	+ O		= OH	+ HO2		2.000E+13	0.00	5900.0
H2	+ HO2		= H2O	+ OH		6.500E+11	0.00	18800.0
CH2O	+ O2		= HCO	+ HO2		1.000E+14	0.00	40000.0
CH2O	+ HO2		= HCO	+ H2O2		3.000E+12	0.00	8000.0
CH2O	+ CH3		= HCO	+ CH4		5.540E+03	2.81	5.86E+3
CH2O	+ M		= HCO	+ H	+ M	3.300E+16	0.00	8.10E+4
HCO	+ HCO		= CH2O	+ CO		3.010E+13	0.00	0.0
HCO	+ OH		= H2O	+ CO		1.000E+14	0.00	0.0
HCO	+ H		= H2	+ CO		1.190E+13	0.30	0.0
HCO	+ O		= OH	+ CO		3.000E+13	0.00	0.0
HCO	+ O		= H	+ CO2		3.000E+13	0.00	0.0
HCO	+ O2		= HO2	+ CO		3.300E+13	-0.40	0.0
HCO	+ M		= H	+ CO	+ M	1.870E+17	-1.00	17000.0
HCO	+ HO2		= CO2	+ OH	+ H	3.000E+13	0.00	0.0
CH4	+ O2		= CH3	+ HO2		7.900E+13	0.00	56000.0
CH4	+ H		= CH3	+ H2		6.600E+08	1.60	10840.0
CH4	+ OH		= CH3	+ H2O		1.600E+06	2.10	2460.0
CH4	+ O		= CH3	+ OH		1.020E+09	1.50	8604.0
CH4	+ HO2		= CH3	+ H2O2		1.000E+13	0.00	18700.0
CH4	+ CH2		= CH3	+ CH3		4.000E+12	0.00	-570.0
CH3	+ HCO		= CH4	+ CO		1.200E+14	0.00	0.0
CH3	+ HCO		= CH2O	+ CH2		3.000E+13	0.00	0.0
CH3	+ H		= CH4			1.900E+36	-7.00	9050.0
CH3	+ H		= CH2	+ H2		9.000E+13	0.00	15100.0
CH3	+ CH3O		= CH4	+ CH2O		4.300E+14	0.00	0.0
CH3	+ CH3		= C2H6			2.120E+16	-0.97	620.0
CH3	+ CH3		= C2H5	+ H		4.990E+12	0.10	10600.0
CH3	+ O		= CH2O	+ H		8.000E+13	0.00	0.0
CH3	+ OH		= CH2	+ H2O		7.500E+06	2.00	5000.0
CH3	+ OH		= CH2O	+ H2		4.000E+12	0.00	0.0
CH3	+ CH2		= C2H4	+ H		3.000E+13	0.00	-570.0
CH3	+ HO2		= CH3O	+ OH		5.000E+13	0.00	0.0
CH3	+ O2		= CH3O	+ O		4.670E+13	0.00	30000.0
CH3	+ O2		= CH2O	+ OH		1.000E+11	0.00	9000.0
CH3	+ C2H4		= CH4	+ C2H3		6.620E+00	3.70	9482.0
CH3	+ CH3		= C2H4	+ H2		1.000E+15	0.00	31000.0
CH2	+ OH		= CH2O	+ H		2.500E+13	0.00	0.0
CH2	+ O2		= HCO	+ OH		4.300E+10	0.00	-500.0
CH2	+ O2		= CO2	+ H2		6.900E+11	0.00	500.0
CH2	+ O2		= CO	+ H2O		2.000E+10	0.00	-1000.0
CH2	+ O2		= CH2O	+ O		5.000E+13	0.00	9000.0
CH2	+ O2		= CO2	+ H	+ H	1.600E+12	0.00	1000.0
CH2	+ O2		= CO	+ OH	+ H	8.600E+10	0.00	-500.0
CH2	+ CH2		= C2H2	+ H2		1.200E+13	0.0	800.0
CH2	+ CH2		= C2H2	+ H	+ H	1.200E+14	0.0	800.0

CH2	+ CO2		= CH2O	+ CO		1.000E+11	0.00	1000.0
C2H4	+ H		= C2H3	+ H2		1.100E+14	0.00	8500.0
C2H4	+ O		= CH3	+ HCO		1.600E+09	1.20	746.0
C2H4	+ O		= CH2O	+ CH2		3.000E+04	1.88	180.0
C2H4	+ O		= C2H3	+ OH		1.510E+07	1.91	3790.0
C2H4	+ OH		= CH2O	+ CH3		6.000E+13	0.0	960.0
C2H4	+ HO2		= C2H3	+ H2O2		7.100E+11	0.0	17110.0
C2H4	+ OH		= C2H3	+ H2O		6.020E+13	0.00	5955.0
C2H4	+ M		= C2H2	+ H2	+ M	1.500E+15	0.00	55800.0
C2H4	+ M		= C2H3	+ H	+ M	2.600E+17	0.0	96570.0
C2H4	+ H		= C2H5			2.600E+43	-9.25	52580.0
C2H6	+ O2		= C2H5	+ HO2		1.000E+13	0.00	48960.0
C2H5	+ O2		= C2H4	+ HO2		2.000E+10	0.0	-2200.0
C2H4	+ O2		= C2H3	+ HO2		4.200E+14	0.00	57590.0
C2H4	+ C2H4		= C2H5	+ C2H3		5.000E+14	0.0	64700.0
C2H5	+ HO2		= C2H4	+ H2O2		3.000E+11	0.00	0.0
C2H2	+ O2		= HCO	+ HCO		4.000E+12	0.00	28000.0
C2H2	+ O		= CH2	+ CO		1.020E+07	2.00	1900.0
C2H2	+ H	+ M	= C2H3	+ M		5.540E+12	0.00	2410.0
C2H3	+ H		= C2H2	+ H2		4.000E+13	0.00	0.0
C2H3	+ O2		= CH2O	+ HCO		4.000E+12	0.00	-250.0
C2H3	+ OH		= C2H2	+ H2O		3.000E+13	0.00	0.0
C2H3	+ CH2		= C2H2	+ CH3		3.000E+13	0.00	0.0
C2H3	+ HCO		= C2H4	+ CO		6.034E+13	0.0	0.0
C2H3	+ C2H3		= C2H2	+ C2H4		1.450E+13	0.0	0.0
C2H3	+ O		= C2H2	+ OH		1.000E+13	0.0	0.0
C2H2	+ OH		= CH3	+ CO		4.830E-04	4.00	-2000.0
C2H2	+ CH2		= C3H3	+ H		1.200E+13	0.0	6620.0
C3H3	+ OH		= C3H2	+ H2O		1.000E+13	0.0	0.0
C3H3	+ O		= CH2O	+ C2H		1.000E+13	0.0	0.0
C2H3			= C2H2	+ H		4.600E+40	-8.80	46200.0
C2H2			= C2H	+ H		2.373E+32	-5.28	130688.0
C2H	+ O2		= HCO	+ CO		5.000E+13	0.00	1500.0
C2H	+ H2		= H	+ C2H2		4.900E+05	2.50	560.0
C2H2	+ O		= C2H	+ OH		4.600E+19	-1.41	28950.0
C2H2	+ OH		= C2H	+ H2O		3.370E+07	2.00	14000.0
C2H2	+ C2H		= C4H2	+ H		9.600E+13	0.0	0.0
C4H	+ H2		= H	+ C4H2		4.900E+05	2.5	560.0
C4H2	+ OH		= C4H	+ H2O		3.370E+07	2.0	14000.0
C4H2	+ O		= C3H2	+ CO		2.700E+13	0.0	1720.0
C3H2	+ O		= C2H2	+ CO		5.800E+13	0.0	0.0
C3H2	+ OH		= HCO	+ C2H2		5.800E+13	0.0	0.0
C3H2	+ CH2		= C4H3	+ H		3.000E+13	0.0	0.0
C3H3	+ C3H3		= C6H5	+ H		2.000E+12	0.0	0.0
C3H2	+ HCCO		= C4H3	+ CO		1.000E+13	0.0	0.0
C2H2	+ OH		= CH2CO	+ H		2.180E-04	4.50	-1000.0
CH2CO	+ H		= HCCO	+ H2		5.000E+13	0.00	8000.0
CH2CO	+ H		= CH3	+ CO		1.130E+13	0.00	3428.0
CH2CO	+ O		= HCCO	+ OH		1.000E+13	0.00	8000.0
C2H2	+ C2H2		= C4H2	+ H2		1.000E+17	0.00	81000.0
C2H2	+ C2H		= C4H3			4.500E+37	-7.68	7100.0
C2H3	+ C2H2		= C4H5			8.100E+37	-8.09	13400.0
C4H5	+ O2		= C2H4	+ CO	+ HCO	4.160E+10	0.00	2500.0
C4H2	+ H		= C4H3			1.100E+42	-8.72	15300.0
C4H3	+ H		= C2H2	+ C2H2		6.300E+25	-3.34	10014.0
C4H3	+ H		= C4H2	+ H2		1.500E+13	0.00	0.0
C4H3	+ OH		= C4H2	+ H2O		5.000E+12	0.00	0.0
C4H3	+ C2H2		= C6H5			3.800E+21	-3.17	6400.0
CH2CO	+ O		= CH2	+ CO2		1.750E+12	0.00	1350.0
CH2CO	+ OH		= HCCO	+ H2O		7.500E+12	0.00	2000.0
C2H3	+ O		= CH2CO	+ H		3.000E+13	0.00	0.0
C3H3	+ O2		= CH2CO	+ HCO		3.000E+10	0.00	2878.0
C3H4	+ O		= CH2CO	+ CH2		2.000E+07	1.8	1000.0
C4H3	+ O2		= HCCO	+ CH2CO		7.860E+16	-1.80	0.0
C6H5	+ O2		= CH2CO	+ CH2CO	+ C2H	7.860E+16	-1.80	0.0
C6H8	+ H		= C6H7	+ H2		1.330E+06	2.53	12240.0
C6H8	+ OH		= C6H7	+ H2O		6.200E+06	2.0	3430.0
CH2CO	+ M		= CH2	+ CO	+ M	2.000E+16	0.00	6.00E+4
C2H	+ OH		= H	+ HCCO		2.000E+13	0.0	0.0
C2H2	+ O		= HCCO	+ H		1.020E+07	2.0	1900.0
C2H2	+ O		= C2H	+ OH		D 4.600E+19	-1.41	28950.0
HCCO	+ O2		= OH	+ CO	+ CO	1.600E+12	0.0	854.0
HCCO	+ CH2		= C2H3	+ CO		3.000E+13	0.0	0.0
C2H	+ C2H		= C4H2			1.800E+13	0.0	0.0
C3H4	+ O		= HCCO	+ CH3		6.300E+12	0.0	2010.0
HCCO	+ HCCO		= C2H2	+ CO	+ CO	1.000E+13	0.0	0.0
CH2O	+ O		= HCO	+ OH		3.800E+13	0.00	3540.0
CH2O	+ H		= HCO	+ H2		2.300E+10	1.05	3270.0
CH2O	+ OH		= HCO	+ H2O		2.430E+10	1.20	-447.0

```
! <-
! -> PAH sub mechanism
A1C2H   + OH                = A1-     + CH2CO           2.180E-04   4.5   -1000.0
A1C2H)2 + OH                = A1C2H-  + CH2CO           2.180E-04   4.5   -1000.0
A2      + OH                = A1C2H   + CH2CO   + H     1.300E+13   0.0   10600.0
A2      + O                 = CH2CO   + A1C2H           2.200E+13   0.0    4530.0
A2R5    + OH                = A2-1    + CH2CO           1.300E+13   0.0   10600.0
C3H3    + C3H3              = A1                        2.000E+10   0.0       0.0
C6H7                        = A1      + H               5.300E+25  -4.42  17300.0
C4H3    + C2H2              = A1-                       1.900E+63 -15.25  30600.0
C4H5    + C2H2              = A1      + H               1.600E+18  -1.88   7400.0
C6H5                        = A1-                       3.500E+46 -10.44  33600.0
A1      + H                 = A1-     + H2              2.590E+14   0.0   16000.0
A1      + OH                = A1-     + H2O             1.060E+08   1.42   1450.0
A1-     + H                 = A1                        1.000E+14   0.00      0.0
C4H3    + C4H2              = A1C2H-                    1.900E+63 -15.25  30600.0
A1      + C2H               = A1C2H   + H               5.000E+13   0.0       0.0
A1-     + C2H2              = A1C2H2                    7.900E+29  -5.15  13700.0
A1-     + C2H2              = A1C2H   + H               2.500E+29  -4.43  26400.0
A1C2H   + H                 = A1C2H2                    1.600E+32  -5.72  11090.0
A1C2H   + H                 = A1C2H-  + H2              2.500E+14   0.0   16000.0
A1C2H   + OH                = A1C2H-  + H2O             1.600E+08   1.42   1450.0
A1C2H-  + H       + M       = A1C2H   + M               1.000E+14   0.00      0.0
A1-     + C2H3              = A1C2H2  + H               9.400E+00   4.14  23234.0
A1C2H2  + H                 = A1C2H   + H2              1.500E+13   0.0       0.0
A1C2H2  + OH                = A1C2H   + H2O             2.500E+12   0.0       0.0
A1C2H-  + C2H2              = A2-1                      5.100E+48 -10.53  28000.0
A1C2H-  + C2H2              = A1C2H)2 + H               2.100E+10   0.85  13700.0
A1C2H)2 + H                 = A2-1                      1.500E+51 -10.77  25500.0
A1C2H   + C2H               = A1C2H)2 + H               5.000E+13   0.0       0.0
A1C2H2  + C2H2              = A2      + H               1.600E+18  -1.88   7400.0
A2      + H                 = A2-1    + H2              2.500E+14   0.0   16000.0
A2      + OH                = A2-1    + H2O             1.600E+08   1.42   1450.0
A2-1    + O2                = A1C2H   + HCO     + CO    2.100E+12   0.0    7470.0
A2-1    + C2H2              = A2R5    + H               1.100E+07   1.71   3900.0
A2R5    + O                 = A2-1    + HCCO            2.200E+13   0.0    4530.0
A2R5-   + O2                = A2-1    + CO      + CO    2.100E+12   0.0    7470.0
A2R5    + H                 = A2R5-   + H2              2.500E+14   0.0   16000.0
A2R5    + OH                = A2R5-   + H2O             1.600E+08   1.42   1450.0
A2R5-   + H                 = A2R5                      1.000E+14   0.00      0.0
! -> Soot oxidation sub mechanism
C(S)    + O2                = O       + CO              1.000E+10   0.00   6800.0
C(S)    + CH3               = H       + C2H2            1.000E+10   0.00   2800.0
C(S)    + OH                = CO      + H               5.000E+10   0.00   2800.0
C(S)    + NO                = CO      + N               2.000E+10   0.00   2800.0
! <-
! -> Toluene sub mechanism
C7H8                        = C6H5    + CH3             1.400E+16   0.0   99800.0
C7H8    + O2                = C7H7    + HO2             5.000E+14   0.0   39080.0
C7H8    + OH                = C7H7    + H2O             1.560E+13   0.0    2583.0
C7H8    + O                 = C7H7    + OH              5.000E+08   1.5    8000.0
C7H8    + H                 = C7H7    + H2              3.980E+02   3.4    3120.0
C7H7    + O                 = C6H5CHO + H               2.500E+14   0.0       0.0
C7H7    + O                 = C6H5    + CH2O            8.000E+13   0.0       0.0
C7H7    + HO2               = C6H5CHO + H       + OH    5.000E+14   0.0       0.0
C7H7    + HO2               = C6H5    + CH2O    + OH    8.000E+12   0.0       0.0
C7H7    + OH                = C7H7OH                    6.000E+13   0.0       0.0
C7H7OH  + OH                = C6H5CHO + H2O     + H     8.430E+12   0.0    2583.0
C7H7OH  + O2                = C6H5CHO + H       + HO2   2.000E+14   0.0   41400.0
C7H7OH  + H                 = C6H5CHO + H       + H2    8.000E+13   0.0       0.0
C7H7OH  + C7H7              = C6H5CHO + C7H8    + H     2.110E+11   0.0    9500.0
C6H5CHO + O2                = C6H5CO  + HO2             1.020E+13   0.0   38950.0
C6H5CHO + OH                = C6H5CO  + H2O             1.710E+09   1.18   -447.0
C6H5CHO + H                 = C6H5CO  + H2              5.000E+13   0.0    4928.0
C6H5CHO + O                 = C6H5CO  + OH              9.040E+12   0.0    3080.0
C6H5CO                      = C6H5    + CO              3.980E+14   0.0   29400.0
C6H5    + CH3               = C7H7    + H               5.700E-02   5.0   15700.0
! <-
! -> Nitrogen sub mechanism
N       + NO                = N2      + O               2.700E+13   0.00    355.0
N       + O2                = NO      + O               9.000E+09   0.00   6500.0
N       + OH                = NO      + H               3.360E+13   0.00    385.0
N       + CO2               = NO      + CO              3.000E+12   0.00  11300.0
N2O     + O                 = N2      + O2              1.400E+12   0.00  10810.0
N2O     + O                 = NO      + NO              2.900E+13   0.00  23150.0
N2O     + H                 = N2      + OH              3.870E+14   0.0   18880.0
N2O     + OH                = N2      + HO2             2.000E+12   0.00  21060.0
N2O     + M                 = N2      + O       + M     7.910E+10   0.00  56020.0
! <-
```

AUTOBIOGRAPHY

Abdurrahman İMREN was born in 27th March 1978 in İstanbul. He graduated from ITU Mechanical Engineering Faculty in 2001. Having accomplished his military obligation in 2002, he has attended Automotive Engineering Programme in ITU Science and Technology Institute.